REACTOR MATERIALS

OCT 15 1969
MICHIGAN STATE UNIVERSITY
LIBRARIES

A Quarterly Technical Progress Review

Prepared for DIVISION OF TECHNICAL INFORMATION, U. S. ATOMIC ENERGY COMMISSION,
by BATTELLE MEMORIAL INSTITUTE, COLUMBUS LABORATORIES

Fall 1969

● VOLUME 12

● NUMBER 3

TECHNICAL PROGRESS REVIEWS

The United States Atomic Energy Commission publishes the Technical Progress Reviews to meet the needs of industry and government for concise summaries of current nuclear developments. Each journal digests and evaluates the latest findings in a specific area of nuclear technology and science. *Nuclear Safety* is a bimonthly journal; the other three are quarterly journals.

Isotopes and Radiation Technology
P. S. Baker, A. F. Rupp, and associates
Isotopes Information Center, Oak Ridge National Laboratory

Nuclear Safety
Wm. B. Cottrell, W. H. Jordan, J. P. Blakely, and associates
Nuclear Safety Information Center, Oak Ridge National Laboratory

Reactor and Fuel-Processing Technology

Reactor Materials
E. M. Simons and associates
Battelle Memorial Institute, Columbus Laboratories

All are available from the U. S. Government Printing Office. See the back cover for ordering instructions.

The views expressed in this publication do not necessarily represent those of the United States Atomic Energy Commission, its divisions or offices, or of any Commission advisory committee or contractor.

Availability of Reports Cited in This Review

United States Atomic Energy Commission (USAEC) reports are available at USAEC depository libraries and are sold by the Clearinghouse for Federal Scientific and Technical Information (CFSTI), National Bureau of Standards, U. S. Department of Commerce, Springfield, Va. 22151. All reports sold by CFSTI are $3.00 for printed copy and $0.65 for microfiche. Each separately bound part of a report is priced as a separate report. Some reports may not be available because of their preliminary nature; however, the information contained in them will generally be found in later progress or topical reports on the subject.

Other U. S. Government agency reports identified in this journal generally are available from CFSTI.

Private-organization reports should be requested from the originator.

United Kingdom Atomic Energy Authority (UKAEA) and Atomic Energy of Canada Limited (AECL) reports are available at USAEC depository libraries. UKAEA reports are sold by Her Majesty's Stationery Office, London; AECL reports are sold by the Scientific Document Distribution Office, Atomic Energy of Canada Limited, Chalk River, Ontario, Canada. UKAEA and AECL reports issued after March 1, 1967, are sold by CFSTI to purchasers in the United States and its territories.

REACTOR MATERIALS

Vol. 12, No. 3 Fall 1969

Contents

Fuel and Fertile Materials (Section I)

Uranium and Uranium Alloys 155
Plutonium 158
Thorium and Its Alloys 162
Uranium and Thorium Oxides 163
Carbide and Nitride Fuels 164
Basic Studies of Irradiation Effects in Fuel Materials 166
References 167

Moderator and Control Materials (Section II)

Graphite 171
Beryllium Metal and Alloys 172
Solid Hydrides 174
Nuclear Poisons 175
References 176

Cladding and Structural Materials (Section III)

Corrosion by Aqueous and Gaseous Media 177
Corrosion by Nonaqueous Liquids and Vapors 180
Cladding Reactions Following Loss-of-Coolant Accidents 186
Radiation Effects on Structural Materials 187
Metallurgy and Mechanical Properties of Common Cladding and Structural Materials 192
Diffusion Studies 196
Metallurgy of Refractory Metals 200
Nonfueled Refractories 202
Concrete 205
References 206

Special Fabrication Techniques (Section IV)

Melting, Casting, and Fabrication of Cast Materials 210
Powder-Metallurgy Materials 211
Plating 212
Explosive Metalworking 214
Welding and Brazing 214
Nondestructive Testing 217
References 218

Superintendent of Documents, U. S. Government Printing Office, Washington, D. C. 20402, $2.50 per year

Reactor Materials

is one of a series of technical progress reviews broadly covering the field of nuclear science and technology. Under the auspices of the USAEC Division of Technical Information, *Reactor Materials* is prepared by Battelle personnel from worldwide literature. It covers properties, behavior, and fabrication processes of materials applicable to nuclear reactor components and associated equipment.

The reader will recognize that the scope of this Review is too broad to permit detailed coverage of every topic. Rather, the authors and editors attempt to combine the highlights of significant new developments into an information summary of current research for both management and the technical specialist. As a rule, enough of the results are presented to define the research and summarize the findings. For readers desiring more information on any particular topic, a complete set of references is provided at the end of each section.

Each quarter, a number of bibliographies, monographs, and books appear on subjects within the scope of *Reactor Materials.* Though the main purpose of this Review is to call attention to findings that are new and significant, such publications are noted in the text because they often represent excellent compilations of available information on important materials topics.

E. M. Simons
D. L. Keller

BATTELLE MEMORIAL INSTITUTE
COLUMBUS LABORATORIES

Issued quarterly by the U. S. Atomic Energy Commission. Use of funds for printing this publication approved by the Director of the Bureau of the Budget on May 12, 1969.

Section

I

Reactor Materials

Fuel and Fertile Materials

Uranium and Uranium Alloys

Unalloyed Uranium

Some mechanical properties of extruded uranium measured by workers at National Lead Company of Ohio[1] over the temperature range 885 to 1235°F (474 to 668°C) are shown in Fig. I-1. Uranium with a fine

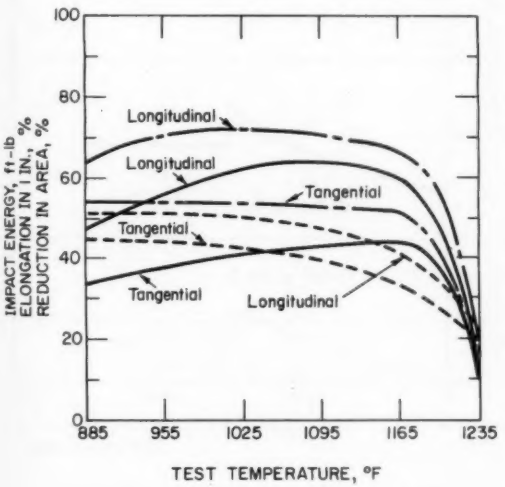

Fig. I-1 Tensile–impact properties of extruded uranium.[1] - - impact energy; ——elongation; —·— reduction in area.

grain structure had lower strength but higher ductility than coarse-grained uranium. As can be seen, the mechanical properties were generally poorer in the tangential (and radial) directions than in the longitudinal direction.

The ignition temperature of irradiated uranium (containing 300 ppm silicon and 300 ppm iron as impurities) was measured[2] in oxygen. Samples irradiated to 0.79% and 1.71% burnup of ^{235}U ignited at 400°C and 360°C, respectively. Unirradiated specimens ignited at 600°C. The nominal surface areas of all samples was about 0.6 cm^2/g, and an effort was made to maintain this value during irradiation by means of cladding constraint. Well-defined ignition did not occur in air with irradiated specimens. However, a greater degree of self-heating and spontaneous thermocycling, beginning at 400°C, occurred with irradiated samples than with unirradiated samples.

Alpha-Phase Uranium Alloys

Thermal cycling has been known to produce pores in several metals with anisotropic expansion coefficients. This was noted[3] in "adjusted" uranium (U–300 ppm Fe–700 ppm Al–50 ppm Si–800 ppm C) cycled between 400 and 600°C and measured quantitatively by means of density measurements as a function of the number of cycles. Magnitudes of density changes ranged from 6% in as-cast adjusted uranium after 5000 cycles to zero in as-cast pure uranium after 10,000 cycles. The voids were intergranular and were often associated with inclusions and grain-boundary triple points. Grain size of the pure uranium was 800 μ, compared with 220 μ for the as-cast adjusted uranium before cycling. Results were consistent with a mechanism for void formation that involves vacancy condensation on a fixed number of sites.[3,4] Thus the anisotropic-expansion stresses that are generated in thermal cycling purportedly cause a vacancy movement and condensation associated with grain boundaries and inclusions.

The specific heat [kcal/(gram atom)(°C)] of U–Zr alloys was found by the Soviets[5] to be related to temperature (°K) by the following equations:

Alpha uranium to 650°C

$$C_p = 2.69 + 9.698 \times 10^{-3}\, T + 1.072 \times 10^{5}\, T^{-2}$$

U–13 at.% Zr to 600°C

$$C_p = 3.56 \times 10^{-1} + 1.425 \times 10^{-2}\, T + 2.59 \times 10^{5}\, T^{-2}$$

U–41 at.% Zr to 600°C

$$C_p = 2.65 \times 10^{-1} + 1.32 \times 10^{-2}\ T + 2.62 \times 10^{5}\ T^{-2}$$

U–61 at.% Zr to 600°C

$$C_p = 3.47 + 9.32 \times 10^{-3}\ T + 7.01 \times 10^{4}\ T^{-2}$$

U–73 at.% Zr to 600°C

$$C_p = 3.08 + 8.43 \times 10^{-3}\ T + 9.83 \times 10^{4}\ T^{-2}$$

U–89 at.% Zr to 600°C

$$C_p = 3.89 + 6.48 \times 10^{-3}\ T + 7.71 \times 10^{4}\ T^{-2}$$

Alpha zirconium to 800°C

$$C_p = 6.15 + 1.927 \times 10^{-3}\ T - 3.485 \times 10^{4}\ T^{-2}$$

Some of these results are shown graphically in Fig. I-2. The discontinuities at about 600°C correspond to initial phase transformations. The other discontinuities with U–41 at.% Zr and U–13 at.% Zr probably result from the added transformations associated with the uranium side of the binary system and correspond roughly to accepted phase relations in the binary system.

Workers at National Lead of Ohio[6] made controlled, dilute alloy additions to uranium to see how they would affect the as-cast microstructure. The uranium used contained <150 ppm total impurities, including interstitials. Binary, ternary, quaternary, and quinary alloys were compounded using C, Fe, Al, and Si as alloying elements in quantities up to 1000 ppm of each.

Precipitates that formed in dilute U–Al and U–Si alloys were studied in Czechoslovakia[7] utilizing the replica method with the electron microscope. Distance between particles and particle size varied as a function of alpha-annealing conditions. A linear relation between hardness and the reciprocal value of distance between globular UAl_2 particles was found to exist in a U–0.1 Al alloy for a constant volume fraction of precipitate. No such relation was observed with a lamellar U_3Si precipitate in U–0.06 Si and U–0.1 Si alloys. The UAl_2 precipitate was similar to the precipitate in adjusted uranium alloys, i.e., U–(0.5–0.12 Al)–(0.02–0.05 Fe).

Trace additions of boron were reported by the French[8] to have important grain-refining effects on beta-treated alpha-uranium alloys. This refining was attributed to the presence of UB_2 nucleation sites.

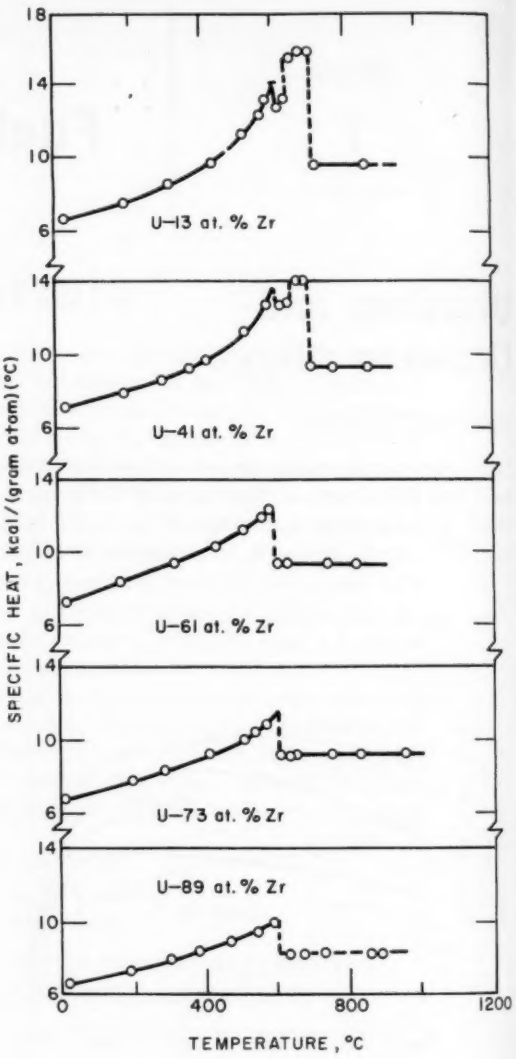

Fig. I-2 Specific heat of various U–Zr alloys.[5]

Kench and Chamberlain have studied creep-deformation effects in uranium* that reportedly occurred with no applied load and under isothermal, elevated-temperature conditions. The minimum creep rate of beta-quenched uranium at 500°C had been well characterized by other investigators for applied tensile stresses of 500 to 11,000 psi. These data, along with data on gamma-quenched uranium and low-stress

*The uranium contained small quantities of aluminum, iron, and carbon.

data,[9] are plotted in Fig. I-3. The creep rates above 500 psi are accurately described by the equation

$$\log \dot{\epsilon} = 2.5 \log \sigma - 13 \qquad (1)$$

where $\dot{\epsilon}$ is the minimum creep rate per hour and σ is the applied tensile stress. This equation is represented by the line in Fig. I-3. The two points labeled

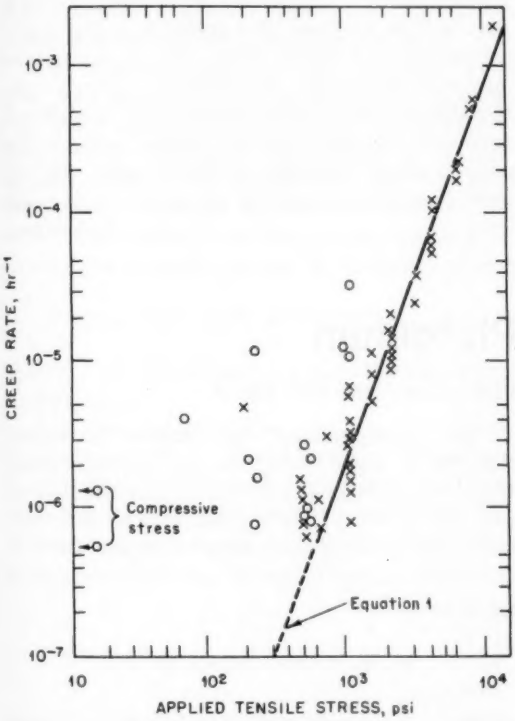

Fig. I-3 Creep rates[9] of uranium at 500°C. X, beta quenched; ○, gamma quenched.

"compressive stress" refer to the slight compressive stresses due to the specimens' weight only. The lack of a decreasing creep rate as stresses below 500 psi were applied to the gamma-quenched material suggested that an unintended tensile stress was present. This was assumed to be the case, and Eq. 1 was altered to

$$\log \dot{\epsilon} = 2.5 \log (\sigma_0 + \sigma) - 13 \qquad (2)$$

where σ_0 is this internal stress. At zero external stress the creep rate is on the order of 10^{-6}/hr. From Eq. 2, σ_0 = 630 psi at $\dot{\epsilon} = 10^{-6}$/hr. The data in Fig. I-3 for gamma-quenched uranium were replotted in Fig. I-4

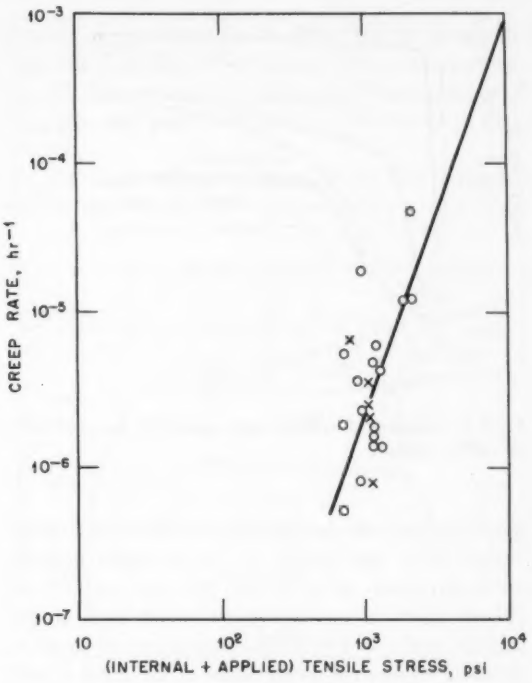

Fig. I-4 Data[9] of Fig. I-3, corrected for 630 psi internal tensile stress. X, beta quenched; ○, gamma quenched.

with 630 psi added to the reported stress values. The straight line represents Eq. 2. The good agreement of the data points with the curve tends to confirm the hypothesis of an internal tensile stress in gamma-quenched uranium.

The authors performed creep tests on beta- and gamma-quenched U–300 ppm Fe–700 ppm Al–1000 ppm C alloy to study these effects and determine mechanisms. Deformation curves with no external stress applied are shown in Fig. I-5. These results indicate that the anomalous creep occurs with both beta- and gamma-quenched uranium, and that creep rates are inversely correlated with grain size. The elongation observed was not caused by thermal cycling since isothermal conditions were maintained to ±2°C for the duration of the tests. It was argued that a UO_2 film could cause a stress state to exist which could result in tensile stresses at the metal–oxide interface. No-load experiments were performed with identical specimens in static and dynamic vacuum. No creep occurred in the static vacuum, but it did occur in the dynamic vacuum. Although the authors did not specify how good the static vacuum was, the dynamic pressure was $<1\ \mu$. More oxygen would probably be available to

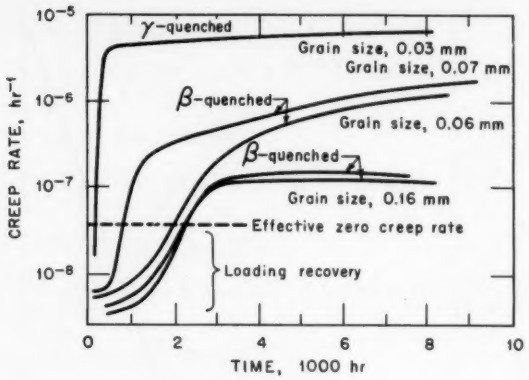

Fig. I-5 Variation of uranium creep rates with time, at 500°C, no applied stress.[9]

the specimen from the dynamic vacuum. Low levels of oxygen were also present in the creep-test environment, specifically up to 22 ppm H_2O and 6 ppm O_2 in 20-psia argon. It was concluded on the basis of this indirect evidence that surface oxidation of uranium results in an internal tensile stress of the order of 600 psi that can cause creep deformation at elevated temperatures in the absence of an external load.

Gamma-Phase Uranium Alloys

Properties and other characteristics of gamma-phase U–Mo alloys have been compiled by the Italians.[10] Properties covered include both mechanical and physical. Some of the characteristics considered are transformation kinetics, dimensional stability, and performance in-pile. Literature through 1967 was included in the survey.

Creep data were obtained for various uranium-base alloys in the U–Zr–Nb, U–Mo–Zr, and U–Nb–Mo systems.[11a] The data were obtained from bend tests conducted in vacuum at 500 and 600°C and under a maximum bending stress of 8.75 kg/mm^2. Hot-hardness studies on these alloys were also performed.[11b] High creep resistance in their respective systems was noted for U–5 at.% Zr–5 at.% Nb, U–10 at.% Mo–10 at.% Zr, and U–15 at.% Mo–15 at.% Nb.

Delta-Phase Alloys

The effects of fabrication and heat-treatment variables on the structure of a U–3.96 Si alloy were studied in Canada[12] using optical microscopy, quantitative metallography, and hardness determinations. It was shown that an optimum temperature exists below the peritectoid temperature where the maximum amount of transformation to U_3Si occurs in a given period of time. The time required to fully transform an as-cast alloy at this optimum temperature is affected by the size of the primary U_3Si_2 dendrites. With a U_3Si_2 particle size of $<12\ \mu$, complete transformation can be achieved in 4 hr.

Corrosion tests in 300°C water were performed for uranium silicide.[13] Proper heat-treatment of U–3.9 Si gives a U_3Si specimen that corrodes at less than 2 mg/(cm^2)(hr) in 300°C water. This is an order of magnitude lower than the maximum corrosion rate tolerable in a water-cooled reactor. U_3Si in a defected, unbonded Zircaloy-2 sheath showed only a slow uniform sheath expansion in 300°C water. All tests were done under isothermal conditions in an ex-pile loop. (J. M. Fackelmann)

Plutonium

Plutonium Metal and Alloys

The investigation of the solubility of selected elements in liquid plutonium and liquid-plutonium alloys is continuing at Los Alamos Scientific Laboratory. The solubility[14] of titanium in liquid plutonium increases with temperature from 1.1 wt.% at 700°C to 10.6 wt.% at 1000°C. At 700 and 750°C the data fit the equation

$$\log N_{Ti} = 1.90 - 5.03 \times 10^3\ T^{-1}$$

where N_{Ti} is the mole fraction of titanium in solution at temperature T in degrees Kelvin. Above the peritectic temperature of 770°C, the data fit the equation

$$\log N_{Ti} = 0.74 - 1.49 \times 10^3\ T^{-1}$$

The solubility[14] of manganese in liquid plutonium increases from 9.3 wt.% at 850°C to 21.0 wt.% at 1000°C. The data fit the equation

$$\log N_{Mn} = 1.52 - 2.27 \times 10^3\ T^{-1}$$

where N_{Mn} is the mole fraction of manganese in solution.

The solubility[15] of niobium in Ga–Pu alloys containing 0 to 10 at.% gallium has been measured over the temperature range of 700 to 1000°C. The solubility decreased as the gallium concentration increased.

For example, at 850°C the solubility decreased from 2.05 at.% niobium in liquid plutonium to 1.75 at.% niobium in a 9.6 at.% gallium alloy. The solubility data fit the equation

$$\log \delta_{Nb}^{Pu+Ga} = N_{Pu} \log \delta_{Nb}^{Pu} + N_{Ga} \log \delta_{Nb}^{Ga}$$

where the δ's are the activity coefficients of niobium in the alloy (Pu + Ga), in liquid plutonium, and in liquid gallium, and the N_{Pu} and N_{Ga} are the atomic fractions of plutonium and gallium in the alloy of interest.

The diffusion behavior of delta plutonium stabilized with aluminum has been studied by electron-microprobe analysis by Los Alamos investigators.[16] Interdiffusion coefficients were measured on face-centered cubic low-aluminum (3.0 and 9.1 at.%) plutonium-alloy couples annealed between 350 and 517°C. Concentration–penetration data fitted by a least-squares technique yielded the Arrhenius relation

$$D = 2.25 \times 10^{-4} \exp(-25{,}500/RT) \text{ cm}^2/\text{sec}$$

where D is the interdiffusion coefficient at the absolute temperature, T.

The phase equilibria of the binary systems Pu–Pr, Pu–Nd, and Pu–Sm have been investigated by Ellinger and coworkers[17] by thermal, micrographic, and X-ray diffraction methods. The maximum solubility of each of these rare-earth metals in both delta and epsilon plutonium was found to be about 2 at.%. No significant solubility was detected in the alpha, beta, gamma, or delta-prime plutonium allotropes. Phase diagrams of these Pu–rare-earth binary systems are shown in Figs. I-6 to I-8.

The plutonium-rich region of the Pu–Hf binary system was also studied in the composition range 0–10

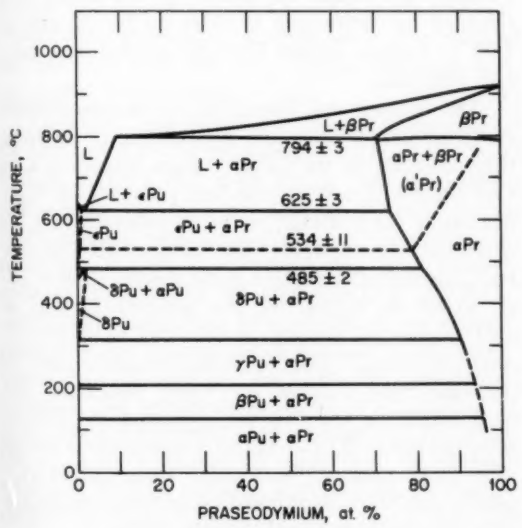

Fig. I-6 The Pu–Pr phase diagram.[17] The field labeled alpha-prime praseodymium simply denotes a region where the cubic form predominates.

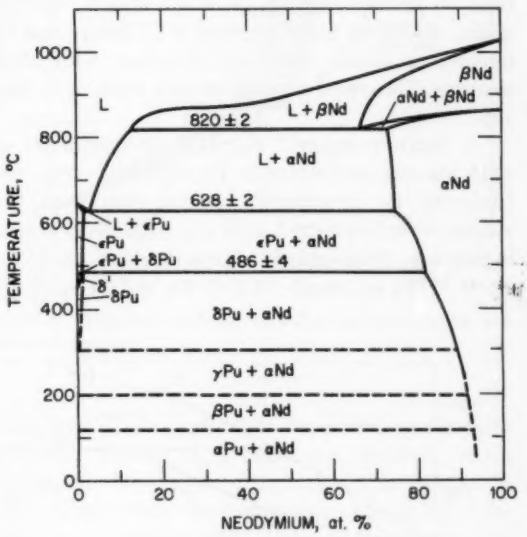

Fig. I-7 The Pu–Nd phase diagram.[17]

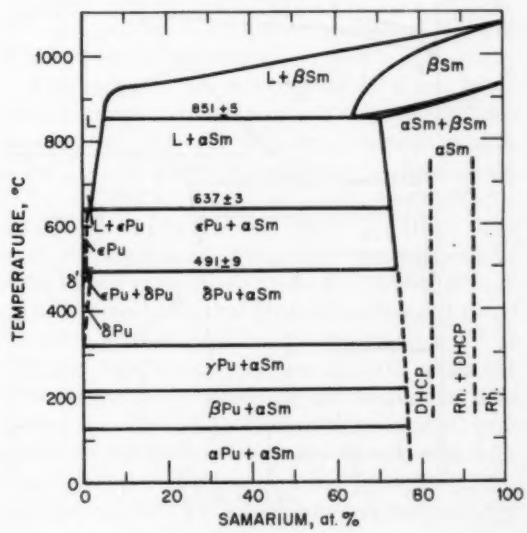

Fig. I-8 The Pu–Sm phase diagram.[17]

at.% hafnium.[18] The maximum solubilities of hafnium in delta and epsilon plutonium were found to be about 7 at.%, in delta-prime plutonium about 1 at.%, and in beta and gamma plutonium less than 0.5 at.%. Both the delta and beta phases can be retained to room temperature in a metastable condition. The phase diagram of this system is shown in Fig. I-9.

Los Alamos has compiled a report,[19] mainly in the form of constitutional diagrams and crystal structure tables, describing phase relations in 75 binary and 17 ternary, or higher, alloys of plutonium with other elements. The report summarizes data available to July 1967.

A Euratom report[20] describes the fabrication of 2115 Masurca fuel elements. The metal-alloy fuel was fabricated by centrifugally casting rods from the vacuum-induction-melted alloy and machining the rods to final size. The rods were of two compositions: 25 Pu (8.4% ^{240}Pu enriched)–74 U–1 Fe, and 24 Pu (3.8% ^{240}Pu enriched)–75 U–1 Fe. The rods were encapsulated in 304L stainless-steel cladding. (D. F. Askey)

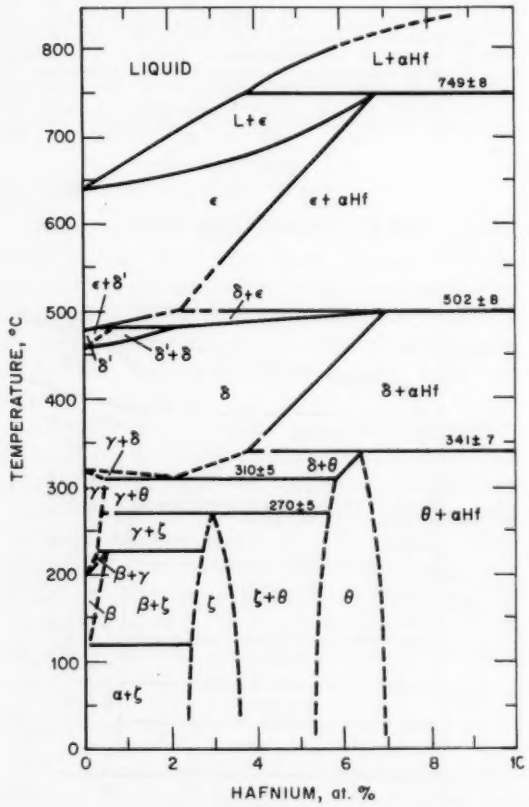

Fig. I-9 The Pu–Hf phase diagram from 0 to 10 at.% hafnium.[17]

Plutonium Compounds

Workers at Argonne National Laboratory[21] prepared Pu–O compositions with O/Pu ratios of 0.29, 0.38, 0.57, 0.85, and 0.99 by arc melting. They concluded that a wide liquid-miscibility gap does exist in the Pu–O system at temperatures near 2500°C. The monotectic temperature in the Pu–Pu_2O_3 region was indicated to be between 1778 and 1863°C.

Rocky Flats Division of Dow Chemical Co.[22] examined the outgassing characteristics of PuO_2 that had been exposed to air. Plutonia exhibited gettering toward water vapor, carbon dioxide, and nitric oxide. Approximately 95% of the adsorbed gases could be removed by vacuum heating at 700°C.

Kruger and Savage[23] measured the heat content of PuO_2 in the temperature range from 192 to 1400°K with an isothermal drop calorimeter. They derived molar thermodynamic properties for the temperature range from 25 to 1800°K.

Battelle–Northwest[24] presented irradiation results for bulk PuO_2 and Pu_2O_3 for burnups in the range from 9 to 55 at.%. Plastic flow of the oxide was reported to be rather extensive, even at the low surface temperature of the fuel, 350°C.

Argonne[25] has fabricated UO_2–15 PuO_2 by hot pressing. A density of 94.8% of theoretical was obtained by compacting at 5100 psi for 30 min at 1500°C. Carbon pickup from the graphite dies averaged 500 ppm.

The Babcock and Wilcox Co.[26] has demonstrated on a laboratory scale the preparation of spherical UO_2–20 PuO_2 by the sol-gel process. Spheres of sizes <44 μ and 420 to 590 μ have been produced for Vipac fabrication. Oak Ridge National Laboratory[27] has developed a process for pelletizing sol-gel UO_2–20 PuO_2 material. Compaction of the powder (O/M = 2.3) at 30,000 to 40,000 psi and sintering in CO_2 at 1450°C gave final densities of 84 to 88% of theoretical. Ayer and Osuna[28] describe a miniature jaw crusher for preparing feed material for Vipac fuel rods. The performance of the unit was evaluated by crushing impacted pieces of UO_2–PuO_2. A typical batch was 60 wt.% 10/18 mesh, 26 wt.% 20/50 mesh, and 14 wt.% smaller than 50 mesh. Material losses during grinding of 860-g batches amounted to 0.2 to 0.5 wt.%.

Battelle–Northwest[29,30a] has measured the thermal conductivity of UO_2–25 PuO_2 as a function of stoichiometry in the O/M range from 2.00 to 1.92.

Calculations indicate that the defect thermal resistance of hypostoichiometric oxides arises from phonon scattering from the lattice strain surrounding oxygen vacancies and Pu^{3+} ions, both of which are larger than the host lattice site which they occupy. General Electric Company[31] reports the lattice parameters for UO_2–25 PuO_2 over an O/M range from 1.999 to 1.923. The material was multiphased, with tentative identification as $(U,Pu)O_{1.6}$, $(U,Pu)O_{1.5}$, and $(U,Pu)O_{2-x}$. The thermal expansion of $(U,Pu)O_{1.999}$ was given for the temperature range from 20 to 1650°C.

Compatibility results for UO_2–20 PuO_2 (O/M = 1.97) in contact with six vanadium alloys were reported by Argonne.[21] All alloys showed an increase in hardness after heat-treatment at 800°C for 1000 hr.

Irradiation performance characteristics for mixed-oxide fuels were reported by numerous investigators. Chalk River[32,33] studied the effect of O/M ratio upon the gas-release behavior for UO_2–0.5 to 1.17 PuO_2. The gas release with material of O/M = 2.04 was higher by an order of magnitude than the value obtained with material of O/M = 1.99. Battelle–Northwest[34] reviewed the Plutonium Recycle Test Reactor trials with UO_2 and UO_2–PuO_2. Gas-release and rupture experiments are described. General Electric presented irradiation results[35,36] for UO_2–20 to 25 PuO_2 up to 128,000 Mwd/metric ton. Swelling rates, microstructural details, and fission-product distribution have been determined. The fuel-pin swelling as a function of burnup in a fast flux is shown in Fig. I-10. Argonne showed the microstructural details and center melting evidence for UO_2–20 PuO_2 Vipac fuel that had operated at 17 to 21 kw/ft.

Karlsruhe[37] has studied the effect of stoichiometry for UO_2–20 PuO_2 as irradiated in the Dounreay Fast Reactor. After 0.96% atom burnup, the microstructural results indicated an increase in size for the fission-product metallic inclusions as the O/M ratio decreased. Battelle–Northwest[38] has also reported microstructural details for irradiated UO_2–25 PuO_2 over an O/M range from 1.94 to 2.00. A fine acicular precipitate was observed which increased in concentration as the O/M decreased and as the fuel temperature increased. The precipitate appeared to be enriched in plutonium and depleted in oxygen relative to the initial MO_{2-x}. Also, a survey-type paper[39] on the thermal properties, swelling behavior, and compatibility characteristics of ceramic fuels for fast-reactor application has been presented by Battelle–Northwest.

Irradiated PuO_2–ThO_2 fuel material has been studied by the Canadians[40] and Battelle–Northwest.[41] At Chalk River the thermal conductivity of ThO_2–1.10 to 2.72 PuO_2 was measured during irradiation. The integrated thermal conductivity of the ThO_2–PuO_2 fuels was higher than that of UO_2, the difference increasing with increasing temperature and reaching about 25% at 1650°C. At Battelle–Northwest, sinterability, melting point, and lattice parameters were established for in-reactor evaluation. Irradiation results for burnups to 3×10^{20} fissions/cm^3 and maximum rod-power generations of over 1000 watts/cm are presented.

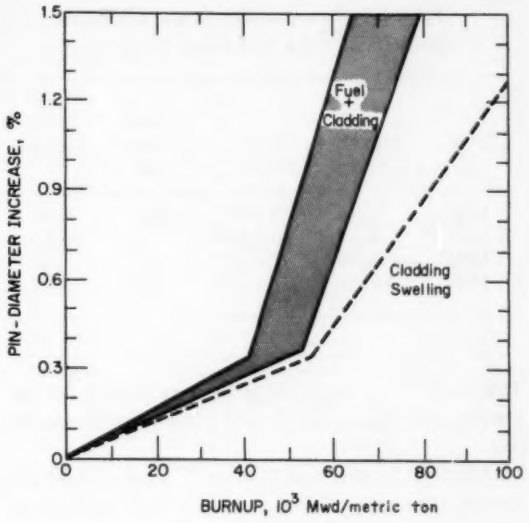

Fig. I-10 Projected diametral increases for mixed-oxide fuel pins and cladding.[37]

Los Alamos[42] has reviewed the U–C and Pu–C systems; compounds, properties, and thermodynamic functions are presented. Differential thermal analysis of $PuC_{2.1}$ indicated[43] the transition temperature for Pu_2C_3 + C/PuC_2 to be 1660 ± 10°C and showed a liquid-phase formation at 2232 ± 10°C. The Pu_2C_3/PuC_2 transition temperature was independent of the carbon concentration over the C/Pu range from 1.6 to 8 (atom ratio). The creep properties of UC–20 PuC (95% of theoretical density) were measured[43] at 1300 and 1400°C under stresses of 2000, 4000, and 6000 psi. The test parameters and results are summarized in Table I-1. Compatibility studies were made[43,44] for UC–20 PuC fuel sodium bonded with claddings of 316 stainless steel and V–15 Ti–7.5 Cr. With the stainless steel, no reaction was observed after 4000 hr at 750°C. With the vanadium alloy, one capsule after 1000 hr at 750°C indicated a reaction.

Table I-1 Test Conditions and Minimum Creep Rates[43] for 95% Dense $U_{0.8}Pu_{0.2}C$

Temp., °C	Stress, ksi	Creep rate, hr^{-1}	Total time, hr	Total deformation, %
1300	2	3.39×10^{-5}	164	0.61
1300	4	1.55×10^{-4}	84	3.0
1300	6	5.9×10^{-4}	16	1.76
1400	2	1.76×10^{-3}	27.5	7.03

This reaction was analyzed as interaction with the free uranium and plutonium present in hypostoichiometric fuel.

Harper, Hedger, and Dalton,[45] have studied the crystal structure of PuC_2 with a high-temperature diffraction unit. The dicarbide was face-centered cubic with a lattice parameter of 5.70 ± 0.01 A at 1710°C. Bender[46] described a metallographic technique that can distinguish between the metallic, dicarbide, and sesquicarbide phases and precipitates of plutonium silicide in sintered U–Pu carbide fuels. Argonne reports[11b] vapor-pressure studies in the Pu–C system. In the Pu_2C_3 + C and Pu_2C_3 + PuC_2 regions and for temperature ranges from 1365 to 1750°C and 1750 to 2026°C, respectively, only Pu(gas) was detected in the vapor phase.

Westinghouse Electric Corporation[47] has investigated the variables for the preparation of hypostoichiometric to hyperstoichiometric U–Pu carbide fuel. The variables included initial carbon content, milling time, binder type, pressing pressure, and firing conditions. Analysis indicated that: (1) initial carbon contents of 4.45 and 4.70 wt.% are required to yield stoichiometric and hyperstoichiometric pellets, respectively, (2) milling times should be 6 hr to achieve density control, and (3) maximum pressing pressures of 20 tsi are sufficient to yield desired densities. Preliminary neutron-radiograph results are given for (U,Pu)C after burnups of 37,189 and 45,472 Mwd/ton in the General Electric Testing Reactor.

The compatibility of UC–15 to 25 PuC, with or without additions of molybdenum, in contact with 316L stainless steel has been investigated by the French.[48] Studies were performed for 1000 hr at 750°C and 500 hr at 950 to 980°C. The addition of molybdenum (10 at.%) to (U,Pu)C improved the compatibility behavior. Precipitates of $(Cr,Fe)_{23}C_6$ were observed in both cases, but the quantities were far lower with U–Pu–C–Mo fuel.

United Nuclear Corp.[49] has reviewed the irradiation performance characteristics for UC-PuC fuels. Irradiation results for burnups in the range from 14,000 to 114,000 Mwd/ton are given. The volumetric swelling rate as measured on high-density pellet fuel was reported as 1.8% per 10,000 Mwd/ton in both thermal and fast reactors up to 114,000 Mwd/ton and 30,000 Mwd/ton, respectively.

Battelle–Columbus[50] reports compatibility and irradiation results for UN–20 PuN. With hypostoichiometric (U,Pu)N in contact with Incoloy 800 for 10,000 hr at 700°C, a fine precipitate was observed to a depth of 180 μ in the Incoloy. Irradiation results are presented for burnups in the range from 39,700 to 64,400 Mwd/ton. Fuel swelling was in the range from 3.1 to 9.9%, and the fission gas released ranged from 0.09 to 1.55% of that generated. Battelle–Northwest[30b] measured the melting behavior of UN–PuN as a function of composition (0, 25, 50, 75, and 100% PuN) and nitrogen pressure (1 to 50 atm).

(M. D. Houston)

Thorium and Its Alloys

The low-melting eutectic in the Th–Fe system was found to be the cause of the hot-short condition that contributed to cracking during fusion welding of thorium. Investigators at Livermore[51] noted that greater than 600 ppm iron in thorium causes severe hot-short cracking. Molybdenum alloying additions improve the weldability of thorium, presumably by combining with the iron to form a higher melting compound.

Diffusion of carbon, nitrogen, and oxygen in beta thorium was studied over the temperature range 1440 to 1715°C by workers at the Ames Laboratory.[52] The diffusion coefficients are given by:

$$D = 0.022 \exp(-27{,}000/RT) \text{ for carbon}$$

$$D = 0.0032 \exp(-17{,}000/RT) \text{ for nitrogen}$$

$$D = 0.0013 \exp(-11{,}000/RT) \text{ for oxygen}$$

Total impurity content for the thorium used was 400 ppm. The interstitial elements were added to high-purity starting material, which was then joined to uncontaminated thorium to form a diffusion couple under high-purity helium. Diffusion times up to 90 min were employed for this study. (R. L. Martin)

Uranium and Thorium Oxides

Properties and Behavior

Investigators at General Electric[53] measured the thermal conductivity of sintered stoichiometric UO_2 in an argon atmosphere. Their results, shown in Fig. I-11, can be expressed by the empirical relation

$$k = 0.0130 + [T(0.4848 - 0.4465D)]^{-1} \text{ watt/(cm)(°C)}$$

for temperatures (T) between 800 and 2000°C and fractional densities (D) between 0.82 and 0.95 times theoretical.

Feith[54] studied the thermal conductivity of powdered ThO_2 having 75% of theoretical density in different atmospheres. The thermal conductivity varied only slightly, if at all, when 1 atm helium, nitrogen, helium plus 52 vol. % nitrogen, or argon was introduced into the powder matrix. However, when the pore volume was evacuated, considerably lower conductivity values were observed. With any of the above gases present, the following thermal-conductivity values (to within about ±10%) were observed:

Temp., °C	Thermal conductivity, watts/(m)(°C)
400	1.25
1000	1.05
1200	1.5

In vacuum the thermal conductivity was about 0.5 watt/(m)(°C) in the temperature range from 400 to 750°C.

The enthalpy of UO_2, as measured at Argonne[25] at temperatures above and below the melting point of UO_2, is shown in Fig. I-12. A value of approximately 18 kcal/mole was observed for the heat of fusion of UO_2.

Sung[55] measured the saturation solubility and diffusivity for helium in $UO_{2.015}$ over a pressure range from 700 to 1300 psi at temperatures from 1200 to 1500°C. The saturation solubility was found to increase with increasing pressure and temperature. The heat of solution for helium in UO_2 was approximately 30 kcal/mole, as compared with a calculated helium strain energy of 5 kcal/mole. The diffusion of helium in UO_2 could be described by the relation $D = D_0$ exp $(-Q/RT)$, where the activation energy Q was found to be 12.7 kcal/mole. This low activation energy was thought to result because helium diffusion was unhampered by defect clustering. Increasing pressure increased the diffusivity by a greater factor than the pressure ratio. The experimental curves of helium concentration as a function of time followed the classical diffusion equations for spherical particles quite well.

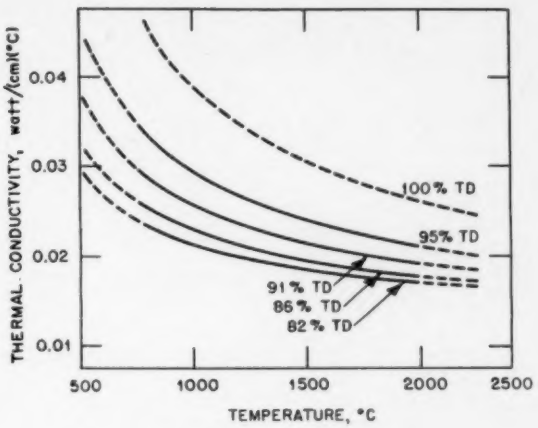

Fig. I-11 Thermal-conductivity curves[53] for UO_2.

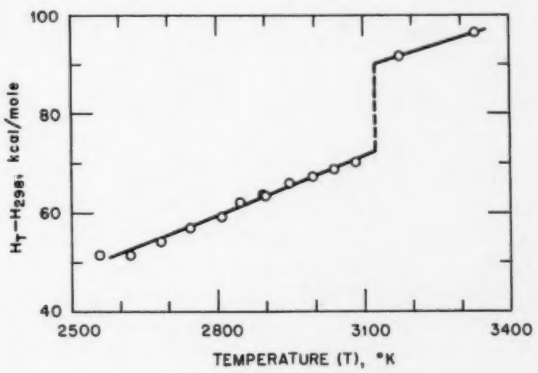

Fig. I-12 Enthalpy[25] of UO_2.

Benz[56] at Los Alamos has investigated Th–ThO_2 phase equilibria using thermal-analysis, X-ray, and microscopic techniques, with the results shown in Fig. I-13. The following conclusions were reached concerning the phase boundaries. The oxygen solubility in solid thorium metal is less than three atoms per thousand. The solid–solid transition of thorium

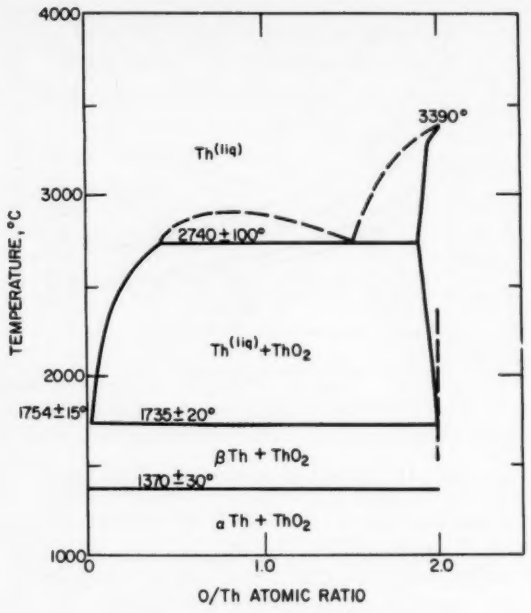

Fig. I-13 The Th–ThO_2 phase diagram.[56]

saturated with ThO_2 occurs at 1370 ± 30°C. A Th–ThO_2 eutectic occurs at 1735 ± 20°C with an O/Th atomic ratio of 0.016 ± 0.005. A monotectic occurs at 2740 ± 100°C with the thorium-rich and the oxygen-rich liquid O/Th atomic ratios of 0.40 and 1.5 ± 0.2, respectively. The thorium-rich ThO_2 solidus varies from an O/Th atomic ratio of 1.985 ± 0.01 at the eutectic to 1.87 ± 0.04 at the monotectic and to 1.997 ± 0.01 at the melting point. (R. H. Barnes)

Fabrication

Oak Ridge investigators[57] are studying the densification behavior of UO_2 powders prepared by the reaction of UF_6 with hydrogen and oxygen in a flame reactor. The true particle size of as-prepared powder is typically less than 0.04 μ. Pellets from as-prepared powders have not generally achieved high densities on sintering, and cracking has been a problem, apparently as a result of the high residual fluorine content. Defluorination of the powders at 1000°C in wet hydrogen for 20 hr reduced the fluorine content to 50 ppm or less. Pellets prepared from this powder exhibited a high degree of structural integrity, but densities of only 92% of theoretical could be achieved.

An arc fusion process has been developed[58] to convert UO_3 to reactor-grade UO_2 having an O/U ratio of 2.00 to 2.05, a particle density >95% of theoretical, and <100 ppm carbon. UO_3 is fed to a carbon-arc furnace having internally insulated walls, which maintain the temperature of the entire charge above the decomposition temperature of UO_3 and eliminate diffusion of oxygen from UO_3 at the walls to the product near the center. The UO_3 powder is continuously added to the furnace by a screw feeder as fusion occurs. Both melting and cooling are done under a flowing blanket of argon. (T. R. Wright)

Carbide and Nitride Fuels

A critical review of the constitution and thermodynamics of the U–C and Pu–C systems[42] has been prepared by Storms at Los Alamos. This is discussed earlier in more detail in the subsection "Plutonium Compounds."

In France, Lorenzelli[59] has examined the U–Pu–C–N system at 1600°C. The UC in the three-phase region of graphite–UC_2–UC was found to contain 22 at. % nitrogen [in good agreement with the findings of Henry et al., as discussed in *Reactor Materials*, **12**(2): 81 (Summer 1969)]. The UC in the three-phase region of U_2C_3–UC_2–UC was found to contain 12 at. % nitrogen, which contrasts strongly with Henry's finding of only 2 at. % nitrogen in this univariant phase at 1700°C. The PuC in the three-phase region of graphite–Pu_2C_3–PuC was found to contain 75 at. % nitrogen.

According to the Japanese,[60] UO_2 apparently dissolves large quantities of UN at 1700°C to form a new phase that separates on cooling into UO_2 and UN containing dissolved oxygen. It is not clear whether the high-temperature phase is a solid solution based on one of the terminal phases or whether it has a new crystal structure.

The UC–stainless-steel compatibility results of Gorle et al. [*Reactor Materials*, **12**(1): 10 (Spring 1969)] have been confirmed at Battelle–Columbus by Fackelmann et al.[61] Studies of the U–C–V system show that at 1500°C UC reacts with vanadium to form V_2C plus a liquid based on uranium metal.

The reactions of UN with various oxides have been examined by the Germans under vacuum conditions at 1100°C; a few have been examined at higher temperatures.[62] The UN did not react with ThO_2 at 1100°C, but reactions were observed with Al_2O_3, BeO, MgO, CeO_2, ZrO_2, TiO_2, and SiO_2. In most cases UO_2 was

one of the reaction products; but the heats of formation of stable intermetallics such as UBe_{13}, and of stable nitrides such as ZrN, play an important role in some of the reactions.

The self-diffusion of ^{233}U in UN has been determined by Reimann and Lundy[63] over the temperature range from 1100 to 1830°C. For a low nitrogen activity, the results from 1100 to 1600°C fit the equation $D = 3.24 \times 10^{-7} \exp(-60{,}000/RT)$. For a high nitrogen activity, the results from 1420 to 1830°C fit the equation $D = 7.54 \times 10^{-2} \exp(-105{,}000/RT)$. These equations give diffusion coefficients of about 10^{-16} cm²/sec at 1100 or 1200°C and of about 10^{-13} cm²/sec at 1700°C. It is indicated that preliminary diffusion-rate data on uranium in UO_2 obtained by the same technique are 2 or 3 orders of magnitude lower than data previously reported for UO_2.

Gautsch[64] has attempted to redissolve krypton in UC under the influence of a neutron flux. His experiments show that large quantities of krypton are adsorbed on the surface of the UC, and the postulated effect of radiation could not be detected under this overriding background. However, desorption experiments showed that some of the adsorbed krypton had dissolved in the UC either during irradiation or during subsequent heat-treatment and was released upon heating, with activation energies between 62 and 85 kcal/mole.

Battelle–Columbus reports[61] that the solubility of xenon in UC is about 4×10^{-13} atom fraction at 1600°C and about 3×10^{-12} atom fraction at 1700°C. Using these solubility data and a model of gas release from UC which interprets the initial rapid release of gas as the breakdown of a metastable solution into a two-phase mixture of UC and gas bubbles, the diffusion rates of xenon in UC were calculated and found to be about 10 times the rates of self-diffusion of uranium in UC, as shown in Fig. I-14.

Table I-2 shows that the swelling and gas-release characteristics of UN, UO_2, and UC under similar

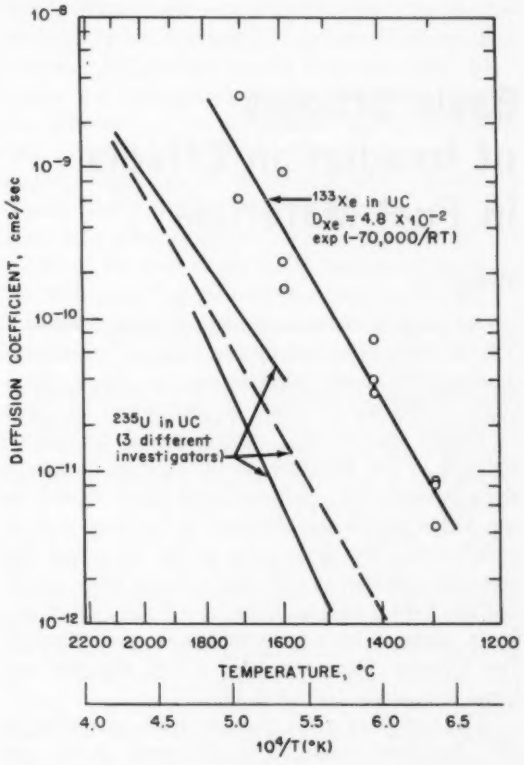

Fig. I-14 Diffusion coefficients[61] for UC.

Table I-2 Comparison of Swelling and Gas-Release Data for UN, UO_2, and UC Irradiated in the HT–BRR-Series Capsules[61]

Fuel	Burnup, 10^{20} fissions/cm³	Average surface temp., °C	Volume increase,* %	Saturation of swelling	Gas release, %	Probable method of gas release
UN	2.4	1670	24	Yes	>97	Rapid migration out of grains and escape through interconnected cores
UO_2	1.9	1700/1470†	20	Yes	79	Sweeping of lenticular voids; some cracking
UC	2.0	1675	34	No	42	Cracking between bubbles

*Volume increase in terms of external dimensions only; swelling into internal voids or axial holes is not included in this number.

†The last three irradiation cycles were at a lower temperature because of the introduction of an extra containment on the capsule.

conditions are basically different. It is suggested[61] that the relatively low vapor pressure of UC compared with those of UN and UO_2, along with its high ductility, may be responsible in part for its lower gas release and greater swelling. A tensile creep specimen of UC elongated 37% in 800 hr at 1400°C and 5000 psi.

(W. Chubb)

Basic Studies of Irradiation Effects in Fuel Materials

Metals

An analysis of fission damage in alpha uranium at 4°K has been presented by the French.[65] Specimens irradiated to several burnups were examined. A coherent model was proposed for fission-particle effects to explain micrographic results and all information gathered in the literature about radiation damage in alpha uranium. The number of point defects created by one initial fission was determined for pure and annealed metal. The importance of the self-anneal that occurs immediately in each displacement spike, as well as that of the anneal resulting from a new fission in a region damaged by a previous fission, was estimated. The focusing distance in the [1 0 0] direction was found to be about 1000 A at 4°K.

The growth of alpha uranium under irradiation at 25°C has been measured by Weinberg, Dural, and Conte[66] as a function of burnup (B) for very low doses. An attempt was made to describe the growth in terms of the customary growth coefficient (G) defined through the relation

$$\ln \frac{l}{l_0} = GB$$

where l is the length along the [0 1 0] direction and l_0 is the initial (zero burnup) length. At low burnups this relation becomes

$$\frac{\Delta l}{l_0} \approx GB$$

For low burnups, $G \approx 45{,}000$. However, it was found to depend strongly on B, indicating that G must be reevaluated if the relation is to be used for higher burnups.

Postirradiation studies at Battelle–Northwest[67] of a Th–1 U (95% ^{235}U) specimen irradiated in NaK at 785 ± 10°C to 0.19 at.% burnup at 50 psi have revealed a very sound structure with little or no porosity. This excellent behavior was attributed to the high melting point of the thorium matrix and the fact that all the uranium was in solution in the thorium at the irradiation temperature.

Ceramics

A critical survey of fission damage in solid nuclear fuels (mainly UO_2) has been conducted at Knolls Atomic Power Laboratory.[68] Part I of this survey, consisting of two chapters, is meant to provide a foundation for analyzing the very complex problems of in-pile behavior of fuels, for example, the in-pile creep of UO_2. Chapter 1 traces the fate of two fission fragments from the instant of fission to their coming to rest in the lattice of the solid. The cumulative effects of a very large number of fissions are considered in Chapter 2. The diffusion of the noble gases krypton and xenon and their isotopes is considered in detail. Part II of this survey will discuss fuel performance and design.

The dynamic re-solution of small gas bubbles in UO_2 has been discussed by the British,[69] for conditions when the dissolved gas both can and cannot diffuse back into the bubbles. In accord with experimental observations, the model predicts that the bubble nucleation density is virtually independent of both the irradiation temperature and the fission rate. Further, the model enables the fraction of gas in dynamic solution and the fraction of gas contained within bubbles to be calculated for different irradiation temperatures.

An interpretation of the trails observed to be left behind migrating bubbles in oxide fuels has been given by Rosenbaum.[70] The bubbles are filled with a gas that has higher solubility in the matrix near a bubble than in the matrix far from a bubble. When a bubble moves rapidly, it leaves a trail of matrix material that is supersaturated with respect to the gas atoms. This model, although not the only conceivable explanation for the bubble trails, is plausible and does fit the observations.

Work on the simulation of fission-fragment damage in U_3Si is currently in progress at Chalk River[71] using bombardments with 2-Mev argon ions. The integrated ion doses have been around 10^{15} to 10^{17} ions/cm^2. An X-ray diffraction study of the bombarded specimens has shown that an almost amorphous surface

layer of thickness corresponding to the ion range was formed in all cases, so that only a few very broad diffraction peaks could be detected. Isochronal (1 hr) annealing studies are in progress; the annealing characteristics are more typical of a recrystallization process or a phase transformation than of the usual mode of recovery of radiation damage, in which defects are progressively annihilated by diffusion to sinks.

The effect of ion-bombardment temperature on the subsequent release of xenon from various materials (some oxides and halides) during postirradiation annealing has been studied by Matzke and MacEwan.[72] For materials resistant to radiation damage, increasing the bombardment temperature had little effect if the temperature was still low enough to avoid appreciable diffusion of the free gas atoms ($T \leq 0.4\, T_{\text{melting}}$). An effect was observed with bombardment doses high enough to cause trapping of xenon, if the bombardment temperature was above that required for migration of the free gas but below that required for escape of the temporarily trapped gas. The retained gas in such samples will be primarily trapped gas, whereas a similar sample bombarded to the same dose at room temperature will contain both free and trapped xenon. A third effect was noted with MgO, which is subject to gross structural damage during irradiation. Samples bombarded at room temperature to an appreciable dose exhibited a large release of gas at low temperature coincident with the annealing of the damage, and samples bombarded to the same dose above the annealing temperature for damage exhibited normal diffusional release.

The effect of power changes on fission-product gas release from UO_2 fuel has been investigated by Soulhier and Notley.[73] The ratio of gas-release rate to gas-generation rate is normally lower at low power than at high power levels. However, it was found that 16 days of high-power operation following a prolonged low-power irradiation resulted in the same percentage release of fission-product gases as that from UO_2 fuel irradiated only at the high power level. On the other hand, the fractional release rate of fission-product gas during a prolonged low-power cycle was not increased by previous irradiation at higher power. These experiments demonstrate the important effects that temporary power (and therefore temperature) increases can have on gas release and suggest a reason for some of the large scatter customarily seen when comparing results of fission-product-gas release from different tests on the basis of time-averaged power outputs. Gas release for a fuel that has a varying power output throughout its lifetime can best be estimated by calculating the release at a maximum power, for the burnup to that time, and adding the incremental quantities released during further periods of operation at lower power. The effect of power excursions of shorter duration than 16 days has not been investigated.

The achievement of high fuel burnup is an essential condition for the economy of fast reactors. In this light a working fuel-element bundle from the Soviet BR-5 reactor was investigated by Kazachkovskii, Votinov, and Lebedev.[74] The fuel-element bundle contained PuO_2 fuel that had attained 6.1% burnup, having been located in the core of the reactor over a period of 5 years (the integrated flux was 2.42×10^{22} neutrons/cm^2). The maximum cladding temperature was 580°C. At the start of the run, the calculated temperature at the center of the fuel-element core was 1400°C. A detailed analysis of the irradiation behavior of the fuel-element bundle was conducted.

Solid-fission-product behavior in U–Pu oxide fuel irradiated in a fast-neutron flux has been investigated by O'Boyle, Brown, and Sanecki.[75] A UO_2–20 PuO_2 fuel pin irradiated in a fast-neutron flux to a burnup of 5.6×10^{20} fissions/cm^3 was examined by electron-microprobe analysis. Two separate types of solid-fission-product inclusions were identified: (1) white metallic inclusions, located in both the equiaxed- and columnar-grain regions, that contained Mo, Tc, Ru, Rh, and Pd; and (2) a gray phase, located in the equiaxed-grain region, that contained strontium, barium, and cerium. The concentrations of molybdenum, technetium, and ruthenium, measured in 42 white metallic inclusions in the columnar-grain region, were found to vary with radial location. The observed partition of solid fission products between the oxide matrix and the inclusions is in agreement with predictions based on the free energy of formation of the fission-product oxides and the oxygen balance between that liberated by the fission process and that required to form stable fission-product oxides. Measurements of the radial distribution of uranium and plutonium confirmed the migration of plutonium up the temperature gradient.

(A. J. Markworth)

References

1. L. G. Wexlin, Elevated-Temperature Mechanical Properties of Uranium with Various Processing Histories, USAEC Report NLCO-1009, National Lead Company of Ohio, December 1968.
2. D. F. Fischer and J. G. Schnizlein, The Ignition of

Irradiated Uranium, *J. Nucl. Mater.*, **28**(1): 124-128 (October 1968).

3. M. V. Speight, Mechanism of Cavity Growth During Thermal Cycling, *J. Inst. Metals*, **96**: 265-267 (September 1968).
4. R. C. Lobb, Density Changes in Uranium Thermally Cycled Between 400 and 600°C, *J. Inst. Metals*, **96**: 262-265 (September 1968).
5. G. Gedorov and Y. Smirnov, Heat Capacity of the Alloy System Uranium–Zirconium, *At. Energ. (USSR)*, **25**(1): 54-56 (1968).
6. L. Wexlin and E. L. Schaich, Microstructures of As-Cast Uranium-Base Dilute Alloys, USAEC Report NLCO-1022, National Lead Company of Ohio, February 1969.
7. J. Truchly and J. Novak, A Study of Morphology and Dispersion of Precipitates in Low Alloy Uranium–Aluminum and Uranium–Silicon Alloys, *Kovove Mater.*, **5**: 135-149 (1967).
8. M. Foure, J. Lauque, M. Colombie, and J. Decours, Influence of Boron on Alpha Crystallization of Uranium Alloys, French Report CEA-R-3498, July 1968.
9. J. R. Kench and J. Chamberlain, Effects of Surface Oxidation upon the Tensile Creep Behavior of α Uranium, *J. Nucl. Mater.*, **28**: 61-72 (October 1968).
10. G. Beghi, Gamma Phase Uranium–Molybdenum Fuel Alloys, Report EUR-4053.*e*, Nuclear Research Center, Ispra, Italy, May 22, 1968.
11. *Physical Chemistry of Alloys and Refractory Compounds of Thorium and Uranium*, Izd-vo "Nauka," Moscow, 1968.
    a. V. B. Kishinevskiy, Resistance Against Creep at 500 and 600°C of Heterogeneous U–Zr–Nb, U–Mo–Zr, and U–Nb–Mo Alloys with 5–30 At.% Additions, pp. 71-81.
    b. V. B. Kishinevskiy, Long-Time Hot Hardness at 500 and 600°C of Heterogeneous U–Zr–Nb, U–Mo–Zr, and U–Nb–Mo Alloys with 5–30 At.% Additions, pp. 73-77.
12. B. S. Wyatt, L. C. Berthiaume, and J. L. Conversi, Metallurgical Structures in a High Uranium–Silicon Alloy, Canadian Report AECL-2761, October 1968.
13. W. T. Bourns, Corrosion Testing of Uranium Silicide Fuel Specimens, Canadian Report AECL-2718, September 1968.
14. D. F. Bowersox, The Solubilities of Selected Elements in Liquid Plutonium. XIII. Titanium and Manganese, USAEC Report LA-3995, Los Alamos Scientific Laboratory, Aug. 23, 1968.
15. D. F. Bowersox, The Solubilities of Selected Elements in Liquid Plutonium. XIV. Niobium in Gallium–Plutonium Alloys, USAEC Report LA-4078, Los Alamos Scientific Laboratory, Jan. 8, 1969.
16. R. E. Tate, G. R. Edwards, and E. A. Hakkila, Diffusion in Stabilized Delta Plutonium, 2. Aluminum, *J. Nucl. Mater.*, **29**(2): 154-160 (February 1969).
17. F. H. Ellinger, C. C. Land, and K. A. Johnson, Binary Systems of Plutonium with Praseodymium, Neodymium, and Samarium, *J. Nucl. Mater.*, **29**(2): 178-183 (February 1969).
18. F. H. Ellinger and C. C. Land, The Constitution of Plutonium-Rich Plutonium–Hafnium Alloys, *J. Nucl. Mater.*, **28**(3): 291-296 (December 1968).
19. F. H. Ellinger, W. N. Miner, D. R. O'Boyle, and F. W. Schonfeld, Constitution of Plutonium Alloys, USAEC Report LA-3870, Los Alamos Scientific Laboratory, January 1968.
20. R. Lesser, J. F. Gueugnon, M. Maurice, and J. Vaane, MASURCA Plutonium Fuel Elements Fabrication, Euratom Report EUR-3663.*e*, Karlsruhe, Germany, October 1968.
21. Argonne National Laboratory, Reactor Development Program, Progress Report, November 1968, USAEC Report ANL-7518, Dec. 27, 1968.
22. J. L. Stakebake and M. R. Dringman, Desorption from Plutonium Dioxide, USAEC Report RFP-1248, Dow Chemical Co., Rocky Flats Division, Nov. 21, 1968.
23. O. L. Kruger and H. Savage, Heat Capacity and Thermodynamic Properties of Plutonium Dioxide, *J. Chem. Phys.*, **49**(10): 4540-4544 (Nov. 15, 1968).
24. J. A. Christensen, High Burnup Plutonium Oxide Irradiations, *Trans. Amer. Nucl. Soc.*, **11**(2): 522-523 (November 1968).
25. Argonne National Laboratory, Reactor Development Program, Progress Report, December 1968, USAEC Report ANL-7527, Jan. 29, 1969.
26. E. H. Dewell (Comp.), Gel-Addition Process Chemical Studies, Quarterly Progress Report No. 9, August–October 1968, USAEC Report BAW-3714-9, The Babcock & Wilcox Co., January 1969.
27. P. Patriarca and W. O. Harms (Comps.) and D. J. Rucker (Ed.), Fuels and Materials Development Program, Quarterly Progress Report for Period Ending September 30, 1968, USAEC Report ORNL-4350, Oak Ridge National Laboratory, February 1969.
28. J. E. Ayer and H. Osuna, A Jaw Crusher for Plutonium Ceramics, *Nucl. Appl.*, **5**: 417-423 (December 1968).
29. R. L. Gibby, The Effect of Oxygen Stoichiometry on the Thermal Diffusivity and Conductivity of $U_{0.75}Pu_{0.25}O_{2-x}$, USAEC Report BNWL-927, Battelle–Northwest, January 1969.
30. A. L. Bement, G. J. Dau, E. A. Evans, and R. E. Nightingale, Reactor Fuels and Materials Development Programs for Fuels and Materials Branch of USAEC Division of Reactor Development and Technology, Quarterly Progress Report, July–September 1968, USAEC Report BNWL-919, (*a*) pp. 5.7-5.9, (*b*) pp. 6.1-6.3, Battelle–Northwest, November 1968.
31. General Electric Company, Advanced Products Operation, Sodium-Cooled Reactors, Fast Ceramic Reactor Development Program, Twenty-Eighth Quarterly Report, August–October 1968, USAEC Report GEAP-5700, November 1968.
32. Atomic Energy of Canada Limited, unpublished data.
33. Ibid.
34. M. D. Freshley, T. B. Burley, and S. Goldsmith, Plutonium Recycle Fuel Evaluations at PNL, USAEC Report BNWL-SA-1979, Battelle–Northwest, November 1968.
35. General Electric Company, Advanced Products Operation, Sodium-Cooled Reactors, Fast Ceramic Reactor Development Program, Twenty-Seventh Quarterly Report, May–July 1968, USAEC Report GEAP-5677, August 1968.
36. W. E. Baily, R. C. Nelson, B. F. Rubin, and C. N. Spalaris, Swelling Rates of Mixed-Oxide Fuel and Cladding in Fast Flux, *Trans. Amer. Nucl. Soc.*, **11**(2): 515-516 (November 1968).

37. M. Coquerelle, J. Gabolde, R. Lesser, and G. Samsel, Uranium/Plutonium Oxide Fuel Irradiation Experiments Related to Fast Reactors, *Trans. Amer. Nucl. Soc.*, 11(2): 516 (November 1968).

38. J. A. Christensen, Nonstoichiometry Effects on the Microstructure of Irradiated UO_2–25% PuO_2 Fuels, *Trans. Amer. Nucl. Soc.*, 11(2): 524 (November 1968).

39. S. Goldsmith, R. J. Jackson, and E. T. Weber, Ceramic Fuels for Fast Reactors, in Fast Reactors Systems, Materials and Components, American Nuclear Society Topical Meeting, Cincinnati, Ohio, April 2–4, 1968, USAEC Report CONF-680419-3.

40. A. T. Jeffs, Thermal Conductivity of ThO_2–PuO_2 During Irradiation, *Trans. Amer. Nucl. Soc.*, 11(2): 497-498 (November 1968).

41. M. D. Freshley and H. M. Mattys, Irradiation of $(Th,Pu)O_2$, in *Thorium Fuel Cycle*, Gatlinburg, Tenn., May 3–6, 1966, R. G. Wymer (Coordinator), AEC Symposium Series, No. 12, pp. 463-473, February 1968.

42. E. K. Storms, The Uranium–Carbon and Plutonium–Carbon Systems, USAEC Report LA-DC-9724, Los Alamos Scientific Laboratory, 1968.

43. Los Alamos Scientific Laboratory, Advanced Plutonium Fuels Program, Quarterly Status Report, October 1–December 31, 1968, USAEC Report LA-4114, Mar. 4, 1969.

44. Los Alamos Scientific Laboratory, Advanced Plutonium Fuels Program, Quarterly Status Report, July 1–September 30, 1968, USAEC Report LA-4073, Jan. 9, 1969.

45. E. A. Harper, H. J. Hedger, and J. T. Dalton, High-Temperature Structure of Plutonium Dicarbide, *Nature*, 219: 151 (July 13, 1968).

46. J. H. Bender, Qualitative Metallography of Uranium–Plutonium Mixed Carbide Fuels, *Metallography*, 1(1): 19-24 (September 1968).

47. A. Biancheria and W. R. Jacoby, Uranium–Plutonium Carbide Development, Quarterly Progress Report for the Period Ending September 30, 1968, USAEC Report WARD-3791-27, Westinghouse Electric Corporation, Advanced Reactor Division, October 1968.

48. M. Mouchnino, Compatibility Comparison of (U,Pu)C and U–Pu–C–Mo with Stainless Steel, French Report CEA-CONF-1031, Mar. 18, 1968.

49. M. M. Shapiro, A. A. Strasser, and B. H. Cherry, Utilization of Carbide Fuels in Fast Reactors, *Trans. Amer. Nucl. Soc.*, 11(2): 518-519 (November 1968).

50. D. L. Keller, Progress on Development of Materials and Technology for Advanced Reactors During October–December 1968, USAEC Report BMI-1857, Battelle–Columbus, January 1969.

51. W. J. Marcellin and P. R. Landon, Cause of Cracking in Thorium During Fusion, *Welding J.*, 47: 575*s*-576*s* (December 1968).

52. D. J. Peterson and T. Carnahan, Diffusion of Carbon, Nitrogen, and Oxygen in Beta Thorium, *Trans. Met. Soc. AIME*, 245(2): 213-215 (February 1969).

53. R. R. Asamoto, F. L. Anselin, and A. E. Conti, The Effect of Density on the Thermal Conductivity of Uranium Dioxide, *J. Nucl. Mater.*, 29: 67-81 (1969).

54. A. D. Feith, The Thermal Conductivity of Thoria Powder from 400 to 1200°C in Various Gases at Atmospheric Pressure, in *Thermal Conductivity, Proceedings of the Seventh Conference, Held at the National Bureau of Standards, Gaithersburg, Maryland, November 13–16, 1967*, National Bureau of Standards Special Publication 302, D. R. Flynn and B. A. Peavy, Jr. (Eds.), pp. 703-709, Superintendent of Documents, U. S. Government Printing Office, Washington, 1968.

55. P. Sung, Equilibrium Solubility and Diffusivity of Helium in Single-Crystal Uranium Dioxide, Thesis, University of Washington, 1967.

56. R. Benz, Thorium–Thorium Dioxide Phase Equilibria, *J. Nucl. Mater.*, 29(1): 43-49 (January 1969).

57. P. Patriarca and W. O. Harms (Comps.) and D. J. Rucker (Ed.), Fuels and Materials Development Program, Quarterly Progress Report for Period Ending June 30, 1968, USAEC Report ORNL-4330, Oak Ridge National Laboratory, November 1968.

58. C. B. Goodlett, Preparation of Reactor-Grade UO_2 from UO_3 by Arc Fusion, USAEC Report DP-1148, Savannah River Laboratory, August 1968.

59. R. Lorenzelli, Contribution to the Study of the System (U,Pu)C,N, French Report CEA-R-3536, May 1968.

60. T. Kubota and S. Takahashi, Microstructural Changes in UN Fuel Elements Under the Influence of a Temperature Gradient, *Nippon Kinzoku Gakkaishi*, 32(7): 665-669 (July 1968).

61. D. L. Keller and W. Chubb, Progress on High-Temperature Fuels Technology During November 1968–January 1969, Quarterly Progress Report, Task 6, USAEC Report BMI-1859, Battelle–Columbus, February 1969.

62. H. Kleykamp, P. Korogiannakis, C. Politis, F. Thuemmler, and H. Wedemeyer, The Reaction of Uranium Mononitride with Metal Oxides, German Report KFK-771, May 1968.

63. D. K. Reimann and T. S. Lundy, Diffusion of U-233 in UN and UO_2 Single Crystals, *J. Metals*, 20(8): 54A (August 1968).

64. O. Gautsch, The Fission Induced Sorption of Krypton in Uranium Carbide, *J. Nucl. Mater.*, 27(3): 310-315 (September 1968).

65. J. Leteurtre, Fission Damage in Alpha Uranium at 4°K, French Report CEA-CONF-1108, 1968.

66. C. Weinberg, J. Dural, and R. R. Conte, Growth of Uranium on Irradiation at 25°C, *Phys. Letters*, 27A(10): 690-691 (Oct. 7, 1968).

67. A. L. Bement, G. J. Dau, E. A. Evans, and R. E. Nightingale, unpublished, Battelle–Northwest, February 1969.

68. R. Bobone, Fission Damage in Solid Fuels, Mainly UO_2: A Critical Survey. Part 1. Atomic and Statistical Damage Mechanisms, USAEC Report KAPL-M-6919, Knolls Atomic Power Laboratory, June 1968.

69. R. S. Nelson, The Stability of Gas Bubbles in an Irradiation Environment, British Report AERE-R-5915, October 1968.

70. H. S. Rosenbaum, Bubble Trails in Oxide Fuels, *J. Nucl. Mater.*, 28(2): 225-227 (November 1968).

71. Atomic Energy of Canada Limited, unpublished data.

72. Hj. Matzke and J. R. MacEwan, The Effect of Bombard-

ment Temperature on the Trapping of Xenon in Some Oxides and Halides, *J. Nucl. Mater.*, **28**(3): 316-323 (December 1968).

73. R. Soulhier and M. J. F. Notley, Effect of Power Changes on Fission-Product Gas Release from UO_2 Fuel, *Nucl. Appl.*, **5**(5): 296-298 (November 1968).
74. O. D. Kazachkovskii, S. N. Votinov, and I. G. Lebedev, Investigation of a Working Fuel Element Bundle from the BR-5 Reactor with Plutonium Dioxide Fuel, *At. Energ. (USSR)*, **24**(2):136-143 (February 1968).
75. D. R. O'Boyle, F. L. Brown, and J. E. Sanecki, Solid Fission Product Behavior in Uranium–Plutonium Oxide Fuel Irradiated in a Fast Neutron Flux, *J. Nucl. Mater.*, **29**(1): 27-42 (January 1969).

Section

II

Reactor Materials

Moderator and Control Materials

Graphite

The role of heteroatoms (oxygen, nitrogen, and sulfur) in the carbonization and graphitization of organic materials, and especially the correlation with the thermal-expansion coefficient of the resulting graphite, has been investigated in the past. In a British study in this subject area,[1] the effects of heteroatoms appeared to fall into two regimes. An apparent discontinuity or possible maximum was noted in the plot of expansion coefficient vs. the square root of the ratio, n, of the sum of heteroatoms to total atoms in the starting raw material used for graphite (carbon) manufacture. In the first regime the expansion coefficient increased with $n^{1/2}$ up to a value of $n^{1/2} \sim 0.25$. In the second regime, above $n^{1/2} = 0.25$, the expansion coefficient dropped abruptly and then remained relatively constant with further increases of $n^{1/2}$. Graphites with a fairly wide range in expansion coefficients were produced from the range of hydrocarbon raw materials, which suggests that structural aspects other than heteroatoms have a major influence on expansion characteristics.

The British have summarized[2] irradiation data for five isotropic graphites on dimensional changes; creep; changes in thermal conductivity, thermal expansion, Young's modulus, and strength; and the effect of radiolytic oxidation in CO_2 coolant on these properties. The data from any of the five graphites indicate that linear dimensional changes induced by fast-neutron irradiation in the moderator of a reactor of the Dungeness B type would be less than 3.5% during the lifetime of the reactor. The creep behavior of the isotropic graphites during irradiation assures that internal stresses resulting from the radiation-induced dimensional changes will be small. At neutron-damage doses slightly higher than the expected peak in a moderator of the Dungeness B type, a marked temperature dependence was observed in dimensional changes in the temperature range 370 to 550°C; and a rapid growth was observed at those high doses in all the materials investigated at temperatures of 500 to 550°C.

Since both the bulk properties and irradiation response of polycrystalline carbon (graphite) are dependent on the degree of orientation of the carbon crystallites, determination of the degree of orientation is a vital characterization. In the present state of the art, the standard Bacon Anisotropy Factor (BAF) method, using commercially available scanning-type densitometers to read X-ray diffraction photographs, requires about 1½ hr per sample. Gulf General Atomic researchers[3] have developed an experimental densitometer that permits calculation of BAF values by a different measuring approach. Their results show that bridging the X-ray diffraction ring with a slit to measure the integrated density, and then scanning around the ring, reduces the time for orientation characterization by a factor of 30 compared with present methods.

The nature of damage to pyrolytic carbon by fission recoils at temperatures between 1200 and 1300°C was studied[4] in two experiments. In the first, a high-density (2.12 g/cm^3) isotropic carbon with a BAF of 1.3 and an apparent crystallite height L_c of 170 A was irradiated at 1200°C. In the second experiment, two types of carbon were irradiated at 1300°C. One carbon type had a density of 1.55 g/cm^3, an L_c of 40 A, and a BAF of 1.0. The other carbon had a density of 2.05 g/cm^3, an L_c of 140 A, and a BAF of 1.3. The microstructure of the latter carbon was granular. In the 1200°C experiment the samples were exposed to 2.7×10^{21} neutrons/cm^2 ($E > 0.18$ Mev) and 3.0×10^{18} fission recoils/cm^2. The 1300°C experiment exposed samples to a fast-neutron dose of 6×10^{20} neutrons/cm^2 ($E > 0.18$ Mev) and 2×10^{18} fission recoils/cm^2. The results of the study show that high-density isotropic or granular carbons are much more susceptible to damage by fission recoils than low-density isotropic carbon. In all cases the damage is so severe that it is clear that, when carbon is used as a coating for nuclear fuel particles, it must be shielded from the fission recoils.

The optical anisotropy exhibited by pyrocarbon has often been used as a convenient indication of

relative crystallite anisotropy. A Gulf General Atomic study[5] indicates that a reliable correlation between the optical and crystal anisotropy is not possible unless coating parameters and pyrocarbon properties affecting polishing and pertinent structural characteristics are identified. This work was performed to determine the influence of surface texture on the optical anisotropy of pyrocarbon and graphite. The results provide proof that a substantial portion of the observed optical anisotropy was caused by reflection of plain or elliptically polarized light from furrowed surfaces. Optical tests and electron microscopy showed that the groove axes are preferentially oriented parallel to the basal plane in graphite and the deposition plane in pyrocarbon. It was further suggested that the structure or polishing characteristics of pyrocarbon vary in such a manner that for nearly isotropic pyrocarbons the grooves are either more random, hemispherical, or absent, and thus no optical anisotropy is observed.

(M. C. Brockway)

Beryllium Metal and Alloys

Physical Metallurgy

A study of gas behavior during annealing of irradiated hot-pressed beryllium was conducted by the Russians.[7] Beryllium samples were given fast-neutron fluences of 2.0×10^{21} and 1.5×10^{22} neutrons/cm^2. Isothermal annealing of the samples was then carried out at 400, 500, and 600°C. The maximum rate of gas evolution was noted at approximately 500°C, at which temperature recrystallization normally begins in beryllium metal. The gas concentrates at the grain pores and migrates out. For beryllium given a fast-neutron fluence of 2.0×10^{21} neutrons/cm^2, the sample density decreased from 1.80 at 600°C to 1.19 g/cm^3 at 900°C owing to swelling of the beryllium. The sample given a fast-neutron fluence of 1.5×10^{22} neutrons/cm^2 showed no change in density on annealing up to 1000°C. The beryllium lattice has only a limited capacity for holding helium gas. At $T = 600$ to 700°C and above, the helium is evolved as fast as it forms.

A book on the physical metallurgy of beryllium has been published by the Soviets.[8] The book is intended for scientists, engineers, and technicians working in the field of the metallurgy of reactor materials and also may be useful to graduate students and students specializing in metal physics, metal science, and physical chemistry. It contains 75 tables, 129 figures, and a bibliography. Of the 813 references, only 140 are Soviet.

The book reviews methods used to produce high-purity beryllium, primarily such methods as vacuum melting, zone melting, and refining. Various physical properties of beryllium metal (electrical, thermal, magnetic, elastic, internal friction, diffusion, etc.), its crystal structure, thermodynamic characteristics, and solidification features are described. A great deal of attention is devoted to the influence of such factors as composition, structure, and heat-treatment on physical properties. Data on the effect of neutron and alpha irradiation upon the structure, physical properties, and mechanical properties of beryllium metal are given. New methods in beryllium research, such as electron microscopy, electron diffraction, high-temperature roentgenography, and spot microbeam analysis of specimens, are described.

Mechanical Metallurgy

Dimensional Stability

The dimensional stability and microplastic properties of beryllium vacuum-hot-pressed Brush Grade I-400 and hot isostatically pressed (HIP) Berylco Grade Super PEL have been studied at Battelle–Columbus.[9,10] The microyield strength (MYS, defined as the 10^{-6} in./in. offset yield) and microcreep properties of these two materials were determined. The MYS for I-400 and Super PEL ranged from 5 to 9 ksi and from 45 to 49 ksi, respectively. The significant scatter in the MYS results among specimens (as much as 40% deviation for I-400) implies that the results were influenced by such factors as inhomogeneity, surface variations, or processing variation. Room-temperature microcreep tests at fractions of the MYS demonstrated that detectable and significant (in terms of μin. tolerances) creep occurs even at these low levels of stress. Moderate thermal cycling between 100 and −50°C also was observed to cause I-400 length changes of about 10 μin./in. after 20 cycles. Residual stresses induced by machining Super PEL beryllium were measured at about 20 ksi and were limited to about 0.002 in. of the specimen surface. Stress levels of this magnitude in I-400 would cause dimensional instability. The MYS and microcreep studies indicated that these properties are sensitive to structural and process factors as yet undefined. Residual stresses, some of which have probably not yet been identified, appeared

to cause most dimensional instability and also to affect the micro–mechanical-property determinations.

Deformation Mechanisms

The *c*-axis compression behavior of beryllium single crystals under a high hydrostatic pressure was studied at Franklin Institute.[11] Three beryllium purity levels were tested at various hydrostatic pressures. These were ingot SR material, 2-pass zone-leveled SR-grade material, and 12-pass zone-refined SR-grade material. Nonbasal slip, primarily on pyramidal, $\{1\,1\,\bar{2}\,2\}$ planes, was observed by both surface trace analysis and transmission-electron microscopy to occur as a result of constraints introduced by testing under a hydrostatic pressure. The higher purity material showed evidence of nonbasal slip at the lower hydrostatic pressure of about 12 kbars, as compared with the 19 kbars necessary to produce nonbasal slip in the lower purity zone-leveled material. However, the amount of pyramidal slip occurring before crystal failure was generally quite small. The hydrostatic-pressure medium appeared to suppress fracture, so that stresses high enough for complex shear processes are tolerated without fracture. Prismatic loops with a $(c+a)$ Burgers vector were observed in the lower purity materials tested. These loops appear to be related to surface extrusions observed on many of the lower purity specimens, but not on the higher purity materials. Nonbasal $(c+a)$ dislocations operating on $\{1\,1\,\bar{2}\,2\}$ planes with a $\frac{1}{2}\langle 1\,1\,\bar{2}\,3\rangle$ Burgers vector were observed by transmission-electron microscopy to dissociate to c and a dislocations, presumably on unloading or after failure. This implies that prestraining to produce mobile $(c+a)$-type dislocations in unalloyed beryllium will not be successful.

The plastic deformation at 4.2 to 300°K of high-purity beryllium monocrystals has been studied by the Soviets.[12] The temperature dependence of the critical resolved shear stress for basal-plane slip under pressure at 4.2 to 300°K and plastic deformation of high-purity beryllium were investigated. Characteristics of the basal slip, strengthening, thickness of the slip layers, and the slip along the pyramid plane were analyzed.

Cleavage-Crack Energy

The energies to initiate and propagate cleavage cracks in beryllium are being determined at Martin Marietta.[13] The double-cantilever cleavage technique was used to determine the energy, ϕ_p, to propagate basal cleavage cracks in beryllium monocrystals. The variations of ϕ_p with temperature, plastic blunting of the crack tip, and purity were studied. In Pechiney SR flake beryllium at temperatures from 77 to 200°K, ϕ_p was found to be 2200 ± 200 ergs/cm^2; the value increased with further temperature increases because of plastic relaxation effects. The crack tip is blunted by the formation of twins or by prismatic and basal slip ahead of the crack tip. The low-temperature value quoted for ϕ_p is in good agreement with Gilman's theoretical estimate of the surface energy of the basal plane in beryllium. A higher value of ϕ_p was obtained for high-purity distilled beryllium and was associated with the increased ductility in this higher purity material. The fracture-initiation energy for basal cleavage, ϕ_I, was estimated from 300°K tensile fracture data to be about 2040 ergs/cm^2. Thus ϕ_I was found to be approximately equal to ϕ_p, as would be expected, since crack initiation and propagation occur in the same plane.

Powder Metallurgy

High-Purity Sheet

The effects of improved purity in wrought polycrystalline beryllium sheet have been investigated at Brush Beryllium Co.[14] The purpose of the program was to study the effect of using zone-refined crystals as a raw material for polycrystalline powder-metallurgy sheet on the mechanical properties of the final product. Three levels of purity of electrolytic-grade beryllium were utilized as the feed material in a casting and zone-refining process. The resulting six-pass zone-refined materials contained approximate total impurity levels (excluding oxygen) as follows: (1) 750 ppm from the most impure starting material, which was a lower purity casting of Brush electrolytic grade, (2) 550 ppm from Brush electrolytic-grade beryllium flake, and (3) 440 ppm from the Pechiney electrolytic SR-grade beryllium flake.

The major experimental problem encountered in this program was one of avoiding contamination, particularly during the powdering processes. Vacuum hot pressing of the powders derived from the zone-refined input materials was performed at 1050°C and 1725 psi for periods of between 45 and 200 min. The low-oxygen powder had very good vacuum-hot-pressing characteristics as exhibited by its ability to be pressed to high densities below the normal pressing temperature of 1075°C. Also, a higher rate of grain growth was

observed during pressing as compared with that of normal powder under the same conditions. The microstructure of the low-oxide pressings was very clean, in contrast to that of commercial material, and was similar to the microstructure of beryllium castings.

The vacuum-hot-pressed beryllium was encased in a mild-steel picture frame, utilizing an Al_2O_3–MgO parting compound. For reductions of 12 : 1 the rolling pack was cross rolled at 790°C, taking 5% reduction per pass until a total reduction of about 3.5 : 1 was achieved. The beryllium sheet was then recanned for finish rolling at 760°C. Materials rolled to only a 6 : 1 reduction employed the finish-rolling sequence only.

The resulting grain size of the −200 mesh high-purity powder-metallurgy sheet ranged from 13 to 16 μ for a reduction of 12 : 1, and from 8.8 to 17 μ for a reduction of 6 : 1. The subsieve input powder resulted in sheet with a grain size of 8.5 to 10.3 μ after rolling reductions of 12 : 1, and of 7.4 to 10.8 μ after reductions of 6 : 1. Metallography revealed that grain-size reduction occurred during initial rolling, but that no further grain-size reduction occurred after a rolling reduction of 4 : 1 was achieved. However, preferred orientation of the basal planes was more pronounced after a 12 : 1 reduction ratio than after a 6 : 1 reduction. Heat-treatment of the sheet for 40 hr at either 780 or 850°C resulted in grain growth and a duplex grain size characterized by islands of large grains heterogeneously dispersed in a matrix of fine grains. The preferred orientation was also decreased by the heat-treatment.

The tensile strength of these high-purity sheets was approximately 80 to 90% of that of commercial sheet, but they had higher tensile elongations when compared with material having equivalent grain size and reduction ratio. The yield strengths decreased with improved purity and increased grain size. The elongations appeared to increase with increases in purity and reduction of grain size.

The major variable observed to affect bend ductility was that of grain orientation incurred by the degree of hot working during rolling. Lowering of the reduction ratio from 12 : 1 to 6 : 1 effected a 20 to 100% increase in the bend ductility, with little or no change in the mechanical properties in the plane of the sheet. The bend ductility of these high-purity materials tended to increase slightly with increasing purity when other variables were held constant, but the beneficial effects of the purification were not outstanding. The influence on bend ductility of the degree of texture was found to be the most significant variable observed.

(F. T. Zurey)

Solid Hydrides

Zirconium Hydride

Using a low-temperature torsion pendulum, Povolo and Bisogni measured the internal friction in polycrystalline wires of zirconium hydride.[15] High-purity zirconium was hydrided to compositions up to 56 at.% hydrogen for the measurements. The internal-friction spectrum showed peaks at −129, −43, and +18°C. From the variation of the peak at −129°C with hydrogen concentration, the low value of the frequency factor, and the similarities between this peak and that obtained in cold-worked high-purity zirconium, it was concluded that the peak is produced by the interaction between dislocations and hydrogen atoms in the hexagonal phase of zirconium. The values obtained for the activation energy, width, and frequency factor of the −43°C peak, together with changes in the peak height with hydrogen concentration in the sample, showed that this peak is produced by the stress-induced migration of the hydrogen atoms within the gamma-hydride phase. The third peak, occurring at 18°C, increases in height with hydrogen concentration, aging time, and deformation. In addition, the values of the frequency factor and the activation energy agree closely with those reported for the peak observed in alloys in the homogeneity range of the hydride. These facts led to the conclusion that the 18°C peak must be associated with the stress-induced motion of the twins in the gamma hydride.

Hydrided Zircaloys

An extensive review of the literature on hydride precipitates in Zircaloys has been made by Ells.[16] After studying 50 references on the subject, he reached the following conclusions:

1. The single-crystal habit plane for hydrides is $\{1\,0\,\bar{1}\,0\}$ in pure zirconium and $\{1\,0\,\bar{1}\,7\}$ in Zircaloy-2 and Zircaloy-4. The factors leading to this difference are not understood.

2. After either hot or cold working of the Zircaloys, the hydrides precipitate in planes whose normal coincides with the direction of the compressive strain. Although the working also establishes a crystallographic texture, the hydride orientation in the polycrystalline material appears to be dependent more on the direction of working than on the texture.

3. When a zirconium alloy is cooled under stress, hydrides tend to form with their normals parallel to

the stress direction. This stress orientation in Zircaloy-2, Zircaloy-4, and Zr–2.5 Nb is much more marked if there is a strong component of basal-plane normal which is also parallel to the direction of stress.

4. If it is desired to fabricate zirconium-alloy tubes to operate under internal pressurization and to avoid formation of radial hydrides, then, in the latter stages of production, it is necessary to have a large amount of compressive strain in the radial direction. Cold drawing with small reduction in diameter and shear forming are particularly suitable for favorable hydride orientation, whereas sinking is particularly unsuitable. The tube-reduction process can be arranged to give satisfactory tubes.

The review by Ells included data obtained by Ambler, which has since been published.[17] This investigation was concerned with the grain-boundary crystallographic directions that are the preferred sites for hydride precipitation. Ambler found that in Zircaloy-2 the preferred grain-boundary directions are at 35 to 40° and at 60 to 65° to the basal planes of the adjacent grains.

Hydrogen transport in Zircaloy-2 has been investigated by Wilkins and Wasylyshyn.[18] They proposed that one solution to hydrogen embrittlement in Zircaloy components is to channel the hydrogen into appendages via thermal diffusion to cold sinks, where hydride precipitation would do no harm. The objective of this particular work was to show that a maximum in the temperature gradient would not be a barrier to thermal diffusion of the hydrogen. They found that such a maximum influenced the hydrogen distribution en route to the steady state by producing alpha-plus-delta two-phase regions, one in the vicinity of the temperature minimum and one adjacent to the cold area. However, when the steady state is reached, the two-phase regions disappear, leaving a region of solid delta-phase hydride at the cold end, with hydrogen in solution below the terminal solubility in the remainder of the Zircaloy sample. (H. H. Krause)

Nuclear Poisons

An investigation was conducted at NASA–Lewis[19] to determine the high-temperature mechanical behavior of HfC and, in particular, to find the temperature at which it becomes plastic and how this plasticity occurs. Transverse rupture tests were conducted from room temperature to 4755°F (2625°C) on both single-phase HfC and on dispersion specimens containing 13 vol.% HfB_2 in HfC. The test specimens were prepared by hot pressing to 95 to 97% of theoretical density. Both materials exhibited decreasing strength with increasing temperature to 4000°F (1207°C), with brittle behavior and transgranular fractures. Above 4000°F the single-phase HfC increased in strength with increasing temperature, exhibited some plasticity, and fractured intergranularly. The two-phase material also showed plastic behavior and intergranular fractures above 4000°F; however, its strength decreased rapidly as the temperature exceeded 4000°F. These results are summarized in Fig. II-1.

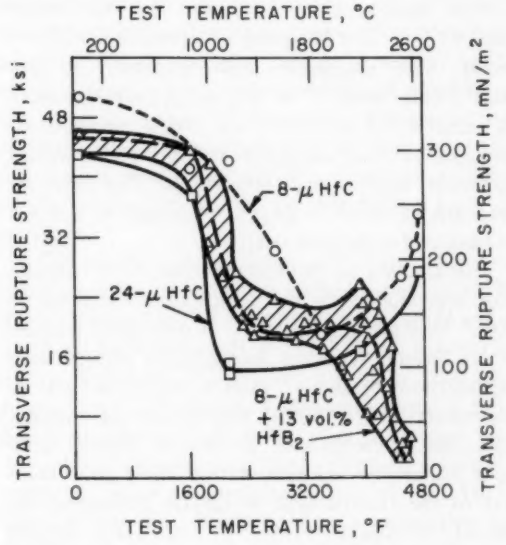

Fig. II-1 Effect of temperature on transverse rupture strength[19] of HfC and HfC + 13 vol.% HfB_2.

Metallographic evidence suggested that the plasticity observed in both materials is a result of grain-boundary sliding. It was concluded that this sliding acts as a stress-relieving mechanism in the single-phase material and prevents premature failure. The HfB_2 present at the grain boundaries of the two-phase material renders the grain-boundary sliding ineffective as a strengthening mechanism and leads to a rapid loss of strength at temperatures where grain-boundary sliding occurs.

Two fuel elements containing 0.05 wt.% B_4C in 6% enriched UO_2 were irradiated in the Saxton reactor to burnups of ~1000 and 5000 Mwd/metric ton at peak heat ratings of 17.2 and 17.8 kw/ft, respectively, by

workers at Combustion Engineering.[20] The elements were fabricated by vibratory compaction to 88 ± 2% of theoretical density, with local boron concentrations maintained within ±20% of the nominal loadings. Postirradiation examination revealed no significant dimensional changes in either element and no axial boron redistribution of any consequence. The boron was found to migrate radially outward in both elements. A correlation was established between the boron redistribution and the thermal gradient during irradiation, but the redistribution of the boron did not appear to be a function of burnup. The effects of this observation on core physics were analyzed and found to be minimal.

Four neutron-absorber elements that had experienced 14.1 to 26.7 Mw-years of service in the SM-1A reactor were examined nondestructively at Oak Ridge[21] and found to be structurally and dimensionally suitable for additional use. These elements are composed of four composite absorber plates welded together to form a square hollow tube. The plates are composed of 37 wt.% Eu_2O_3 dispersed in stainless steel and clad in stainless steel.

The reaction of gadolinium oxide with hafnium oxide was studied in the temperature range up to 1900°C by Russian scientists.[22] A cubic solid solution of the fluorite type was found to be formed with concentrations of above 7 mole % Gd_2O_3 in HfO_2 at temperatures above 1500°C. Gadolinium and hafnium hydroxides, coprecipitated at 250 to 1700°C, contained metastable low-temperature cubic solid solutions of the fluorite type at Gd_2O_3 concentrations from 2 to 33 mole %. (D. E. Lozier)

References

1. V. Y. Labaton, M. J. Jenkins, and T. Kilner, The Role of Hetero-Atoms in Carbonisation, British TRG-Report-1738, July 5, 1968.
2. P. T. Nettley, J. E. Brocklehurst, W. K. Martin, and J. H. W. Simmons, Irradiation Experience with Isotropic Graphite, British TRG-Report-1762, Sept. 11, 1968.
3. C. L. Chang and K. F. Powell, A Densitometer for Determining Preferred Orientation of Pyrolytic Carbon, USAEC Report GA-8514, Gulf General Atomic Incorporated, Feb. 7, 1969.
4. J. C. Bokros, Fission-Recoil Damage to Pyrolytic Carbon, USAEC Report GA-9054, Gulf General Atomic Incorporated, Dec. 10, 1968.
5. O. M. Stansfield, Optical Anisotropy in Pyrolytic Carbon and Graphite, USAEC Report GA-9125, Gulf General Atomic Incorporated, Jan. 1, 1969.
6. Reference deleted.
7. T. M. Guseva and E. F. Davydov, Study of Gas Behavior During Annealing of Irradiated Hot-Pressed Beryllium, *At. Energ. (USSR)*, **25**: 152-153 (August 1968).
8. I. I. Papipoy and G. F. Tikhinskii, *Fizicheskoe Metallovedenie Berilliya (Physical Science of Beryllium Metal)*, 451 pp., Atomizdat, Moscow, 1968.
9. A. G. Imgram, M. E. Hoskins, J. E. Sovik, R. E. Maringer, and F. C. Holden, Study of Microplastic Properties and Dimensional Stability of Materials, Report AFML-TR-67-232, Part II, Battelle–Columbus, August 1968.
10. R. E. Maringer, M. M. Cho, and F. C. Holden, Stability of Structural Materials for Space-Craft Application, Final Report, Battelle–Columbus, Apr. 16, 1968.
11. V. Damiano, J. Hanafee, and G. London, Investigation of the Deformation of Beryllium Single Crystals Under High Pressure, Final Report, AFML-TR-68-13(AD-832975), Franklin Institute Research Laboratories, March 1968.
12. I. A. Gindin et al., Plastic Deformation of High-Purity Beryllium Monocrystals at 4.2 to 300°K, *Fiz. Metal. Metalloved.*, **26**: 157-163 (July 1968).
13. R. K. Govila and M. H. Kramdar, Determination of Energies To Initiate and Propagate Cleavage Cracks in Beryllium, RIAS–Martin Marietta Corp., September 1968.
14. J. G. Theodore, B. B. Lympany, and W. M. Beaver, Effects of High Purity in Wrought Polycrystalline Beryllium Sheet, Report AFML-TR-67-338, Brush Beryllium Co., June 1968.
15. F. Povolo and E. A. Bisogni, Internal Friction in Zirconium–Hydrogen Alloys at Low Temperatures, *J. Nucl. Mater.*, **29**(1): 82-102 (January 1969).
16. C. E. Ells, Hydride Precipitates in Zirconium Alloys, *J. Nucl. Mater.*, **28**(2): 129-151 (November 1968).
17. J. F. R. Ambler, Grain-Boundary Hydride Habit in Zircaloy-2, *J. Nucl. Mater.*, **28**(3): 237-245 (December 1968).
18. B. J. S. Wilkins and A. Wasylyshyn, Diffusion of Hydrogen up a Thermal Gradient in Zircaloy-2, *J. Nucl. Mater.*, **29**(2): 235-237 (February 1969).
19. W. A. Sanders and H. B. Probst, High-Temperature Mechanical Properties of Polycrystalline Hafnium Carbide and Hafnium Carbide Containing 13 Volume Percent Hafnium Diboride, Report NASA-TN-D-5008, National Aeronautics and Space Administration, Lewis Research Center, January 1969.
20. S. S. Christopher, J. J. Koziol, and D. E. Mahagin, Irradiation Testing of UO_2 Fuel Elements Containing Burnable Poison Additions, *Nucl. Appl.*, **6**(1): 47-55 (January 1969).
21. A. E. Richt and V. O. Haynes, Inspection of Europium-Bearing Control Rods from the Army SM-1A Station Medium Power Reactor, USAEC Report ORNL-TM-2349, Oak Ridge National Laboratory, January 1969.
22. E. N. Isupova, V. B. Glushkova, and E. K. Keler, Study of the System Gd_2O_3–HfO_2 in the Region Rich in Hafnium Dioxide, *Izv. Akad. Nauk SSSR, Neorg. Mater.*, **4**: 1732-1737 (October 1968).

Section III

Reactor Materials

Cladding and Structural Materials

Corrosion by Aqueous and Gaseous Media

Corrosion of Zirconium Alloys

Experimental data on the effect of fission-fragment, neutron, and gamma radiations on the oxidation of zirconium alloys were reviewed at Chalk River.[1] It is concluded that both fast neutrons and free oxygen or oxidizing radiolytic species must be present simultaneously before irradiation can have an effect on oxidation in high-temperature water. Hydrogen uptake under irradiation appears to be largely independent of the oxidation process in water and steam. Enhanced oxidation under irradiation is explained qualitatively on the basis that only one of the main processes in oxidation (ionic transport) is affected by radiation, and thus control of the oxidation rate switches to the other process (electronic transport).

Studies on the effects of radiation on the aqueous corrosion behavior of Zircaloy-2, Zircaloy-4, Zr–3 Nb–1 Sn, Zr–2.5 Nb, Zr–1.2 Cu–0.28 Fe, and Zr–1.2 Cr–0.08 Fe* are continuing at Battelle–Northwest.[2] Exposure conditions were 174 days in *p*H 10 NH_4OH at 270 to 280°C. Radiation-enhanced corrosion occurred on all alloys at a fluence of 1.7×10^{21} neutrons/cm^2 (>1 Mev), but only on the Zr–Cr–Fe alloy at a fluence of 1×10^{20} neutrons/cm^2 (>1 Mev). Corrosion and hydriding were lowest on the alloys containing niobium. The in-flux hydriding rates followed the general trend of the in-flux corrosion rates. Prefilming in 400°C steam adversely affected the corrosion rates of Zircaloy-2, Zircaloy-4, Zr–Cu–Fe, and Zr–Cr–Fe alloys in the high-flux exposure.

Corrosion of Aluminum Alloys

The results of the second year's work on stress-corrosion-crack initiation and development in thick plates of 2219-T37, 7075-T6, 7079-T6, and 7039-T6 aluminum alloys have been reported by Alcoa.[3] Most of the tests were conducted in $NaCl–AlCl_3$ solutions at *p*H 1. Cracks in 7075-T6, 7079-T6, and 7039-T6 alloys always initiated on "former" grain boundaries perpendicular to the stress and, in many cases, at boundaries between grains having considerably different orientation. Cracks propagated along these same paths, following the straightest possible path perpendicular to the stress. Stress level affected quantity and propagation rate of cracks but had no effect on crack-initiation sites or propagation paths. There were no indications that dislocations, constitutent particles, dispersoid particles, or precipitate particles had any direct effect on crack initiation.

The second annual report on the mechanism of stress corrosion of aluminum alloys has been issued by TYCO laboratories.[4] Experiments were carried out in 1*M* NaCl buffered to *p*H 4.7 at 30°C on commercial alloys 7075 and 2219 and on pure-alloy laboratory heats. Tests on nonstressed specimens revealed grain-boundary attack of Al–4 Cu alloy in tempers both susceptible and nonsusceptible to stress corrosion, and failed to produce intergranular attack in Al–7.5 Zn–2.4 Mg, thus indicating that a preexisting corrodible path is not a prerequisite to cracking. Continuous application of stress was shown to be necessary to produce stress-corrosion cracking in the 2219 alloy. However, preexposure of the unstressed 7075 alloy to the environment shortened the time it took for failure to occur after a stress was applied. This implies that true corrosion has a significant influence on stress corrosion in the 7075 alloy.

Corrosion of Iron-Base Alloys

Steels

The Experimental Boiling Water Reactor (EBWR) pressure vessel has been reexamined[5] following the plutonium recycle program (September 1965 to July 1967). During this time the vessel and cladding accumulated 4830 hr of exposure to water at 489°F (254°C) and a maximum flux of ~3×10^{17} neutrons/

*Unless otherwise specified, compositions are in weight percent.

cm^2 (>1 Mev). No accelerated corrosion was observed on the SA-212B pressure-vessel steel where cracks completely penetrated the 304 stainless-steel cladding. (These cracks had been located in a previous examination conducted in 1964 and 1965.)

The results of a long-term corrosion test in high-temperature water with several alloys have been summarized by Chalk River.[6] Specimens were exposed 677 days to *p*H 10 water (LiOD or ND_3 additions) at 250°C and 20 ft/sec. Corrosion rates are summarized below.

Alloy	Descaled corrosion rate, mg/(dm^2)(day)	Metal release rate, mg/(dm^2)(day)
Carbon steel	0.3	0.2
2¼ Cr–1 Mo	0.2	0.1
Cor-Ten	0.4	0.3
304 stainless steel	<0.1	<0.1
Monel 400	0.7	0.9
Inconel 600	<0.1	<0.1

A new environmental cause of stress-corrosion cracking of mild and low-alloy steels has been described by the Japanese.[7] Transgranular cracking occurred in U-bend specimens with a 1-week exposure to water at 104°F (40°C) in an autoclave that was pressurized with 35-psia CO_2 and 178-psia CO.

Stainless Steels

The hydrogen embrittlement of stainless steel has been studied by Lawrence Radiation Laboratory.[8] Notched and unnotched tensile bars of 304L and 310 stainless steels were fractured in hydrogen or helium at 10,000 psi and ambient temperature. The results indicated that hydrogen embrittlement occurs in an austenitic steel which is unstable with respect to the formation of strain-induced alpha (bcc) and epsilon (hcp) martensite when plastically strained in high-pressure hydrogen. A stable austenitic steel (310) was not embrittled under these same test conditions.

The effect of explosive shocking on the corrosion and stress-corrosion-cracking behavior of 304 and 310 stainless steels has been studied at Du Pont.[9] The pressures of explosive shocking ranged from 90 to 550 kbars. The intergranular corrosion of the two steels in boiling nitric acid and ferric sulfate–sulfuric acid was only mildly affected by explosive shocking of solution-annealed or sensitized material. Stress-corrosion tests of up to 1100 hr in 42% boiling $MgCl_2$ on as-explosively shocked pieces (no external applied stress) revealed that stress-corrosion cracking due to residual stresses occurred above 200 kbars in 304 stainless steel and above 300 kbars in 310 material.

Corrosion of Copper- and Hafnium-Base Alloys

The effect of morpholine additions at high *p*H (9.5 to 9.9) on the corrosion of copper-base feedwater-heater materials has been studied at Chalk River.[6] At temperatures of 50 to 160°C and dissolved oxygen contents of 0.01 to 0.05 ppm, the following corrosion rates were observed after 90 days' exposure:

70/30 cupronickel	<0.1 mg/(dm^2)(day)
90/10 cupronickel	<0.1 to 0.2 mg/(dm^2)(day)
Arsenical admiralty	<0.1 to 0.2 mg/(dm^2)(day)
Low-silicon bronze	0.1 mg/(dm^2)(day)

The above corrosion rates were considered acceptable.

In a program[10] to develop oxidation-resistant hafnium alloys, a number of quaternary and higher alloys based on the Hf–20 to 30 Ta system met the goal of 100 hr of life in air at 2500°F (1370°C). However, most of these alloys oxidized rapidly at 1600°F (870°C), presumably because of the inability of the alloy to heal cracks in the oxide at low temperatures. Alloys in the Hf–Ta–Cr–B–Al system resisted oxidation at both 1600 and 2500°F, the optimum composition being Hf–24.5 Ta–0.66 B–1.2 Cr–0.12 Al. (W. E. Berry)

Corrosion of Refractory Metals

Uncoated Refractory Metals

The oxidation behavior of unalloyed niobium has been studied by the Germans[11] between 400 and 1000°C. The results indicate that, after a parabolic initial stage, oxidation obeys the linear rate law. The latter begins after a breakaway reaction connected with the appearance of Nb_2O_5 nucleation sites on the surface. Oxidation below 800°C at atmospheric pressure shows three regions of different temperature dependence, i.e., 400 to 500, 500 to 600, and 600 to 800°C. These are discussed in terms of microstructure and oxide phases involved.

The Japanese[12] have investigated the oxidation of niobium and Nb–2 to 7 at.% Zr at 485 to 935°C in dry air using thermogravimetric, X-ray diffraction, metallographic, and microhardness measurements. Five structural modifications of the dominant product Nb_2O_5 were identified, and the transition temperature of each

modification was observed to increase with increasing substrate zirconium content. It was confirmed that there is an intimate relation between thermal transformations of Nb_2O_5 and changes in scale morphology. Anomalous weight-gain curves were obtained and explained in terms of cavity formation which reduced the cross-sectional area of ion transport in the Nb_2O_5 scale. The Russians[13] have also investigated films formed on Nb–Zr alloys using X-ray diffraction.

The oxidation of Nb–V, Nb–Zr, and Nb–Zr–V alloys has been measured[14] in air at 500 to 900°C. Addition of 1 to 5 wt.% vanadium slightly improved oxidation resistance, whereas 10 to 20 wt.% vanadium had no beneficial effect. The addition of zirconium or zirconium and vanadium gave similar results.

Adsorption-rate sticking probabilities for oxygen (ratio of absorption rate to corresponding oxygen flux) on niobium and Nb–1 Zr have been studied[15] at temperatures of 885 to 1100°C and oxygen pressures between 10^{-7} and 10^{-5} torr. The absorption rates were derived from the pressure drops, and oxygen fluxes were obtained from constant-pressure measurements. Sticking probabilities between 0.047 and 0.15 were found.

The reaction of CO and carbon-free tantalum foils above 1700°C has been followed using a mass spectrometer and electron beam.[16] Scans made on reaction products formed at 0.1 to 20 x 10^{-7} torr indicated only TaO. The rate of TaO vaporization is first order with respect to CO pressure and has an activation energy of 102 ± 2 kcal/mole. The carbon produced on the tantalum surface diffuses into the foil.

In a field-ion microscope investigation at U. S. Steel,[17] the induction period for oxide formation on tungsten was found to be inversely proportional to the 0.8 power of oxygen pressure and exponentially related to $1/T$, with an activation energy of 21 ± 2 kcal/mole. The particles appear to be irregularly shaped, and their distribution is crystallographically nearly homogeneous. It is proposed that the length of the induction period is determined primarily by the rate of oxygen penetration in the tungsten lattice.

The field-emission microscope has been used[18] to study the influence of foreign gases on the initial oxidation stages of molybdenum at 380 to 755°C and tungsten at 670 to 980°C, at oxygen pressures of 1 x 10^{-7} to 1 x 10^{-5} torr. An increase in incubation time and activation energy for molybdenum oxide formation was found to be associated with an added partial pressure of CO. Emission anisotropy was marked for molybdenum in oxygen and oxygen + CO atmospheres. CO, CO_2, N_2, and CH_4 all affected kinetics and morphologies of tungsten oxidation. Little emission anisotropy for tungsten was found in oxygen, but emission anisotropy tended to increase with the introduction of each foreign gas.

Oxygen adsorption on the (1 0 0) surface of molybdenum single crystals was examined[19] by low-energy electron diffraction between 25 and 850°C. The thermal characteristics and formation kinetics of the four ordered structures found are discussed.

Various studies have been made on aqueous corrosion of refractory metals. The corrosion resistance of unalloyed niobium has been measured in HCl, H_2SO_4, and NaOH solutions.[20] The most aggressive effects were noted in 30% NaOH. The behavior of Nb–Ta alloys in mineral acids and K_2CO_3 solutions has been reported.[21] The anodic behavior of tungsten in KOH was studied potentiostatically, with emphasis on passivation and surface polishing.[22] Dislocation etch pitting was investigated[23] on tungsten single crystals in chloride solutions during anodic polarization.

Coated Refractory Metals

Silicide and aluminide coatings are under study[24] for protection of niobium alloys (D-43, Cb-752, C-129Y, XB-88, and Cb-132M) for hundreds of hours to 2500°F for application in gas-turbine engines and aerospace environments. The coatings were modified with elements such as Ti, Cr, V, and Mo. Vanadium was deposited by an activated vacuum-pack process, whereas molybdenum was deposited by chemical-vapor deposition from $MoCl_5$. The Ti–Al–Si system was promising for low-temperature applications, giving over 500 hr of protection at 1600°F (870°C).

Of the many combinations investigated, the V–CrTi–Si system was most promising. In oxidation-erosion tests this system protected substrates up to 200 hr at 2200°F (1205°C) and 100 hr at 2400°F (1315°C). In oxidation-erosion, ballistic-impact, and slow-thermal-cycle tests, this system was comparable to the Cr–Ti–Si system. Although lifetimes to initiation of coating failure were similar in many tests, propagation and growth of oxidation sites were notably slower in the vanadium-modified coating. Such behavior suggests that a self-healing tendency is the principal advantage of the V–CrTi–Si over the Cr–Ti–Si system.

The British[25] have developed a $NbSi_2$–1 Fe–1 Cr + glaze coating for protection of niobium alloys such as F48 and SU-16 (Nb–11 W–3 Hf–2 Mo–0.08 C). The modified silicide was applied by pack cementation and the glaze by a slurry–sinter process. The best glaze

composition studied was 68.4 SiO_2–19.5 Al_2O_3–2.0 CaO–0.17 MgO–5.0 K_2O–5.0 Na_2O, which improved coating performance by filling microcracks present in the silicide. The coating gave about 100 hr of cyclic-oxidation protection at 2010 to 2370°F (1100 to 1300°C), generally under simulated gas-turbine-engine exhaust products. The oxidation resistance was found to be similar to that of Cr–Ti–Si coatings developed in the United States. Room-temperature tensile and miniature Charpy-impact tests showed that the silicide-glaze coating maintained the ductility of the uncoated alloy even after oxidation or creep exposure in air for 100 hr up to 2280°F (1250°C). The Cr–Ti–Si coating tended to embrittle F48 niobium-impact specimens. The coatings slightly reduced the creep strength of F48 and SU-16 niobium alloys at 2010 to 2280°F.

A niobium alloy that develops its own protective coating upon air exposure has been investigated by Wah Chang.[26] The alloying additions are 28 to 30 Hf, 13 to 16 W, 0 to 4 Ta, 1 to 2 Zr, and 0.07 to 0.33 C. The hafnium provided the oxidation resistance by forming a 0.03- to 0.04-in.-thick coating after 24 hr at 2400°F (1315°C). Inward diffusion of oxygen was nominal within the estimated maximum exposure period for candidate applications in gas-turbine engines. The other additions impart strength and creep resistance. At 1400°F (760°C) the yield and tensile strengths were 80,000 and 100,000 psi, respectively, and the elongation was over 15%.

The oxidation behavior of the following four systems has been evaluated in supersonic airstreams by NASA:[27] Durak B and Vought IX silicide-coated TZM molybdenum, and Cr–Ti–Si- and Cr–$MoSi_2$-coated Cb-752 niobium. Cyclic (8 min) coating life was measured on blunt-nose models at surface temperatures of 2600 to 3000°F (1425 to 1650°C) at air stagnation pressures behind the shock wave of 0.03, 0.1, and 5.5 atm. Except for the Vought coating which gave erratic protection, coating life was under 32 min at the two lower pressures and about 1 hr at 5.5 atm. The uncoated-alloy controls oxidized catastrophically by liquid-phase formation in less than 30 sec at 2900 to 4000°F (1595 to 2205°C), depending on stagnation pressure.

The oxidation of W–Si-coated Ta–10 W has been studied between 1830 and 3090°F (1000 and 1700°C) at an oxygen partial pressure of 150 torrs in helium[28] for times up to 1 hr. The TRW coating was prepared by chemical-vapor-depositing tungsten and vacuum-pack siliciding. The Solar coating (TNV-13) was applied as a 95 W–5 Ti slurry, sintered, pack silicided in argon near 1 atm, and impregnated with glass frit. Oxidation of the TRW-coated sample was logarithmic, with oxidation resistance improving with increasing temperature in the range 1830 to 2730°F (1000 to 1500°C). At 3090°F the coating failed catastrophically. Oxidation of the TNV-13 coating was parabolic between 1830 and 3090°F. Electron-microprobe analyses suggest that the difference can be ascribed to the titanium content of the Solar coating. (B. C. Allen)

Corrosion by Nonaqueous Liquids and Vapors

Corrosion of Iron-, Nickel-, and Cobalt-Base Alloys by Sodium

Typical weight-change data on inserts of three candidate cladding alloys from 5000-hr tests in Brookhaven's sodium thermal-convection loops[29] (velocity ~0.1 ft/sec) are shown in Fig. III-1. Note that in all cases the corrosion rate increases with increasing nickel-plus-chromium content and decreases with time, the cobalt-base alloy S-1 corroding the slowest.

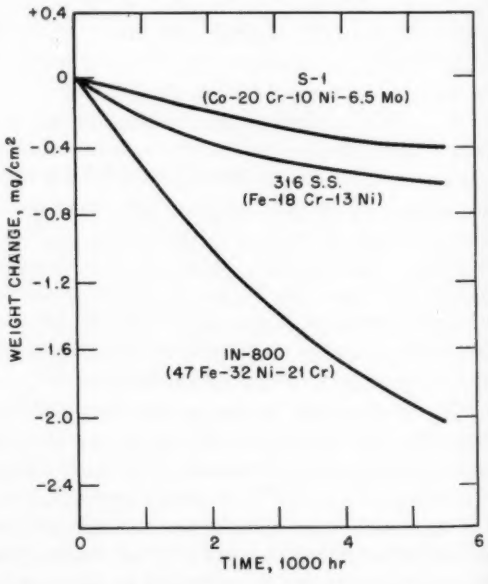

Fig. III-1 Effect of time on corrosion rate of three alloys in 760°C hot-trapped sodium in a 321 stainless-steel thermal-convection loop.[29]

Figure III-2 summarizes some U. S. and U. K. data on the temperature dependence of corrosion of stainless steels by sodium containing different amounts of oxygen. The consistency among investigators is rather good. Note that increasing the oxygen level in the sodium from 4 to 12 ppm increased the corrosion rate of the stainless steels at 710 to 760°C by factors of 3 or 4. The same test on HA-25 (Co–20 Cr–10 Ni–15 W–3 Fe) resulted in a factor of 3 *decrease* in the rate of weight loss. The HA-25 surface was found to be strongly enriched in iron when the sodium contained 12 ppm oxygen but not when it contained 4 ppm oxygen.

Atomics International's continuing stress–rupture program on stainless steels in sodium has yielded further interesting results,[30] including the following:

1. At temperatures of 1000 and 1200°F (540 and 650°C), the second-stage-creep behavior of 10 to 15% cold-worked 304 or 316 stainless steel is the same in a helium environment as in a high-purity static sodium environment.

2. The strain-rate behavior of 10 to 15% cold-worked 304 stainless steel in high-purity static sodium up to 1300°F (700°C) is not affected by copperplating the steel or by saturating the sodium with copper.

3. The stress–rupture life of annealed 304 stainless steel under 1:1 biaxial stress in static sodium seems to be the same as that found for uniaxial stress. However, the elongation at rupture is substantially lower unde biaxial stress (8% vs. 40% under 28,000-psi stress i 1200°F sodium).

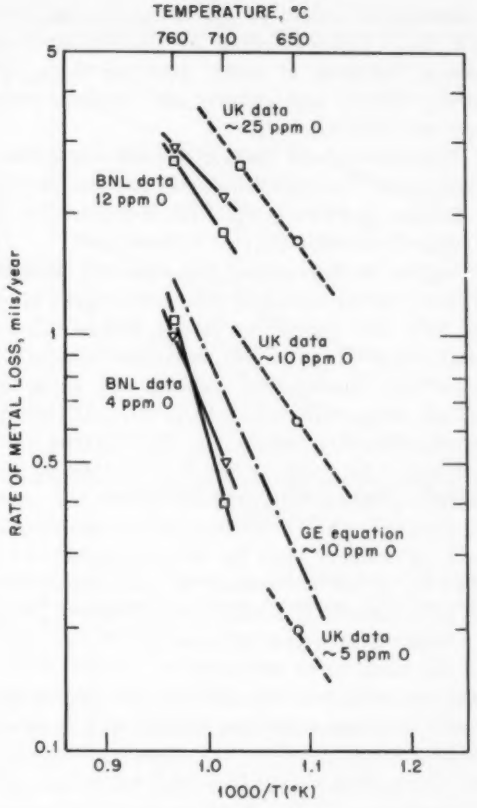

Fig. III-2 Temperature dependence of the corrosion rates of stainless steels with different oxygen contents.[29] □, 321 stainless steel; ▽, 304 stainless steel; ○, many alloys.

As discussed in the previous review, General Electric workers noted that sodium (<10 ppm oxygen, 17 ft/sec) attacks Incoloy 800 about three to four times as fast as it does 316 stainless steel under identical conditions. The researchers caution,[31] however, that the effect of composition on corrosion rate cannot be divorced from sodium velocity, temperature, and oxygen content. For example, since the corrosion rate of austenitic steels is strongly dependent on the oxygen content of the sodium, whereas that of nickel-base alloys is not, it is quite possible for stainless steels to corrode faster than the Incoloy 800 when the oxygen content of the sodium is high.

As part of the program to study what happens when a liquid-metal-cooled fast breeder reactor (LMFBR) sodium-heated steam generator springs a leak, workers at Atomic Power Development Associates[32] directed sodium–water reaction jets on target tubes of 2¼ Croloy, Incoloy 800, and stainless steel and examined their "wastage" patterns. All evidence indicates that the attack results from abrasion and erosion, rather than from corrosion. Also, the stainless steels and Inconel 800 resisted wastage better than did the Croloy.

Surface-tension and wetting studies of sodium in contact with stainless steel and nickel were carried out by the British.[33] Variations in oxygen content of the sodium from 5 ppm to saturation (as high as 80 ppm) had no noticeable effect on surface tension over the temperature range 150 to 265°C. However, increasing the oxygen in the sodium accelerated the wetting of nickel and inhibited the wetting of stainless steel. The investigators attribute this difference to the difference in wettability of the respective complex oxides formed. The reaction product on nickel is thought to have a higher surface energy, a weaker structure, or higher solubility in sodium than the $FeO \cdot 2Na_2O$ film expected on stainless steels. Wetting was found to

be strongly influenced by the surface-cleaning procedure used. Electropolishing of stainless steel and chemical polishing of nickel gave the most rapid wetting, whereas acid cleaning and abrasion, respectively, were least effective.

The results of the Battelle–Columbus sessile-drop wetting tests[34] of high-density UN and stainless steel by sodium are shown in Fig. III-3. It appears that the UN wets more readily than the stainless steel.

Argonne workers suggest that a paste of uranium–ceramic powders in sodium is an economically attractive fluid fuel for a fast reactor breeder blanket. Consideration was given[35] to the compatibility of such pastes with stainless-steel claddings and containers. Markedly hypostoichiometric UO_2, UC, or UN was not deemed promising because the free uranium could react with constituents of the stainless steel to form low-melting eutectics. Hyperstoichiometric UO_2 could lead to excessive Na_2O formation, which aggravates the attack of stainless steel by sodium. Hyperstoichiometric UC would be expected to cause carburization and embrittlement of stainless steel. However, release of nitrogen from hyperstoichiometric UN was considered less likely to be deleterious to stainless steel. A rough test series was run exposing 304 stainless-steel coupons to sodium containing 88 to 93 wt.% of various uranium–ceramic powders in capsules at 1400°F (760°C) for 1000 hr. The UO_2 (O/U = 2.007) and UN (plus some beta U_2N_3) pastes appeared to be compatible with the stainless steel, whereas the hyperstoichiometric UC (5.24 wt.% carbon) paste caused the expected carburization. The UN paste was considered most attractive.

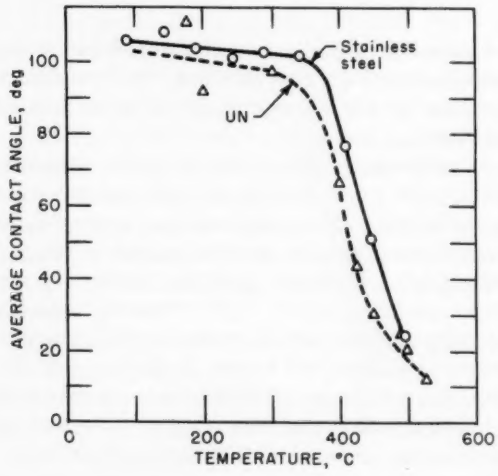

Fig. III-3 Wetting of 304L stainless steel and UN by sodium.[34]

Corrosion of Refractory Metals and Alloys by Sodium

By analyzing vanadium tabs from sodium-filled vanadium capsules with various amounts of Na_2O added, workers at Oak Ridge noted[36] that essentially all the oxygen had transferred from the sodium to the vanadium after 500 hr at 600°C or 100 hr at 800°C. Also, the amount of vanadium found in the sodium was independent of initial oxygen content of the sodium, being about 40 ppm at 600°C and 200 ppm at 800°C. This behavior is in contrast to that of the Nb–Na or Ta–Na system, where metal concentration in the sodium increases sharply with oxygen additions to the sodium and the niobium or tantalum does not getter oxygen from the sodium unless the starting oxide content of the sodium is very high. Another distinction is that the vanadium samples in these capsules showed no evidence of attack, whereas both niobium and tantalum contaminated to the same high oxygen levels (1600 to 1900 ppm) suffer rapid intergranular attack by 600°C sodium.

Brookhaven workers[29] confirmed the observations by Argonne and others that vanadium alloys gain weight very slowly in hot-trapped sodium (<1 ppm oxygen) and lose weight rapidly if the oxygen level is increased. The same effect was observed with Nb–1 Zr alloy specimens. However, TZM (Mo–0.5 Ti–0.08 Zr) specimens were unaffected after 2000 hr in flowing hot-trapped sodium and continued to show no weight change when the oxygen level in the sodium was increased to ~4 ppm.

Several vanadium-base alloys developed by Westinghouse[37] for LMFBR fuel-pin cladding are showing considerably lower corrosion rates than the V–20 Ti alloy in low-oxygen–sodium (<10 ppm) loop experiments. Some representative results are presented in Figs. III-4 and III-5 for Vanstar-7 (V–3.3 Fe–9.1 Cr–1.3 Zr–0.05 C) and Vanstar-9 (V–6.4 Fe–5.3 Nb–1.3 Zr–0.05 C), along with V–20 Ti for comparison. The corrosion kinetics appear to follow the parabolic law $\triangle w2 = K_p t$, where $\triangle w$ is the total weight gain, K_p is a temperature-dependent parabolic rate constant, and t is the exposure time. Room-temperature tensile tests of Vanstar-7 and -9 specimens that had been exposed for 500 hr to 690°C sodium at 5 ft/sec showed increases in strength and marked decreases in ductility as a result of the exposures. When

the tensile tests were run at 800°C, however, the alloys retained considerable ductility.

The corrosion of TIG welds in SNAP-8 tantalum tubing containing 55 to 520 ppm oxygen by eutectic NaK containing about 10 ppm oxygen was investigated by General Electric workers.[38] Specimens were exposed in tantalum capsules for either 100 hr at 1200°F (650°C) or 1000 hr at 1350°F (730°C). Metallography showed no evidence of attack in specimens containing 220 ppm oxygen or less, although all of the 1350°F specimens suffered modest weight losses (presumably because of oxygen gettering by the NaK).

Specimens with 270 ppm oxygen suffered 2 to 4 mils penetration in the heat-affected zone, whereas those with 520 ppm oxygen were much more severely attacked. Of these, curiously, the ones tested at 1200°F for 100 hr were completely penetrated (20 mils), whereas those tested at 1350°F for 1000 hr were attacked to a depth of only about 8 mils.

The phenomenon of reduced corrosion at increased temperatures and exposure times is explained by the researchers as follows. Oxygen in the tantalum can diffuse to the surface and dissolve in the NaK much faster at 1350 than at 1200°F. In fact, at 1350°F, this diffusion and dissolution occur so fast that the oxygen concentration in the tantalum region where corrosion is advancing along grain boundaries and crystallographic planes can be reduced to below the corrosion threshold and thereby retard the penetration into the specimen. This concept is consistent with the observed reductions in oxygen content of all tantalum specimens following exposure to NaK, with the greatest reductions occurring after the 1350°F exposures.

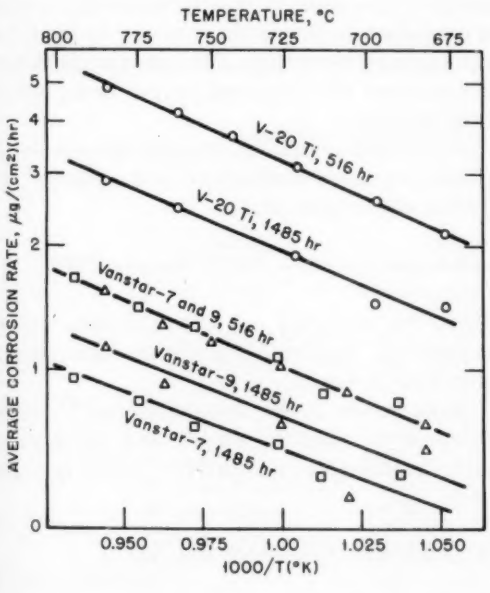

Fig. III-4 Effects of time and temperature on the corrosion rate of vanadium alloys in sodium containing <10 ppm oxygen and flowing at 5 ft/sec (Ref. 37).

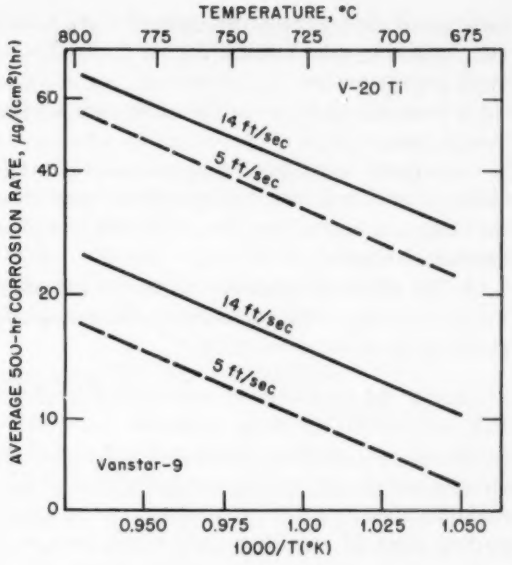

Fig. III-5 Effect of velocity on corrosion rate of two vanadium alloys exposed to sodium containing <10 ppm oxygen (Ref. 37).

The large grain size and long transverse grain boundaries in the fusion zone of high-oxygen specimens account for the deeper corrosive attack noted there, as compared with attack in the heat-affected zone. Corrosion in both the fusion and heat-affected zones of specimens containing 270 ppm oxygen was more severe than in the base metal. Contamination of the TIG atmosphere (helium) with up to 250 ppm of air during welding had no observable effect on the corrosion resistance of the welds to NaK.

The conclusion from this study is that welded and unwelded tantalum in the SNAP-8 boiler will not be attacked by the NaK unless the tantalum contains 270 ppm oxygen or higher—a circumstance that is unlikely to develop accidentally, by virtue of the inaccessibility of the Ta–NaK interface to oxygen.

Reactions of Graphite and B_4C with Sodium

The compatibility of liquid sodium with various types of irradiated and unirradiated graphite was

investigated by Battelle–Northwest[39] by heating encapsulated samples at 1000°F (540°C) for 100 hr. Major conclusions are:

1. Irradiated graphite expands more than unirradiated graphite.

2. Graphite irradiation temperature is a major factor in sodium-graphite compatibility—the lower the irradiation temperature, the greater the growth on exposure to sodium.

3. The degree of graphite crystallinity influences the compatibility with sodium, more anisotropic samples being more severely affected.

During the exposures of unirradiated graphites, TSX and TSGBF graphites expanded from 0.4 to 1.05%, pyrolytic graphite delaminated and cracked, an isotropic sample that had been graphitized at 2825°C cracked, most samples containing carbon black cracked, and CSF graphite suffered a 20% decrease in coefficient of thermal expansion. The growth of CSF graphite in contact with sodium reached saturation in 1½ hr at 400°C, 4 hr at 350°C, 7 hr at 300°C, and >12 hr at 250°C. At 540°C, growth of transverse CSF, TSX, and CSGBF graphites in sodium was complete (0.85 to 1.12%) in <2 hr.

The irradiated samples increased in length by 0.95 to 2.40% upon exposure to 540°C sodium, depending on degree of crystallinity, irradiation temperature, and fast-neutron fluence. A sample of CSF graphite irradiated at 80°C to 2.2×10^{20} neutrons/cm^2 ($E > 0.18$ Mev) expanded to about 2½ times its original length upon exposure to molten sodium at 120°C. Irradiated (2.2 to 3.5×10^{20} neutrons/cm^2 at 300 to 475°C) boronated graphite (7 wt.% boron as B_4C) expanded 5.6 to 8% after 100-hr exposures to 540°C sodium, which is more growth than nonboronated samples suffered—presumably because of the greater damage from the $^{10}B(n,\alpha)^7Li$ reaction.

In similar studies in England,[40] Brocklehurst arrived at the same conclusions. He measured expansions as high as 12% when irradiated graphite was exposed to 600°C sodium and noted that heavily damaged specimens disintegrated upon exposure to sodium. He concluded that the sodium–graphite reaction is strongly dependent on the radiation-induced changes in electronic properties of the graphite, and also noted that smaller quantities of sodium are absorbed by graphite when it is under a compressive stress.

To study the compatibility of B_4C with sodium in stainless-steel systems, workers at Battelle–Northwest[41] are exposing −10 +20-mesh B_4C in sodium-filled capsules. Metallographic examination of B_4C from a 100-hr, 500°C capsule and several 1000-hr capsules showed that particle cracking was common. Sodium penetration appeared to occur along parallel graphite flakes that were present as a minor phase.

Solubility of Materials in Liquid Metals

The solubility of nickel in sodium as measured at Brookhaven[29] is given by

$$S(\text{wppm Ni}) = 0.0046T(^\circ\text{C}) - 1.40 \text{ from } 450 \text{ to } 600^\circ\text{C}$$

which gives ~0.6 ppm at 450°C and ~1.4 ppm at 600°C. These values are about an order of magnitude lower than those of Rodgers et al.[42] and two orders of magnitude higher than those of Baus et al.[43]

Brookhaven solubility measurements of iron in sodium deviate in similar fashion from those of the above investigators, being ~0.3 ppm at 486°C and ~0.85 ppm at 550°C. However, they are in line with more recent measurements by Atomics International[44a] and the United Kingdom[45] at higher temperatures and fit the equation

$$\log S(\text{wppm Fe}) = 7.05 - 5730/T(^\circ\text{K}) \text{ from } 486 \text{ to } 700^\circ\text{C}$$

The solubility appears to be independent of the oxygen in the sodium so long as the sodium is no more than 20% saturated with oxygen. The apparent solubility of iron increases with increasing oxygen in the sodium above this value.

A new (but apparently not final) equation for the solubility of carbon in sodium has been presented[30] by Atomics International. This is

$$\log S(\text{wppm C}) = 1.55 - 360/T(^\circ\text{K}) \text{ up to } 900^\circ\text{C}$$

Efforts are continuing to refine the data and to reconcile the apparent disagreement with measurements made elsewhere.

Measurements in the United Kingdom[44b] of the solubilities of bismuth, copper, and tellurium in sodium containing 10 ppm oxygen yielded the equations

$$\log(\text{at.\% Bi}) = 5.0038 + 4188.9/T(^\circ\text{K}) \text{ at } 252 \text{ to } 563^\circ\text{C}$$

$$\log(\text{at.\% Cu}) = -0.5173 + 2018.7/T(^\circ\text{K}) \text{ at } 222 \text{ to } 640^\circ\text{C}$$

$$\log (\text{at.\% Te}) = 0.7514 + 1282.2/T(^\circ\text{K})$$

at 222 to 572°C

Values for bismuth measured by Atomics International[30] compare well with the above.

Table III-1 summarizes results of the Atomics International experimental solubility program[46] involving refractory metals and alloys in potassium or lithium. The addition of up to 2 wt.% of a gettering element (zirconium, hafnium, or titanium) to tantalum and niobium dramatically reduces the apparent solubility of the metal in potassium or lithium. All solutes except rhenium are more soluble in potassium than in lithium.

Oak Ridge measurements of the solubility of crystal-bar thorium in molten bismuth[47] gave the relation

$$\log S(\text{wppm Th}) = 7.677 - 3850/T(^\circ\text{K})$$

from 480 to 900°C

Since these data are in excellent agreement with those indicated by reductive extraction experiments at 600 to 700°C, it appears that the presence of lithium, uranium, rare earths, and other elements in low concentrations has little influence on the solubility of thorium in bismuth.

The Soviets[48] are considering the use of molten lead, aluminum, or tin as the coolant in a UC_2-fueled reactor with graphite as the structural material. By equilibrating graphite with each of the three metals at 1100°C for 2 hr, they found the solubilities of carbon to be 0.09 at.% in lead, 0.04 at.% in tin, and 0.009 at.% in aluminum. The equilibrium concentrations of uranium in the systems Al(Sn,Pb)–C–U decreased in the reverse order, being greatest in aluminum and least in lead. The solubility of UC_2 in tin in the presence of graphite increased from 0.05 mole % at 1000°C to 0.35 mole % at 1750°C.

The solubility of vanadium in molten potassium containing <20 ppm oxygen was found by workers at NASA–Lewis[49] to follow the law

$$\log S(\text{wppm V}) = 5.18 - 4500/T(^\circ\text{K})$$

from 1012 to 1341°K

The optical-spectrographic and wet-chemical methods used were not sufficiently sensitive to measure the solubilities of titanium and zirconium in potassium, although indications are that the solubilities are both below 10 ppm up to 1333°K.

Corrosion by Potassium

At United Nuclear,[50] molten potassium with controlled additions of up to 200 ppm oxygen was circulated between 1200 and 1600°F (650 and 870°C) in 316 stainless-steel loops containing strings of Nb–1 Zr and stainless-steel test specimens in the heater legs. The oxygen additions were apparently gettered rapidly by the Nb–1 Zr, since they had no observable effect on the stainless-steel corrosion rates, while causing a

Table III-1 Solubilities of Metals in Potassium and Lithium[46]

Solute	Solubility in potassium		Solubility in lithium	
	wppm	Temp. range, °C	wppm	Temp. range, °C
Ta from T-111*	$\log S(\text{wppm}) = 2.099 - [2090/T(^\circ\text{K})]$	1200–1600	0–3	1200–1600
Ta from ASTAR-811C*	6–10	1200–1600	0–3	1200–1600
Ta from Ta–0.5 Zr	500–3000	1200–1600		
Nb from Nb–1 Zr	~6	1200–1400		
Mo from Nb–0.5 Zr	10–15	1200–1600		
Mo from Mo–0.5 Zr	~100	1200–1400		
Mo from TZM*	~12	1400		
Hf from ASTAR-811C*			6–10	1200–1600
Hf (zone refined)	~100	1200–1400	~6	1200–1400
Zr (zone refined)	60–100	900–1200		
W (vapor deposited)	40–80	1200–1600	0–3	1200–1600
Re	<1	1200–1600	0–2	1200–1600
Mo			2–15	1200–1600

*T-111 = Ta–8 W–2 Hf; ASTAR-811C = Ta–8 W–1 Hf–1 Re–0.025 C; TZM = Mo–0.5 Ti–0.07 Zr.

pronounced increase in the initial rate of Nb–1 Zr surface removal. However, there were no identifiable oxide films or microstructural changes in the Nb–1 Zr specimens, which remained ductile. The initially high corrosion-weight-loss rates in the Nb–1 Zr decayed with time, returning essentially to normal rates (<0.1 mil/year) in about 2500 hr if no further oxygen was added. Increasing the potassium flow velocity by a factor of 18 had no obvious effect on the weight-loss rate of the Nb–1 Zr.

DiStefano has summarized[51] the Oak Ridge results of over 67,000 hr of testing of the refractory alloys Nb–1 Zr, D-43 (Nb–10 W–1 Zr), T-111 (Ta–8 W–2 Hf), TZM (Mo–0.5 Ti–0.1 Zr), and C-129Y (Nb–10 W–10 Hf–0.1 Y) in boiling-refluxing potassium at 1100 to 1400°C. (Note that all of these alloys contain an active gettering element.) No serious corrosion interactions were observed in any of the tests, the weight changes of insert specimens being directly related to migration of oxygen. Similar tests on Nb–1 Zr with 1200°C refluxing sodium, rubidium, and cesium failed to show any significant difference in the corrosiveness of the various alkali metals, there being essentially no attack in each case.

Corrosion by Lithium

Examination of 82 insert specimens from a T-222 (Ta–10.2 W–2.3 Hf–0.014 C) thermal-convection loop[36] after 3000 hr of lithium circulation at 1350 to 1140°C and 2.5 ft/sec disclosed very small hot-zone weight losses (0.8 mg/cm^2, max.) over about two-thirds of the loop and minimal cold-zone weight gains (2.0 mg/cm^2, max.) over the remaining third. A significant transfer of hafnium from the hotter to the cooler regions was noted, with surfaces near the heater entrance analyzing as much as 60 wt.% hafnium.

Corrosion by Mercury

A great deal of effort has gone into the evaluation of 9 Cr–1 Mo steel as the construction material for the mercury boiler in the SNAP-8 space power system. A report has been issued by Aerojet-General[52] summarizing earlier capsule and loop-test findings and describing an analytical method used to predict corrosion behavior, along with a final set of loop experiments to confirm the analysis. This work led to the following conclusions:

1. Corrosion of 9 Cr–1 Mo steel by flowing mercury is by dissolution of the alloy constituents in the mercury.

2. The corrosion rate is velocity dependent, suggesting that the rate-controlling step is diffusion transport of solute molecules through the laminar sublayer adjacent to the wall.

3. Corrosion rates can be calculated by a mass-transfer equation which indicates that, under the fully wetted condition required for good heat transfer, 9 Cr–1 Mo steel is not suitable for 10,000-hr service in the SNAP-8 boiler.

4. Materials like tantalum and niobium, which are essentially insoluble in mercury, are preferable to 9 Cr–1 Mo steel. (E. M. Simons)

Cladding Reactions Following Loss-of-Coolant Accidents

Workers at Argonne[53] are studying the effect of violent meltdown on stainless-steel-clad UO_2 fuel rods in a sodium-cooled reactor by subjecting the rods to high temperature in a sodium-filled autoclave. The internal pressure of the fuel rods is monitored by the motion of a pressure transducer. The results of the first experiment involving three transients are summarized in Table III-2. The center fuel rod of the array failed

Table III-2 TREAT Meltdown Experiment with Stainless-Steel-Clad UO_2-Core Fuel Rods Submerged in Sodium[53]

	Transient		
	1	2	3
Reactor characteristics			
Integrated power, Mw-sec	312	481	495
Peak power, Mw	1048	1790	2310
Period, msec	90	70	63
Results			
Peak temperature,* °C	470	710	
Maximum indicated motion, cm	2.3	3.8	7.4
Maximum piston velocity, cm/sec	1.6	8.5	27
Appearance of fuel rod	Intact†	Intact†	Split
Energy calculations			
Fission-energy input, cal/g of UO_2	214	330	340

*Measured by thermocouple in sodium 3 in. above bottom autoclave head.

†Determined from neutron radiographs of autoclave assembly.

during the third transient, and 24.3 g of UO_2 was released into the sodium coolant, which was at a temperature between 600 and 700°C. The cladding rupture appeared as a ragged tear in the wall of the tubing, and there was no sign of the cladding having melted.

(H. S. Rosenberg)

Radiation Effects on Structural Materials

A survey[54] on in-pile mechanical properties of reactor structural and fuel materials, by Knolls, includes a state-of-the-art summary of in-reactor Zircaloy properties, a tabular summary of information given in the cited literature, and a bibliography with abstracts.

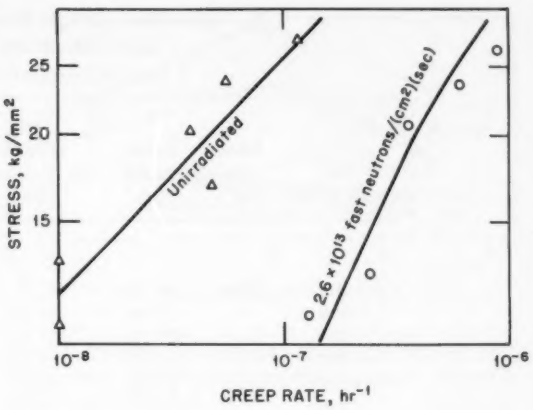

Fig. III-6 Tubular creep rates of Zircaloy-2 after 9000 hr under stress[6] at 258°C.

Zirconium Alloys

The effect of neutron radiation and hydrogen content on the failure stress of flawed Zircaloy-2 pressure tubes has been investigated by the British.[55] These tubes were 18% cold drawn and had an inside diameter of 3.25 in. and a wall thickness of 0.165 in. It was found that at 300°C the failure stress was not affected by 200 ppm hydrogen, whereas at 20°C the precipitated hydrides reduced the failure stress sharply. Irradiation up to a fast fluence of 7×10^{20} neutrons/cm^2 increased the failure stress at both room temperature and 300°C, the increase being minimal at the higher temperature. A combination of hydrogen and irradiation reduced the failure stress of the pressure tubes at room temperature. However, at 300°C the failure stress of the irradiated and hydrided pressure tube was higher than that of the unirradiated material. A summary report[56] that discusses the properties of both unirradiated and irradiated Zircaloy-2 pressure tubing has been issued by Battelle–Northwest.

A fast flux of 2.6×10^{13} neutrons/(cm^2)(sec) was found by the Canadians[6] to cause a 10-fold acceleration of creep in cold-worked Zircaloy-2 at 258°C, as shown in Fig. III-6. Also, they were able to obtain good correlation between uniaxial and biaxial (pressure-tube) in-pile creep rates for Zr–2.5 Nb by using texture coefficients to adjust the tube stresses and normalizing all data to the same temperature and fast-neutron flux.

Research at Chalk River[57] indicates that the radiation-induced increase in yield strength of a Zr–2.7 Nb alloy is dependent on the amount of niobium in solution. Structures containing niobium in metastable solution were found to undergo significantly larger yield-strength increases than did aged alloys in which the excess niobium had precipitated out of solution. The enhanced yield-strength increases are believed to be due to stabilization of defect clusters by niobium atoms that are in metastable solution. Irradiation at 300°C caused larger increases in yield strength than irradiation at 100°C for material containing the same amounts of niobium in supersaturated solution.

Stainless Steels and Superalloys

Review articles on effects of irradiation on stainless-steel and refractory-metal alloys were presented[58] at the American Nuclear Society Topical Meeting on Fast Reactor Systems, Materials, and Components in Cincinnati, Ohio, on April 2–4, 1968.

Tensile properties of 316 stainless steel, irradiated by Battelle–Northwest at 900°F (480°C) in the Experimental Breeder Reactor II (EBR-II) to a total fluence of 0.8×10^{22} neutrons/cm^2, are shown[39,59] in Table III-3. These results confirm the previously reported trends for irradiated stainless steel, wherein elevated-temperature ductility is significantly reduced by irradiation. Both the strength and ductility of the irradiated material are highly sensitive to strain rate during testing.

The postirradiation stress-rupture properties of 304 stainless steel at 1000 and 1100°F (538 and 593°C), as determined by Battelle–Northwest,[60] are shown in Fig. III-7. It is apparent that high-temperature irradiation causes significant reductions in rupture life at both testing temperatures. Comparable reductions were ob-

Table III-3 Tensile Properties of 316 Stainless Steel[39] Unirradiated and Irradiated at 900°F to a Total Fluence of 0.8×10^{22} neutrons/cm²

Test temp., °F	Strain rate, min^{-1}	Elastic limit, ksi	Yield strength (0.2% offset), ksi	Ultimate tensile strength, ksi	Elongation, %		Reduction in area, %
					Uniform	Total	
			Irradiated				
RT	0.002	31.70	42.85	85.04	39.24	46.41	65.04
600		23.64	31.98	71.32	24.72	30.32	59.50
800		23.98	31.30	72.20	22.72	27.60	54.47
900		19.92	29.11	67.64	28.87	33.72	47.97
1000		27.24	33.82	63.33	18.13	19.40	35.77
1100		22.36	33.58	54.07	10.99	12.12	30.89
1200		18.70	31.87	43.90	4.63	5.14	22.76
1400		16.26	24.39	26.50	2.42	5.59	8.13
1000	0.2	19.2	28.70	63.52	17.82	23.21	53.60
1100		19.11	29.02	60.73	22.07	32.06	60.16
1200		20.33	30.08	55.61	20.70	28.21	44.72
1400		18.70	26.50	38.86	8.21	16.28	25.20
			Unirradiated				
RT	0.002	15.3	34.85	77.0	63.80	76.0	77.10
572		19.2	25.9	85.5	47.6	56.5	78.6
700		12.2	18.4	70.6	39.2	44.4	66.2
800		8.5	11.9	65.7	41.8	49.4	60.7
900		11.9	16.7	71.1	39.3	46.9	61.7
1000		12.4	16.9	68.7	46.2	52.8	61.7
1100		12.9	15.9	64.7	42.7	50.6	60.7
1200		11.7	14.3	55.7	35.6	40.1	43.8
1300		12.4	16.7	44.0	23.9	35.3	41.8
1400		10.0	14.0	30.8	14.9	53.8	62.7
1500		14.4	16.3	24.9	10.5	55.9	60.7

tained in 1200°F (650°C) stress-rupture tests on tubular material that had been irradiated in sodium in the EBR-II to a fluence of 0.8×10^{22} neutrons/cm² ($E > 0.1$ Mev).

General Electric workers[61] have continued their measurements of the ductility of irradiated ring specimens using an expanding mandrel inside the ring to strain it to failure and determining the ductility of the ring by measuring its diameter after failure. Results of such tests at 1300°F (705°C) are summarized in Fig. III-8. As can be seen, the ductility obtained in these tests is significantly better than that shown by simple tensile specimens irradiated at the same conditions and tested at the same temperatures. This phenomenon was discussed in the Summer 1969 issue of *Reactor Materials*.

Tensile and creep-rupture properties of several heats of Incoloy 800 were determined by Oak Ridge[62] at 700 and 760°C after irradiation. It was found that optimum postirradiation ductility was obtained with a titanium addition of 0.1 wt.% and small grain size. The ductility appeared to be independent of the carbon content. Aging the Incoloy 800 before irradiation in order to agglomerate the carbide particles had no effect on tensile ductility at 760°C. Typical test results are shown in Fig. III-9.

Figure III-10 shows that measurable creep occurs in 304 stainless steel during irradiation[59] under 35,000-psi stress at 175°C.

The creep rate of irradiated A-286 steel at 660°C has been shown to depend on its helium content, which is generated from boron.[63] Specimens had been irradiated in the Engineering Test Reactor (ETR) at 50°C to a fast fluence of 4.9×10^{19} neutrons/cm² and a thermal fluence of 6.2×10^{20} neutrons/cm². Figure III-11 shows that the minimum creep rate de-

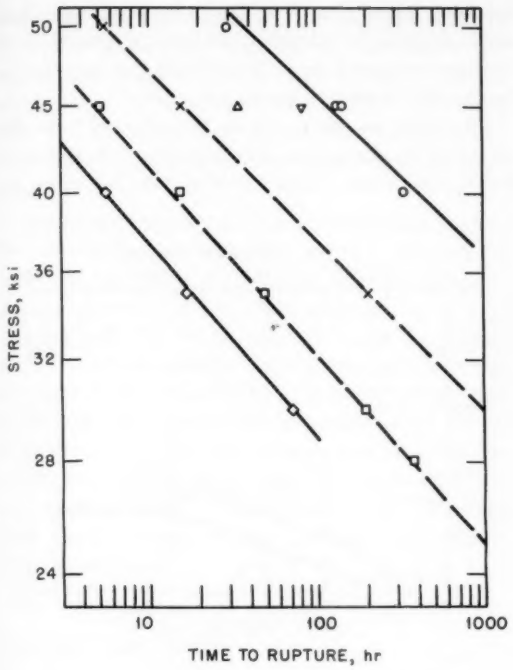

Fig. III-7 Postirradiation creep-rupture properties of 304 stainless steel.[60] 1000°F (538°C) tests: ○, solution-treated control; ×, solution treated and irradiated at 900°F to ~10^{22} neutrons/cm^2 (total); △, solution treated and irradiated at 800°F to ~3 x 10^{21} neutrons/cm^2 (total); ▽, solution treated and irradiated at 800°F to ~10^{21} neutrons/cm^2 (total). 1100°F (593°C) tests: □, solution-treated control; ◇, solution treated and irradiated at 900°F to 10^{22} neutrons/cm^2 (total).

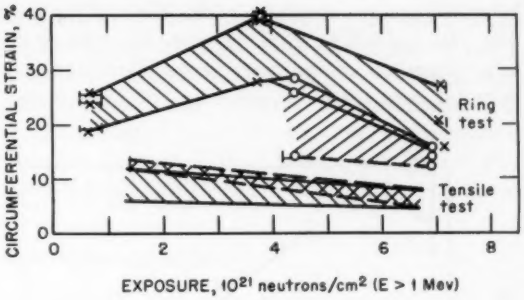

Fig. III-8 Ductility of irradiated mill-annealed 304 and 316L stainless steels obtained from two types of tests[61] at 1300°F. ○ ▨, 304; × ▧, 316.

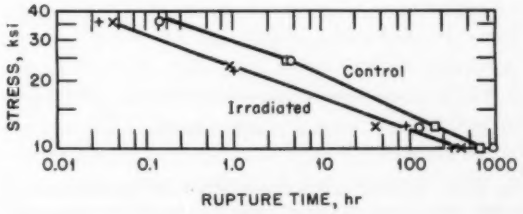

Fig. III-9 Creep rupture of experimental Incoloy 800 containing 0.13 wt.% carbon and 0.10 wt.% titanium.[62] Specimens were irradiated or soaked (controls) at 760°C and tested in air at 760°C. ×○, annealed at 1150°C; +□, annealed at 1150°C and aged 100 hr at 800°C.

creases with increasing helium content. The variation in helium content was obtained by varying the boron content. The decreasing creep rate is attributed to pinning of dislocations by fine helium bubbles.

Charpy V-notch specimens of 403 stainless steel were irradiated to a fast fluence of 6.07 x 10^{19} neutrons/cm^2 (>1 Mev) at 300°C. Impact-test results,[6] shown in Fig. III-12, illustrate that the upper shelf energy was reduced below the 30 ft-lb criterion by irradiation. The reduction of impact strength is attributed to irradiation, since aging some of the controls for 1352 hr at 300°C without irradiation had no adverse effect on impact strength.

The effect of small titanium additions on the irradiation response of cobalt alloys is being investigated at Brookhaven.[29] Cold-worked and recrystallized (16 hr at 870°C) specimens of Co–21 Cr–10 Ni–5 W–5 Mo–8 Fe containing from 0.09 to 0.64 wt.% titanium were irradiated to a fast fluence of

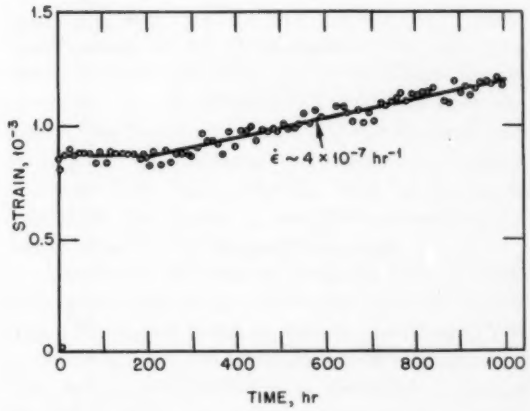

Fig. III-10 Creep of annealed 304 stainless steel during irradiation[59] at 175°C and 35,000 psi.

1.3×10^{20} neutrons/cm^2 ($E > 0.82$ Mev) and tested at 650, 750, and 800°C. Although irradiation reduced the total elongation of the experimental alloys, the ductility (at least 20% elongation at 650°C) was considerably higher than that shown by irradiated cobalt alloys without the titanium additions. The variation of titanium content from 0.09 to 0.64% did not result in appreciable changes in tensile properties.

Research is continuing at Brookhaven[64] on the effect of irradiation on the superplastic behavior of Fe–Cr–Ni alloys. Table III-4 shows the effect of

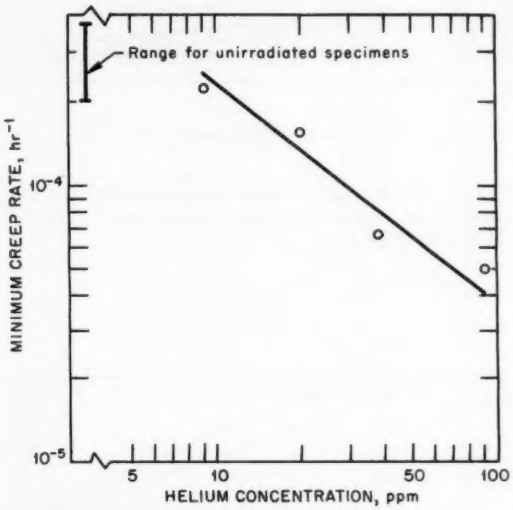

Fig. III-11 Effect of calculated helium atom concentration in A-286 steel on its minimum creep rate at 655°C under 38.7 kg/mm^2 stress.[63]

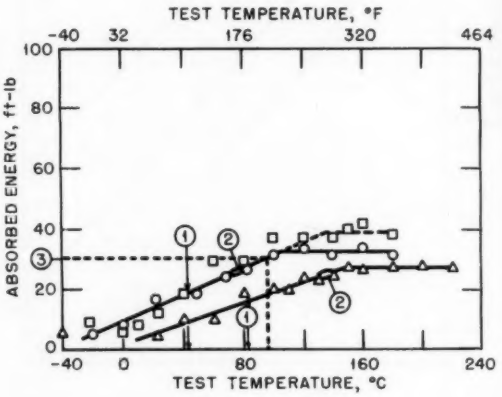

Fig. III-12 Effect of irradiation on the impact properties of 403 stainless steel.[6] ① 50% energy level; ②50% shear fracture; ③30 ft-lb energy level. ○, unirradiated; □, aged 1352 hr at 300°C; △, irradiated to 6.07×10^{19} neutrons/cm^2 (>1 Mev).

Table III-4 Effect of <100°C Irradiation on Tensile Properties of Superplastic Ni–38 Cr–20 Fe Alloy[64]

(Strain Rate: 0.2%/min; Starting Condition: 1200°C for 1½ hr and Water Quenched; Cold Swaged 85%)

Treatment	Exposure fluence, 10^{20} neutrons/cm^2 (E> 0.82 Mev)	Test temp., °C	Yield strength, ksi	Tensile strength, ksi	Total elongation, %
Aged at 760°C for 8 hr	0	650	46.3	51.0	30
	0	650	30.8	34.0	52
	0	750	25.8	28.4	27
	1.3	650	29.3	32.5	53
	1.3	650	27.2	31.4	52
	1.3	750	25.8	27.6	24
Aged at 927°C for 8 hr	0	650	31.4	35.0	73
	0	750	11.8	13.4	83
	1.3	650	36.0	39.8	35
	1.3	750	14.0	15.3	77
Aged at 1038°C for 8 hr	0	650	38.3	41.0	54
	0	750	10.8	12.8	125
	1.3	650	38.6	42.5	28
	1.3	750	14.2	15.1	150
	1.3	800	7.1	8.2	175

irradiation and heat-treatment on tensile properties of Ni–38 Cr–20 Fe alloy. Note that the best postirradiation tensile properties were obtained on a material which was water quenched from 1200°C, cold swaged 85%, and then aged for 8 hr at 1038°C. The above treatment resulted in an austenitic matrix with islands of ferrite.

Significant improvements in postirradiation rupture life of Hastelloy N at 650°C can be obtained by modifying the alloy with minor additions. For example, additions of 0.5 wt.% hafnium or 2 wt.% tungsten and 0.5 wt.% titanium result in rupture lives[47] which are comparable or even superior to that of unirradiated Hastelloy N. It had previously been found that the postirradiation stress-rupture life of Hastelloy N at 650°C was independent of irradiation temperature in the range 43 to 650°C. However, it was subsequently found[36] that irradiation at 700°C and above can shorten the rupture life by as much as three orders of magnitude.

Pressure-Vessel Steels

At the Naval Research Laboratory, the response of A-533B and A-533C steel plate and weld metal to irradiation embrittlement was determined by impact testing.[65] The material was irradiated at 550°F (290°C) with fast fluences ranging from 0.5 to 2.3×10^{19} neutrons/cm^2. Consistently high radiation-embrittlement sensitivity was observed for A-533B electroslag and A-533B and A-533C submerged-arc weld deposits. Also, considerable variation in embrittlement sensitivity was found in plates from different heats. It appears that the variation in degree of radiation embrittlement between heats is related to differences in chemical composition (more embrittlement with high copper and phosphorus contents, as indicated in the Summer 1969 issue of *Reactor Materials*). The response of A-533 plate and weld metal to 550°F irradiation did not appear to be measurably influenced by either strength class (Class 1 vs. Class 2) or the particular grade of steel (Grade B vs. Grade C). The steels did not exhibit significant variation in 550°F irradiation response across the thickness of the plate. Similarly, there were no marked variations in radiation sensitivity between longitudinal and transverse test orientations in individual plates.

The combined effects of irradiation and stress on samples of A-302B and A-350LF1 steels were also investigated.[66] Charpy V-notch specimens were loaded in uniaxial tension at 75% of their yield strength while being irradiated at 430 and 550°F (220 and 290°C). Impact testing of the irradiated Charpy V-notch specimens indicated that the shift in transition temperature was similar whether the specimens were irradiated under stress or not. The postirradiation annealing response of the low-alloy A-302B steel also was found to be unaffected by stress during irradiation.

Miscellaneous Materials

Specimens of pure copper, Cu–0.85 Al and Cu–0.95 Mg have been irradiated (fast fluence of 8.2×10^{19} neutrons/cm^2) and tested in tension at temperatures[67] up to 650°C. The results indicate that irradiation causes an increase in strength and a decrease in ductility at low testing temperatures. At higher testing temperatures (above about 500°C), the displacement type of radiation damage is removed, and the preirradiation tensile properties of pure copper are restored. However, the copper alloys behaved somewhat differently than pure copper in that the elongation of the irradiated specimens was not restored at elevated testing temperatures. It was suggested that the copper alloys, like austenitic stainless steels and nickel-base alloys, were embrittled by helium at elevated temperatures. Since all the materials contained about 0.1 wt.% boron, it was concluded that the helium which was generated from the boron behaved differently in pure copper than in the copper alloys.

Basic Mechanisms of Radiation Damage

It has been found that saturation of radiation damage occurs in iron after large fast fluences.[39] These results, shown in Fig. III-13, indicate that softening (oversaturation) can occur in a material with further irradiation after a certain fast fluence has been exceeded. The best explanation for the above-mentioned behavior is the dynamic rearrangement of defect aggregates into larger clusters, with an attendant decrease in the number of point defects surviving the damage event at high fluences.

Distribution of voids in irradiated 304L stainless steel, as determined by transmission electron microscopy (TEM), was found by Battelle–Northwest[39] to be dependent on the thickness of the stainless-steel foil. As the foil thickness is decreased, a smaller number of large voids will be found in a cubic centimeter of material. Also, as the thickness of the foils is increased, the number of small voids per cubic

centimeter of material is decreased. This study indicates that considerable care should be taken in evaluating the "average void diameters" which are given by different investigators.

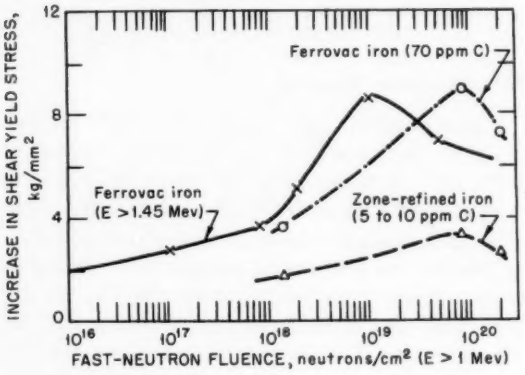

Fig. III-13 Effect of fast-neutron irradiation on shear yield stress of iron.[39]

TEM observations, on 304 stainless steel irradiated in EBR-II to a fluence of 10^{22} neutrons/cm^2, indicated the presence of pseudomorphs.[59] These pseudomorphs are believed to result from the filling of voids by atoms during fast reactor operation. Some characteristics of the pseudomorphs are:

1. They are spherical or polyhedral in shape, depending on the shape of the associated radiation-produced void.
2. Their volume percent increases with increasing fast fluence.
3. When pseudomorphs are coincident with voids, the voids are almost always centrally located within the pseudomorphs.
4. Their size is on the order of 200 to 500 A, somewhat larger than the radiation-induced voids, which are 80 to 300 A in diameter.
5. They do not appear to be associated with a strain field.
6. They appear to be stable during high-temperature annealing.

It was found that the irradiation of 25% cold-worked 304 stainless steel in the EBR-II at 380°C to a fluence of 1.6×10^{22} neutrons/cm^2 did not cause a measurable density decrease.[59] This result was consistent with TEM observations, in that no voids were observed in the irradiated 304 stainless steel. (M. Kangilaski)

Metallurgy and Mechanical Properties of Common Cladding and Structural Materials

Zirconium Alloys

A thorough review of the hydride precipitates in zirconium alloys has been issued.[68] The review discusses the habit planes of the hydrides, hydride orientation in unstressed polycrystalline material, and the effect of stress on hydride-platelet orientation. A review of the present state-of-art of Zircaloy-2 heavy-water pressure-tube technology has been prepared.[56] This Battelle–Northwest publication covers design, specifications, production, use, and operational standards of pressure tubes. Also included are data on mechanical properties, welding of Zircaloy-2 and stainless steel, and effects of irradiation on mechanical properties.

Tensile tests were performed by General Electric[69] on Zircaloy-2 specimens at room temperature and 350°C to gain a basic understanding of ductility in Zircaloy-2. Specimens with a variety of textures were utilized. Some were tested in simple tension, and others were tested under plane-strain loading. The plane-strain tensile tests utilized specimens which had a narrowed-down gauge section that was 0.05 in. long and 16 mils thick. In all tests the simple tensile specimens exhibited higher ductility but lower strength than the plane-strain tensile specimens. The test results showed that, as the frequency of basal planes moved away from the tensile axis, the elongation to fracture increased in simple tension but decreased in plane-strain tension. Accompanying this decrease in ductility was an increase in strength. At 350°C the same general trends persisted, but there was a marked decrease in ductility with decreasing strain rate.

Grain boundaries are preferred sites for precipitation of zirconium hydride platelets, provided they lie in certain directions relative to adjacent grains.[70] The most favorable sites are those grain boundaries which make angles of 35 to 40° and 60 to 75° with the basal planes of the adjacent grains.

Studies are in progress at General Electric to determine the mechanical behavior of Zircaloy-4 at temperatures high enough to cause melting of the material.[71] These temperatures are envisioned when a

Zircaloy-4-clad fuel pin loses its coolant as a result of a nuclear accident. Figure III-14 illustrates the failure mode of Zircaloy-4 tubes as a function of internal steam pressure and heating rates. These results indicate that brittle fracture is favored by low pressures and high heating rates, whereas high pressures promote ductile fracture.

The ultimate strength of Zircaloy-4 at temperatures up to 1800°C is shown in Fig. III-15. In all of these tensile tests, Zircaloy-4 was quite ductile, showing total elongations generally in the 60 to 80% range. The ultimate strength is independent of strain rate at testing temperatures below 900°C. Above 900°C the strength is slightly lower for slower strain rates.

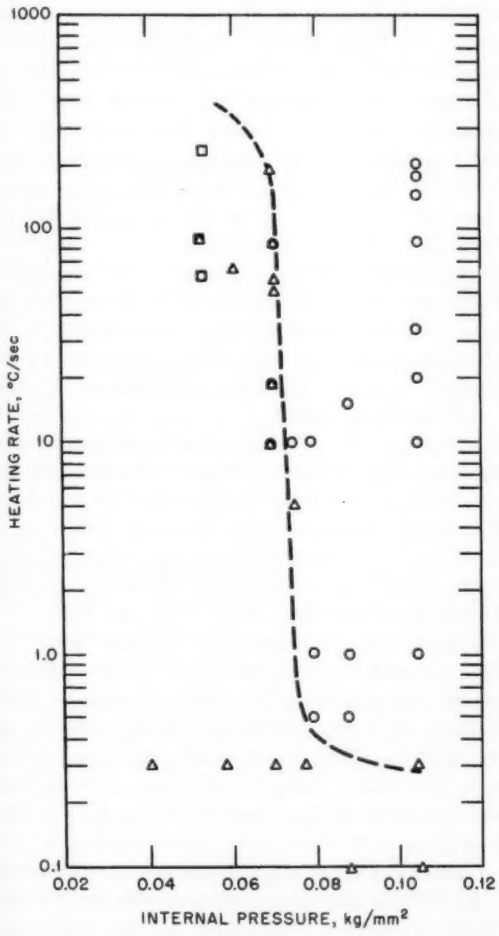

Fig. III-14 Mode of failure for Zircaloy-4 tubing in steam for various internal pressures and heating rates.[71] □, neither burst nor expanded fully; △, burst; ○, expanded.

Creep tests at 300 and 400°C have been performed on Zr–2.5 Nb pressure tubes.[39] These tubes were given various treatments before testing, including (1) 30% cold work; (2) water quenching from 880°C, followed by 15% cold work and aging 24 hr at 500°C; and (3) water quenching from 880°C, followed by aging 24 hr at 500°C. Figure III-16 shows both the rupture times and creep rates for specimens given the different treatments. These results show that the 15% cold work between quenching and aging does not significantly affect the creep performance of Zr–2.5 Nb pressure tubes at 400°C.

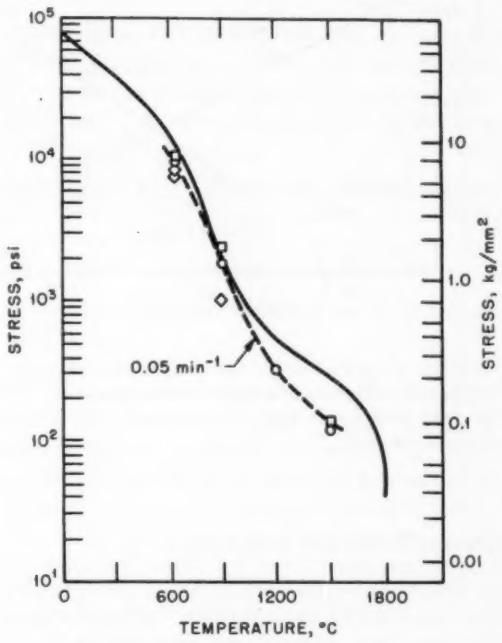

Fig. III-15 Ultimate tensile strength of Zircaloy-4 sheet tested in helium.[71] —, data obtained at 1.13 cm/min crosshead speed (in argon); ◇, 0.005 min^{-1}; ○, 0.05 min^{-1}; □, 0.1 min^{-1}.

The hardenability of Zr–1.2 Cr–0.1 Fe containing 1400 ppm oxygen was found by the Canadians[72] to depend on cooling rate. At cooling rates below 2000°C/sec, the hardness of the material increased with increasing cooling rate. A steady maximum hardness of 360 VHN was obtained for cooling rates above 2000°C/sec. The hardness of 360 VHN was found to be independent of beta quenching temperature, time at quenching temperature, and beta grain size.

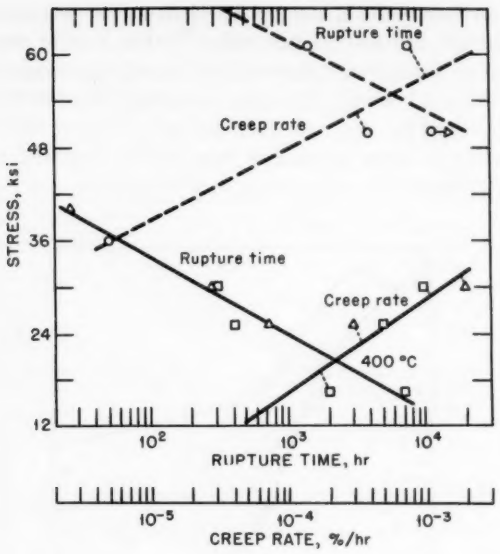

Fig. III-16 Creep data for Zr–2.5 Nb alloy pressure tubing.[39] ○, 30% cold worked; △, heat-treated (880°C, water quenched, 15% cold worked and aged; □, heat-treated (880°C, water quenched and aged).

Stainless Steels and Superalloys

The available mechanical-property data for 304, 316, 321, and 347 stainless steels at elevated temperatures have been collected and tabulated by General Electric.[71] Emphasis is on tensile and creep properties. The February and May 1968 issues of *Metals Engineering Quarterly* have been devoted entirely to stainless steels. The areas that are discussed include mechanical properties, corrosion applications, and forming properties. The American Society for Metals has published four timely books covering the selection,[73] forming,[74] joining,[75] and machining[76] of stainless steels.

An attempt has been made by the Canadians[77] to improve the wear resistance of 304 stainless-steel journals through different surface treatments. The treatments consisted of one or more of the following: shot blasting with glass shot, shot blasting with chilled-iron shot, heating in air, heating in argon, or heating in vacuum. The treated journals were tested against Wankesha 88 bearings at loads ranging from 20 to 80 lb and speeds of 40 and 180 rps. The testing environment was *p*H 7 water at 80°F (27°C). In general, the treated journals were found to have better wear resistance than the untreated journals. The improvement in wear resistance was attributed to oxidation. The best wear resistance was obtained by glass-shot blasting the surface and then heating the journals in air at 800°C for 21 hr.

Surface damage resulting from electrical-discharge machining (EDM) and electrochemical machining (ECM) was found[78] to reduce significantly the fatigue endurance limit of Inconel 600, 304 stainless steel, Inconel X-750, 17-4PH stainless steel, and Haynes Stellite 25. The strength reduction factor (K_f) was found to be as large as 2.77 if the deleterious effects of arc strikes are included. The effects of EDM and ECM were found to be more prominent for high-strength materials like 17-4PH stainless steel and Inconel X-750.

Metallographic examinations were completed on 304 stainless-steel specimens that had been tested at 650°C in alternating tension–compression strain fatigue.[71] These specimens had been tested under a total strain of 2.0% in both tension and compression at a strain rate of 4×10^{-3}/sec. During testing, the specimens were given various strain wave forms, the main variable being the hold time at maximum strain. The hold time at maximum strain in tension, compression, or both was 0, 30, or 60 sec for the different specimens. All the strain wave forms caused transgranular fracture except in specimens that were held at maximum strain in tension for 30 or 60 sec with zero hold time at maximum strain in compression. The above-mentioned specimens failed intergranularly and showed the grain separation characteristic of failed stress-rupture specimens.

In India, the effect of 2.6 wt.% niobium on the mechanical properties of austenitic stainless steel (23 Cr–19 Ni–0.04 C) was determined.[79] It was found that double isothermal aging, 20 min at 850°C and 18 hr at 650°C, of samples which were water quenched from 1320°C gave maximum hardness and tensile properties at both room temperature and 700°C. Cold rolling of the water-quenched material before isothermal aging at 775°C for 20 hr also improved the mechanical properties. Structural examination of the stainless steel was performed by light microscopy, transmission electron microscopy, and X-ray diffraction. The added strengthening imparted by niobium was attributed to the formation of Fe_2Nb and NbC phases.

The stress-rupture properties of SANDVIK 12R72HV (15 Cr–15 Ni–1.4 Mo–0.4 Ti–0.0065 B) at 700°C are shown (Fig. III-17) to be considerably superior to those of 347 stainless steel.[80] The improved strength is attributed to the addition of molybdenum, titanium, and boron. The fracture mode

of SANDVIK 12R72HV is considerably less intergranular than that of 347 stainless steel at 700°C. It is believed that the beneficial effect of the boron addition (promotion of transgranular fracture at high temperatures) will override the potential deterioration of mechanical properties due to helium formation from the boron by (n,α) reactions during irradiation.

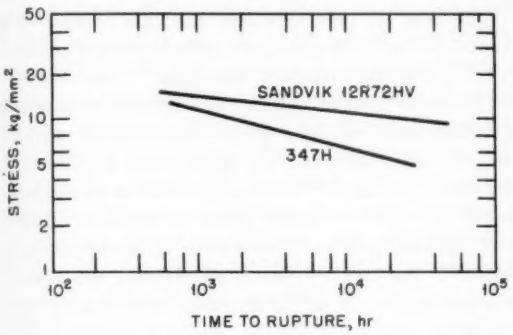

Fig. III-17 Stress-rupture properties of SANDVIK 12R72HV and 347 stainless steel[80] at 700°C.

Inconel 718 is being considered[81] as a high-strength structural material for selected components in the Fast Flux Test Facility (FFTF). Some of the possible applications include fuel-element grid spacers, safety and accelerator springs, and flow-duct contact pads. A thorough state-of-the-art survey of the alloy has been published which includes tensile creep, fatigue, and stress-relaxation properties. Also included are possible effects of radiation on these properties.

Pressure-Vessel Materials and Alloy Steels

A complete issue of *Nuclear Engineering and Design* (July 1968) containing 13 papers was devoted to reactor pressure vessels and their technology. These papers were concerned with pressure-vessel fabrication, inspection, radiation effects, and research programs in progress.

An interim report has been issued on evaluation of advanced pressure-vessel materials.[82] The materials covered in this report are stronger and otherwise more advanced than the currently used ASTM A-302B and A-533 steels. Tensile properties, toughness, thermal stability, and weldability of these materials were evaluated. The materials that were considered and some of the pertinent conclusions are:

1. *7.5 Ni–Cr–Mo.* This steel has been eliminated from the program because of lack of applications experience and because of weldability problems.

2. *12 Ni–5 Cr–3 Mo Maraging Steel.* Best combinations of toughness and high strength are obtained by aging at 900°F (480°C) for 3 hr. The steel shows generally high promise and will be studied in thicknesses up to 4 in.

3. *Martensitic PH13 Cr–8 Mo Steel.* In spite of good plate strength and ductility, this steel requires further study before heavy-section materials are procured because of possible problems with weld ductility and notch toughness.

4. *Inconel 718.* In spite of good high-temperature strength and microstructural stability, poor weld toughness and weld efficiency cast doubt on the potential of this alloy for pressure-vessel service.

5. *HP–9 Ni–4 Co–0.2 C.* Work on this alloy has just been initiated.

The effect of chromium content on the isothermal tempering characteristics of 0.3 C–3 Mo–Cr steels was determined by the Japanese[83] by varying the chromium content from 2 to 12 wt.%. These steels were tempered at temperatures ranging from 400 to 700°C for up to 1000 hr. A tempering parameter $P = T(20 + \log t) \times 10^{-3}$ is utilized for discussing the tempering results. In the higher chromium steels, the peak of hardness shifts to the lower parameter side. On isothermal tempering the following reaction in carbides takes place: $Fe_3C \rightarrow M_2C \rightarrow M_7C_3 \rightarrow M_6C$ for steels containing 2 wt.% chromium and $Fe_3C \rightarrow M_2C \rightarrow M_{23}C_6 + M_6C$ for steels with 5 to 12 wt.% chromium. In higher chromium steels, iron carbide transforms more rapidly to alloy carbide, and the rate of growth and agglomeration of alloy carbide becomes smaller.

The effect of intermittent thermal cycles on the creep properties of Cr–Mo alloy steels (ASTM A-20063T) was investigated.[84] In these tests a steady-state creep rate at 600°C was established, after which the load was removed and the specimen was heated to a higher temperature (650, 700, or 750°C) and held there for 24 hr. Then the specimen was cooled down to 600°C and the original load was reapplied. It was found that generally the secondary creep rate at 600°C is reduced by cycling to higher temperatures without load. However, a significant factor to consider in the life of the component is the amount of primary creep strain that is undergone by the specimen each time at reloading. Therefore, in predicting creep life of a component that is thermally cycled, consideration

should be given to both the steady-state secondary creep rate and the strain in primary creep.

Aluminum Alloys

High-temperature mechanical properties of SAP 895 were found to be sensitive to the Al_2O_3 particle distribution.[85] If a rod of SAP was slightly worked perpendicular to its original extrusion direction, its mechanical properties at 450°C were significantly reduced. However, as the degree of reduction in the perpendicular direction was increased, the mechanical properties improved. After an 8:1 transverse reduction, the original properties were restored. After further working, the mechanical properties exceeded the original values, with the uniform elongation improving by 100% after a 30:1 reduction in the transverse direction. The improved properties are attributed to breaking up and dispersion of the Al_2O_3 particles by secondary working. (M. Kangilaski)

Diffusion Studies

General Diffusion Studies and Reviews

A tabulation of diffusion coefficients and activation energies compiled by Kubaschewski for selected elements in niobium and its alloys of Mo, Ta, U, W, and Zr is included in a review of diffusion rates in solids in a special publication[86] of the International Atomic Energy Agency. This article surveys current methods for measuring diffusion, with emphasis on metallic-ion, metalloid-ion, and noble-gas diffusion in solids.

A special diffusion apparatus that permits continuous measurements of impurity-atom transport rates in solids was used at Brookhaven[87] to measure the diffusion of fission-product iodine in spherical specimens of UC. The diffusion specimen was inductively heated, and the ^{131}I released from the specimen was carried by a purified helium stream to a cooled graphite trap so as to separate the ^{131}I from the less volatile products. The collection rate of ^{131}I was continuously monitored with a radiation detector. The diffusivity of iodine in UC was calculated by measuring the collection rate and then determining the percent released from the specimen (by extracting and measuring the activity of the iodine remaining in the specimen after the experiment was completed). The author found that the amount of ^{133}I released during the initial burst was negligible compared with amounts released through the solid via diffusion. The apparatus can be adapted to a wide variety of volatile and semivolatile impurity diffusion studies.

Zener diffusion parameters have been calculated[88] for some of the rare-earth metals, with the results shown graphically in Fig. III-18. No data were available to permit these theoretical values to be compared with diffusion parameters obtained from experimental measurements.

A review of problems and concepts related to diffusion processes in refractory carbides is included in a 1968 book on refractory materials.[89] The article briefly reviews diffusion theory as it pertains to binary and ternary systems, develops the equations for diffusion, and then discusses the application of derived equations to diffusion in carbide systems of particular interest in which sufficient data are available from either tracer-diffusion experiments or layer-growth studies. In the binary systems the reviewer evaluates the interpretation of diffusion terms and simplifying assumptions applied to the UC and NbC systems. In ternary systems, he summarizes the general rules of Kirkaldy and Brown concerning the construction of diffusion paths on a ternary isotherm. These rules assist in solving metallurgical problems from metallographic data (obtained, for example, from carbide diffusion couples). These rules are used to evaluate results from a study of carburization in some Ta–W alloys. A summary of the diffusion data for different refractory-carbide systems is presented which includes a tabulation of tracer-determined coefficients of diffusion for various carbides, a list of "average" interdiffusion coefficients as they are reported in the literature, and a

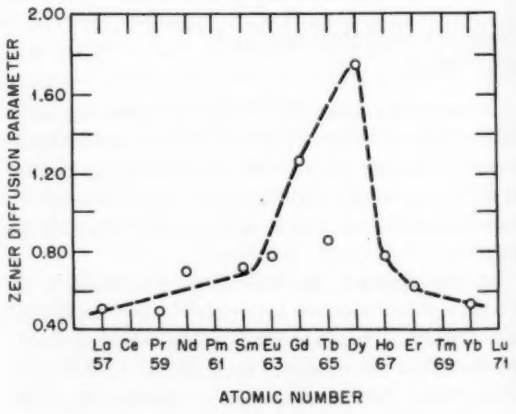

Fig. III-18 Calculated Zener diffusion parameters for the rare-earth metals.[88]

compilation of isothermal parabolic rate constants determined from layer-growth data.

Diffusion in Metallic Fuel Systems

Diffusion in uranium carbide was studied[90] using radioactive tracers ^{14}C and ^{235}U applied as carbides on the diffusion surfaces of arc-cast UC pellets and sintered UC pellets. After diffusion anneals between 1266 and 1684°C for ^{14}C in UC and between 1505 and 1863°C for ^{235}U in UC, the couples were hand ground, and activity-distribution profiles were obtained by scintillation counter (for ^{14}C) and by gamma-ray spectrometer (for ^{235}U). Volume diffusion predominated, but significant contributions from grain-boundary diffusion were evident at low temperatures in arc-cast hypostoichiometric UC. Temperature-dependence curves for ^{14}C in UC followed the equation $D = 1.75 \exp(-63{,}000/RT)$ cm²/sec. For ^{235}U in UC the equation was $D = 8.47 \exp(-104{,}000/RT)$ cm²/sec. The carbon contents of the arc-cast UC pellets ranged from 4.7 to 5.6 wt.%. The activation energy for diffusion and the frequency factor D_0 were affected considerably by changes in the carbon content.

Kimmel, Bar-Or, and Rosen[91] studied the growth of intermediate phases in nickel-plated uranium specimens diffused at 530 to 735°C for 2 hr to 10 days. The specimens were polished, air oxidized, and evaluated metallographically and by microprobe analyses. Two intermetallic compounds, UNi_5 and U_6Ni, were studied below 600°C. Between 600 and 680°C, a third phase, U_7Ni_9, appeared, and its growth increased rapidly with temperature. Above 680°C a fourth phase having a nickel concentration of 46.11 wt.% appeared and grew, whereas the UNi_5 phase decreased in width. Parabolic growth of the layers separately and together was observed up to 640°C, above which the fourth phase began to form and alter the total growth rate. The authors proposed a model based on diffusion-controlled layer growth, in which the diffusion coefficient and the flux of atoms are constant within each layer, to calculate the diffusion coefficients in each phase from the Arrhenius-type equation:

$$D_s\delta_s = A_s \exp[-Q_s/RT]$$

where D_s = diffusion coefficient in layer s
δ_s = solubility range within that layer s
A_s = preexponential coefficient containing a concentration percent factor
Q_s = activation energy for diffusion in layer s

Values of A_s and Q_s for the various intermediate layers are given in Table III-5.

The growth rates of the layers were slightly higher than those obtained by other investigators; but the method and conditions of preparing the diffusion couples in each case were also different, which could contribute to the slight differences in results between investigators.

Table III-5 Activation Energies and Preexponential Coefficients of Various Layers[91]

	U_6Ni	U_7Ni_9	UNi_5
A, (cm²/sec)(at.%)	3.14	850	0.0074
Q, kcal/mole	43 ± 3	53 ± 3	31 ± 3

Plutonium diffusion in nickel was investigated by the French,[92] using nickel saturated with $Pu + Pu_2Ni_{17}$ against a pure-nickel couple and heating the couples between 1025 and 1125°C. Since the solubility of plutonium in nickel was only 130 to 320 ppm, the concentration–penetration curves could be determined. The activation energy for diffusion was 51,000 cal/mole, and the frequency factor was 0.14 to 1.14 cm²/sec.

Diffusion in Refractory-Metal Systems

Using the exceptionally precise anodizing chemical-dissolution-sectioning technique on polycrystalline tungsten, Oak Ridge investigators[93] studied the diffusion of ^{95}Nb in tungsten at 1399°C for 8 hr. The slope of the concentration–penetration curve varied considerably in the first 3 μ, resulting in diffusion coefficients that ranged from 3.77×10^{-8} cm²/sec near the original interface to 1.3×10^{-12} cm²/sec at points 3 μ away from the original interface. These values are compared to the lattice diffusion coefficient of about 3×10^{-18} cm²/sec for ^{95}Nb in monocrystalline tungsten, showing the influence of short-circuiting paths on the measured diffusion coefficients. The investigators emphasize that these observations may help explain some "anomalous" diffusion curves found in past work with certain body-centered cubic metals.

Results of titanium diffusion in titanium-modified Hastelloy N at temperatures between 800 and 1250°C were also reported by Oak Ridge.[93] This study was undertaken to determine whether the selective removal of titanium from the alloy during corrosion is a diffusion-controlled phenomenon. After the specimens

were diffusion annealed, they were analyzed by serial sectioning and gamma spectroscopic detection of ^{44}Ti. The data fit the equation $D = 15.3 \exp(-72{,}000/RT)$ cm^2/sec.

A study of carbon diffusion in rhenium was completed in France[94] by heating carburized rhenium ribbon in oxygen at temperatures between 1500 and 2000°K. Allowing that carbon diffusion in rhenium was the rate-limiting process, the rate of CO expulsion was determined by mass spectroscopy and used to determine the diffusion coefficients. An activation energy of 53,000 ± 5000 cal/mole was found, and the frequency factor was 0.1 ± 0.04 cm^2/sec.

In India, studies have been made on the diffusion of niobium in aluminum,[95] chromium and iron in Zircaloy-2,[96] and molybdenum in zirconium.[97] A combination of diffusion paths was suggested by the data in the Nb–Al experiments. The diffusivity of niobium within a 20-μ depth into aluminum followed the equation $D = 1.656 \times 10^{-7} \exp(-19{,}650/RT)$ cm^2/sec. Diffusion of chromium and iron in alpha and beta Zircaloy was studied by measuring the residual activity of isotopes after diffusion anneals between 650 and 1250°C. The results are shown in Table III-6.

Table III-6 Diffusion of Chromium and Iron[96] in Zircaloy-2

Diffusing element	Temperature range, °C	Frequency factor, cm^2/sec	Activation energy, cal/mole
Cr	650–780	2.91×10^{-6}	35,620
Cr	980–1250	6.31×10^{-2}	51,040
Fe	650–780	2.56×10^{-8}	27,110
Fe	980–1250	1.03×10^{-2}	46,767

In the phase-transition range 780 to 980°C, the authors suggest using a statistical average of diffusivity on each phase to determine the average diffusion of the element in Zircaloy-2. The residual-activity method was also used in the study of molybdenum diffusion in zirconium. Short-circuiting diffusion paths apparently contributed to some anomalous effects in both phases. The authors analyzed the curvature in temperature-dependent plots above 1000°C for possible high-temperature enhanced-diffusion mechanisms and developed a composite equation to describe diffusion of molybdenum in beta zirconium.

The Soviet literature describes a number of diffusion studies conducted with refractory metals. The interdiffusion of tantalum and tungsten was studied[98] with ground samples held at 2000°C for 48 hr. Concentration curves were plotted from X-ray microanalytical data. The diffusion coefficient of tantalum was strongly sensitive to the tungsten concentration in the interface; it decreased from 4.7×10^{-11} to 0.8×10^{-11} cm^2/sec as the tungsten concentration increased from 10 to 50 wt.%, and then it increased gradually to 1.9×10^{-11} cm^2/sec as the tungsten concentration was increased from 50 to 90 wt.%.

In another study, diffusion of iron, chromium, and tungsten in titanium and its alloys was examined[99] using titanium samples prepared from powder. The powder was molded into slabs and sintered at 1300 to 1500°C for 4 to 6 hr. Porosity of samples used was less than 2%. In some cases the titanium slabs were deformed by 10% reduction before diffusion annealing. Radioactive isotopes ^{51}Cr, ^{59}Fe, and ^{185}W were applied to the faces of the specimens, and the specimens were diffusion annealed at 700 to 1323°C in a resistance furnace for 1 hr to several days; the diffusivity was then determined by layer removal and measurement of residue activity in the specimens. Diffusion in titanium and titanium alloys was generally found to be linear on an Arrhenius-type plot. Some results are shown in Table III-7. Large deviations from a normal temperature-dependent curve for iron diffusion in titanium at 750°C were caused by phase transformations. The influence of the phase transformation on chromium and tungsten diffusion was not established. The addition of alloying elements to titanium causes an increase in the diffusivity of chromium and iron in titanium but results in a decrease in the diffusivity of tungsten in titanium.

Table III-7 Diffusion Constants for Titanium and Titanium-Base Alloys[99]

Diffusing element	Solvent	Activation energy, kcal/gram atom	Frequency factor, cm^2/sec
Cr	Ti	68	800
Cr	Ti*	67	200
Fe	Ti*	50	20
W	Ti*	49	0.3
Cr	Ti + 10% Cr	50	0.4
Fe	Ti + 10% Cr	45	2
W	Ti + 10% Cr	47	0.03
Cr	Ti + 10% W	48	0.5
W	Ti + 10% W	58	0.4

*Deformed 10%.

Diffusion in Miscellaneous Metallic Systems

A study of ^{233}U diffusion in single-crystal and polycrystalline UO_2 has been carried out by Reimann and Lundy.[100] After depositing ^{233}U onto single crystals of UO_2 and annealing in a mixed CO/CO_2 atmosphere at 1400°C for 4.34×10^5 sec, the investigators could detect no penetration of the tracer within the limits of the spectrometer. The true lattice diffusivity of ^{233}U in UO_2 at this temperature was determined to be no more than 10^{-17} cm^2/sec, but this is 2 to 3 orders of magnitude lower than the lattice-diffusion values obtained by other investigators who used polycrystalline UO_2 in their studies.[101] The discrepancy strongly suggested that diffusion in polycrystalline UO_2 occurred by short-circuiting paths. To check this, the authors subjected a polycrystalline sample of UO_2 to the same process as was carried out on the single crystal, except that the diffusion anneal was made at 1385°C for 9.25×10^5 sec. The sample also had a gradient of grain sizes—large on one side, small on the other. Tracer penetration into the sample from the small-grain side was considerable, whereas that into the large-grain side was nil. Autoradiographic inspections verified that tracer penetration occurred exclusively via the grain boundaries.

Diffusion of Gases and Permeation Studies

A method for measuring rates of hydrogen permeation in metals at room temperature is described[102] which permits measurements on the order of 10^{-17} cm^2 (STP)/(sec)(cm^2)/mm of metal. Tritium gas and conventional counting equipment are used, and techniques for determining the very low permeation rates at room temperature are described and illustrated.

In a Soviet study[103] the activation energy for diffusion of hydrogen in face-centered cubic metals was calculated from semiempirical determinations of energies associated with certain lattice positions of the hydrogen atoms. The activation-energy values ranged from 7000 cal/mole for silver to 10,000 cal/mole for nickel. The authors discuss the possible mechanisms for hydrogen diffusion in these metals suggested by their results.

Peterson and Hammerberg[104] contributed additional data to the literature of hydrogen diffusion in body-centered cubic metals with their study of diffusion in barium. Barium hydride was formed at one end of barium bars encapsulated in stainless steel except for this end. The hydrogen concentration was maintained at the solubility limit during the diffusion anneal by reacting the exposed end with hydrogen. After the diffusion run, the hydride surface layer was removed, the stainless-steel jacket was machined off, and serial sections were vacuum-fusion analyzed for hydrogen content. In the range 200 to 620°C, the data fit the equation $D = 4.0 \times 10^{-3} \exp [(-4540 \pm 570)/RT]$ cm^2/sec. The author interprets the activation energy to be a variation in bonding energy of the hydrogen with penetration distance, rather than the energy associated with a lattice strain at the saddle point.

Helium diffusion in tantalum was investigated[105] by measuring the dissipation of elastic energy as a function of temperature and vibration frequency. The tantalum specimen was vacuum annealed and then held in a helium atmosphere at 800°C for several hours; this produced dissipation peaks at certain frequencies. The shape of the peaks or the shift in peaks with frequency can be used to calculate the activation energy. For helium in tantalum the activation energy was 0.05 ev, and the preexponential factor was 4.4×10^{-10} cm^2/sec.

In a study of ^{133}Xe diffusion in CsI single crystals,[106] the single crystals were grown containing ^{133}I which decayed to ^{133}Xe. The time rate of ^{133}Xe release was measured at low gas concentration, and the data fit the equation $D = 0.57 \exp [(-1.01 \pm 0.04 \text{ ev})/RT]$ cm^2/sec. At high gas concentrations, radiation damage created traps that decreased gas diffusion rates. Rare-gas-diffusion measurements on uranium-doped crystals produced anomalous diffusion results that were traced to inhomogeneities in the uranium. Diffusion of ^{133}Xe from CsI and CaF_2 crystals cut at different crystal orientations appeared to be influenced by crystal orientation.

The permeation and diffusion behavior of deuterium in Pyrex glass was studied[107] for temperatures between 100 and 300°C. The glass bulb was blown and annealed at 600°C for 30 min; the diameter was then measured with a cathetometer. Thicknesses were originally calculated; but, after permeation studies were completed, thicknesses were measured by breaking the bulbs. Calculated values were in good agreement with the measured value of 0.047 mm. Deuterium gas was admitted to the bulb, and the gas flux through the bulb was measured. The bulb temperature was controlled with heater tape and insulation wrapped around the bulb envelope. The absolute rate of permeation was calculated from peak heights after the gas flux was steady, and the diffusion coefficient was calculated from the time course of gas flux from the bulb after

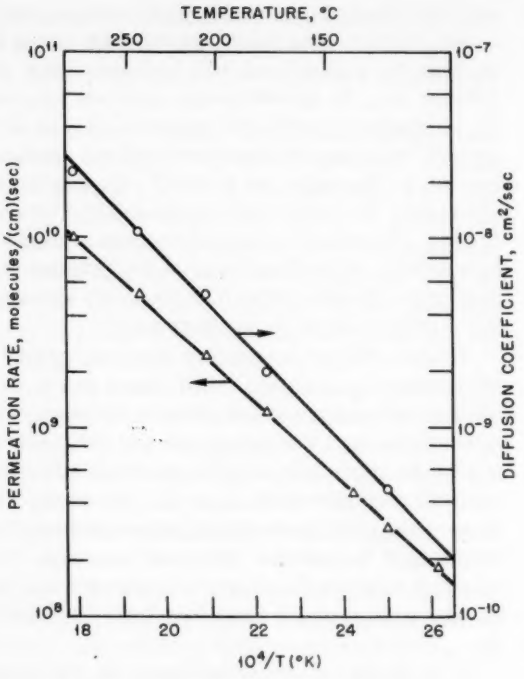

Fig. III-19 Temperature dependence of diffusion and permeation of deuterium in Pyrex glass.[107]

the deuterium was pumped out. These results are presented in Fig. III-19, showing the temperature dependence of permeation and diffusion of deuterium in Pyrex glass. (A. N. Ashurst)

Metallurgy of Refractory Metals

The results of a preliminary study on the properties and heat-treatment of Mo–Hf–C alloys were reported by NASA–Lewis.[108] Nine alloys, containing up to 1.83 at.% hafnium and 1.07 at.% carbon, were prepared by consumable-electrode arc melting, extrusion, and swaging to ¼-in.-diameter bar. The properties evaluated include recrystallization behavior, heat-treatment response, and tensile, creep, and stress-rupture strengths at temperatures to 3000°F (1620°C).

Useful combinations of room-temperature ductility and hot strength were found in most of these alloys, as indicated in Table III-8, which compares tensile properties for a few of these alloys with those of the commercial TZM and TZC alloys. A comparison of the stress-rupture strengths of these alloys in the as-wrought or stress-relieved condition at 2400°F (1315°C) (vacuum of less than 5×10^{-5} torr) is given below.

Alloy composition, (balance Mo), at.%	Stress to cause rupture at 2400°F in 50 hr, ksi
0.18 Hf–0.42 C	40.5
0.39 Hf–0.65 C	35.5
CbTZC	33
TZC	24–30.5
TZM	14

Heat-treatment experiments showed that the 2400°F tensile strengths of the Mo–Hf carbon alloys could be further increased by appropriate solution treatments and/or prestraining at 3000°F. These results suggest that the Mo–Hf–C alloys have a high-temperature-strength advantage over commercial TZC and TZM alloys. This advantage is tentatively attributed to the higher thermodynamic stability of HfC as compared with the carbides found in the other alloys.

As part of a project to develop refractory-metal alloys suitable for high-temperature structural applications,[109] the Bureau of Mines applied solid-solution and precipitation-hardening techniques to niobium and tantalum alloys. Thirty-three alloys were evaluated to determine their formability, strength, and oxidation resistance. Of the elements used for alloying, the most effective strengtheners were W, V, Hf, N, and B. Three alloys had tensile strengths near 40,000 psi at 1200°C: Nb–1 N–5 W–5 V–10 Hf (No. 4), Nb–15 Hf–5 W–0.5 B (No. 31), and Nb–15 Hf–5 W–1 B (No. 32). Oxidation resistance of the high-strength alloys was good. Alloy 4 gained only 34 mg/cm² at 1200°C and 21 mg/cm² at 1000°C in 2 hr. This is better than a twofold improvement over unalloyed niobium. Hot-forming studies were conducted without any protection from oxidation.

Radial heat-flow measurements of the thermal conductivity of W–26 Re have been made over the temperature range 300 to 2200°C by Feith of General Electric.[110] The results of this study identify a small positive temperature coefficient, with conductivity values ranging from 56.0 watts/(m)(°C) at 300°C to about 69.0 watts/(m)(°C) at 2200°C. Measurements of the electrical resistivity for both W–26 Re and for

Table III-8 Tensile Properties of Selected Mo–Hf–C and TZM and TZC Alloys[108]

Alloy content, (balance Mo), at.%	Test temp., °F	Tensile properties: As wrought or stress relieved — Ultimate strength, ksi	Yield strength, ksi	Elongation, %	Reduction in area, %	As recrystallized — Ultimate strength, ksi	Yield strength, ksi	Elongation, %	Reduction in area, %
0.18 Hf–0.42 C	RT			4	3	80.1	54.4	38	49
	2400	71.4	68.9	12	59	33.6	17.9	48	78
	3000	25.6	24.9	22	98	13.7	8.8	65	98
0.39 Hf–0.65 C	RT	151	139	12	31	86.9	60.6	35	44
	2400	70.7	67.7	18	57	35.3	22.6	37	85
	3000	21.2	19.5	20	88	15.1	10.1	59	98
0.96 Hf–0.82 C	RT	195	145	8	8	90.4	56.2	27	37
	2400	66.8	64.2	14	67	46.4	28.1	24	79
	3000	29.1	27.3	25	76	15.4	14.5	39	93
TZM*	RT	108.7	105.4	28	75				
	2400	47.8	46.3	18	>98				
	3000	10.3	7.6	75	>98				
TZC†	RT	112.1	98.8	30	59				
	2400	47.1	46.5	18	86				
	3000	22.2	21.8	35	>98				

*Commercial heat; composition was Mo–0.5 Ti–0.096 Zr–0.016 C.
†Commercial heat; composition was Mo–1.2 Ti–0.172 Zr–0.11 C.

unalloyed tungsten were employed to calculate the electronic contribution to the thermal conductivity of the W–Re alloy. At 300°C the electronic contribution was calculated to be about 65% of the thermal conductivity, whereas at 2200°C the conductivity was about 90% electronic.

The high-temperature properties of chemical-vapor-deposited (CVD) tungsten, in particular the grain stability and bubble formation, are directly related to fluorine impurities in fluoride tungsten. Workers at Oak Ridge[36] found that samples which contained 6 ppm fluorine had very few bubbles on the grain boundaries and showed some grain growth after being annealed at 1800°C. At higher annealing temperatures (2500°C), extensive grain growth took place, and bubbles with an average diameter of 1.7 μ covered about 18% of the grain-boundary area. When the fluorine content was increased to 30 ppm, no grain growth occurred at 2500°C, and bubbles with an average diameter of 2.3 μ covered about 38% of the boundary area. In tungsten deposited from WCl_6 rather than WF_6, a different type of behavior occurred. Although the chloride tungsten contained 7 ppm fluorine, much greater grain growth occurred, and little or no bubble formation was observed by electron microscopy.

The reasons for this anomalous behavior are not known, but they may result from a difference in the nature of the fluorine impurities in the chloride material due to the difference in deposition conditions. Chloride tungsten is usually deposited between 900 and 1100°C, whereas fluoride tungsten is normally deposited between 500 and 700°C. The reaction product of the fluoride deposit is HF, and that of chloride deposits is HCl. The trace impurities in the deposition system are very likely different, too. Of particular interest is the increase in efficiency of thermionic emitters made from chloride tungsten rather than fluoride tungsten, due to the higher bare-work function of the (1 1 0) preferred orientation that can be obtained under special deposition conditions in chloride tungsten. Fluoride tungsten normally has a (1 0 0) preferred orientation that approaches a more random structure for those deposition conditions which produce a lower fluorine content.

The scavenging of oxygen from dislocation and grain-boundary sites by rhenium in solid solution in tungsten appears probable and is believed by Novick and Machlin[111] to be the basis of the increment in ductility known to be associated with the addition of rhenium to tungsten. The assumption that rhenium acts to increase the lattice solid solubility by the

formation of ReO complexes was found to be in quantitative agreement with data derived from field-ion-microscope observations.

In a Lawrence Radiation Laboratory study,[112] tungsten, W–25 Re, and W–30 Re alloys were plastically deformed in the 1400 to 1900°C temperature range at creep stresses up to 10,000 psi in a vacuum of less than 10^{-8} torr. For tungsten the activation energy for creep was calculated to be about 100 kcal/mole, i.e., considerably less than an earlier value of 140 kcal/mole found for volume self-diffusion. The rate-controlling deformation mechanism during creep was ascribed to dislocation climb. For the W–25 Re alloy, two distinct rate-controlling mechanisms, dependent on grain size, were operative, with activation-energy values of 100 and 62 kcal/mole, corresponding to dislocation glide and grain-boundary sliding, respectively. Solid-solution alloying of tungsten with rhenium was ineffective in promoting creep resistance. The activation energy for W–30 Re also amounted to 100 kcal/mole and was associated with the dislocation-glide model. Creep strength in this last alloy was not enhanced by sigma-phase precipitates in grain boundaries.

Microstructural investigations, using optical and replica electron microscopy, have been conducted by General Electric[113] to characterize the modes of high-temperature creep deformation and failure in rolled sheet of high-purity arc-cast and powder-metallurgy tungsten. The observations indicate that, whereas arc-cast material deforms in a ductile fashion and fails transgranularly, powder-metallurgy material is relatively brittle and fails intergranularly by the formation and linkup of creep cavities. At lower temperatures (<2000°C), these cavities were irregular in shape and tended to be flattened along the grain boundaries, whereas at higher temperatures the cavities exhibited polyhedral shapes. Measurements showed that creep porosity in the powder-metallurgy samples accounted for approximately 16% of their total deformation. Although these studies failed to show any evidence of precipitation which might explain the basic difference in failure mechanisms of the two types of tungsten, the occurrence of sintering pores in the powder-metallurgy material probably contributes to its embrittlement.

In addition to the work described above, General Electric has examined the microstructure of wrought, arc-cast, polycrystalline tungsten after creep-rupture testing.[114] The stress levels for these tests ranged from 0.21 to 5.62 kg/mm² (300 to 8000 psi) over the temperature range 1600 to 3000°C. By means of optical and electron microscopy and Laue X-ray diffraction techniques, the subgrain sizes, dislocation densities, and subgrain-boundary tilt angles and dislocation contents were determined and correlated with the creep conditions. These observations showed that subgrain sizes were independent of test temperature and were inversely related to creep stress, that the density of free dislocations depended upon both temperature and stress, and that subgrain misorientations were generally small, averaging less than 0.5°. Crystallographic analysis indicated that tilt, twist, and mixed-type subgrain-boundary dislocation networks were formed during creep. These networks were composed principally of dislocations having $a/2\langle 1\,1\,1\rangle$ Burgers vectors, with short $a\langle 1\,0\,0\rangle$ segments at nodal points.

The yield strength of a dispersion-hardened W–3.8 vol.% ThO_2 alloy in both the recovered and recrystallized conditions was examined by King and was compared with those of pure tungsten over the 325 to 2400°C temperature range.[115] Results for the recrystallized alloy indicated that Orowan's mechanism for fine-particle strengthening is obeyed during yield. In the recovered alloy, yield strength was further enhanced by the retained substructure, which is stable up to temperatures in excess of 2700°C. The yield stress of the alloy in the recovered state was greater by a factor of about 5 than that of recrystallized pure tungsten. After the alloy was recrystallized at 2850°C, its yield strength was greater by a factor of 2 than that of pure tungsten annealed at the same temperature. Contributions to the yield strength of a dispersion-hardened alloy are believed to come from the yield strength of the single-crystal matrix, the Orowan-related yield stress, and the substructure-related yield stress. (J. H. Peterson)

Nonfueled Refractories

Carbide–Carbon Composites and Alloys

Researchers at Los Alamos[116] have reported preliminary data on the mechanical and physical properties of extruded carbide–graphite composite materials. The compositions investigated ranged from 0 to 40 vol.% NbC in graphite. The extruded, heated (to 2500°C) composites attained a density of 84% of theoretical. The mechanical and physical properties of the composites are shown in Tables III-9 and III-10. In general, it was shown that the compressive and flexure strengths, compression deformation, modulus of elas-

Table III-9 Mechanical Properties of Extruded NbC–C Composites[116]

Nominal vol.% carbide	Filler carbon*	20°C compressive strength, ksi	20°C flexure strength, ksi		90-min compressive deformation	
			1/3 point	3 points	Cyclic†	Single point‡
10	S-97	14.0	7.7	8.2	0.80	0.08
20	S-97	15.2	7.2	10.0	0.10	0.08
30	S-97	19.2	10.1	11.0	0.15	0.18
40	S-97	24.6	11.5	12.2	0.20	0.20
40	1008	22.2	12.1		0.10	0.00

*The S-97 flour was obtained from Speer Carbon Company; nominal Fischer particle size = 4.75 μ. The 1008 flour was S-97 flour ground to a nominal Fischer particle size of 0.6 μ.
†Nine 10-min cycles at 2500°C, 500 psi.
‡One 90-min cycle at 2500°C, 500 psi.

Table III-10 Physical Properties of Extruded NbC–C Composites[116]

Nominal vol.% carbide	Filler carbon*	Density, g/cm³			Electrical resistivity at 20°C, 10^{-6} milliohm/cm	Coefficient of thermal expansion (20 to 2000°C), 10^{-6}/°C		Dynamic modulus at 20°C, 10^6 psi
		Theoretical	Calculated	Immersion		Across grain	With grain	
10	S-97	2.93	2.46	2.48	927	5.71	4.30	3.20
20	S-97	3.62	3.02	3.05	584	6.19	5.35	3.69
30	S-97	4.39	3.68	3.70	317	6.73	6.25	5.18
40	S-97	5.12	4.25	4.27	183	7.23	6.80	7.08
40	1008	5.15	4.10	4.32	239	7.21		

*The S-97 flour was obtained from Speer Carbon Company; nominal Fischer particle size = 4.75 μ. The 1008 flour was S-97 flour ground to a nominal Fischer particle size of 0.6 μ.

ticity, and thermal expansion increased with increasing carbide content. The electrical resistivity decreased rapidly with increasing carbide content. It was demonstrated that the graphite flour used in the preparation of the composites can greatly affect mechanical and physical properties.

The preparation of HfC–C alloys utilizing arc-melting and centrifugal-casting methods has been investigated by Adams et al.[117] The alloys contained between 6.3 and 13.5 total wt.% carbon and 2 wt.% zirconium. The mold material for casting was graphite. An interesting method was employed to hold the mold together for initial casting but to allow the mold to part before severe casting shrinkage had occurred. This involves using iron wire to hold a two-piece mold together. After partial solidification of the cast carbide, the iron wire melts, allowing the mold to separate and permitting the cast part to contract freely during complete solidification. The thickness of the graphite mold is used to assist in controlling the solidification rate of the part. In general, electrical resistivity of the composites increased as the carbon content increased up to 1400°C. For example, the 10.4 wt.% carbon material exhibited a room-temperature resistivity of 35 μohm-cm as compared with 171 μohm-cm at 1400°C. The coefficients of linear expansion for 5.1 and 12.3 wt.% carbon structures were 6.33 and 6.42 x 10^{-6}/°C between 100 and 900°C. The reactions of the HfC–C composites with various refractory metals are reported in Table III-11. Mechanical properties of the cast composite structures are shown in Table III-12. It was noted that the higher graphite-content composites, owing to their crack-arresting characteristics, were better able to resist gross failure. Quality castings containing 9 to 13.5 wt.% carbon could be produced by arc-melting and centrifugal-casting methods, but crack-free, single-phase HfC castings and compositions near the eutectic composition could not be prepared.

Other studies by the Albany Metallurgy Research Center, Bureau of Mines,[118] have been performed on NbC–C fusion-cast and hot-pressed alloys and hot-

Table III-11 Minimum Melting Temperatures Observed for Refractory Metal–Hafnium Carbide Combinations[117]

Refractory metal	Temp., °C
Vanadium	1790
Zirconium	1850
Titanium	1655
Niobium	2310
Molybdenum	2350
Tantalum	2680
Tungsten	2730

Table III-12 Tensile Properties of Cast HfC–C Composites[117]

Carbon wt.%	Temp., °C	Tensile strength, psi	Modulus of elasticity, 10^6 psi
8.9	20	12,450	33.7
9.9	20	14,135	*
10.0	20	8,580	*
12.4	20	4,135	*
10.4	1050	15,890	20.6
10.8	1050	15,300	19.3
12.5	1050	18,300	16.3
9.9	1400	18,720	15.2
10.5	1400	13,850	*
10.8	1400	16,080	18.1
10.0	2400	18,700	15.5
11.3	2150	16,340	17
11.6	2150	16,350	*
10.0	2400	12,580	7.3
11.4	2400	11,895	6.1
11.5	2400	13,510	7.4

*Not determined.

pressed ZrC–C composites. Both fusion-cast and hot-pressed alloys oxidized noticeably at about 500°C, and with sharply increasing rapidity above 600°C. The air oxidation rate of alloys increased with increasing carbon content. For example, at 600°C the oxidation rate for the hypereutectic niobium alloy was about three times as fast at that for the NbC. The ZrC–C was more resistant to oxidation in air than the NbC–C material.

The coefficient of linear thermal expansion for commercial hot-pressed NbC–C and ZrC–C between 20 and 2400°C was relatively independent of carbon content between 11 and 20 wt.% carbon. Coefficients for both NbC–C and ZrC–C ranged between 7.2 and 7.8×10^{-6}/°C for the 20 to 1200°C range and from 9 to 11×10^{-6}/°C for the 1200 to 2200°C range. The resistivity of hypoeutectic NbC–C alloys was similar whether the materials were fusion cast or hot pressed. The resistivity increased with increases in either temperature or carbon content. The resistivity of castings was slightly lower than the resistivity of hot-pressed composites. For hypereutectic NbC–C alloys, however, the resistivity of castings increased very markedly with increased carbon content, whereas the resistivity of hot-pressed composites increased gradually with increased carbon content. This difference in resistivity behavior was attributed to the difference in the shape of free graphite in the microstructures. The resistivity of hypoeutectic hot-pressed ZrC–carbon alloys, however, was noted to be considerably higher than that of fusion-cast material. The hot-pressed alloys exhibited anisotropic properties.

Rossi and Carnahan[119] discuss the mechanical properties of group IV refractory-metal carbides fabricated by arc-melting techniques as related to microstructure. The relations between microstructure and properties of composites of the group IV carbides and graphite are presented and shown to be strongly dependent on total carbon content. Of particular importance is the enhanced resistance of hypereutectic carbide–graphite alloys to thermal-stress environments. Although material in this composition range is mechanically weaker than hypoeutectic alloys, the thermal-shock resistance is attributable to its inherent capacity for absorption of elastic energy released by a propagating crack and the ability of graphite flakes to blunt a crack tip.

Refractory-Metal Carbides

Several Russian investigators[120] have reported their findings on the effect of high pressure on the structure and hardness of some refractory carbides. The carbides of Cr, Nb, Ta, and W were subjected to 1.4×10^6 psi pressure at 1400°C. A noted increase in microhardness was measured within the range of 2600 to 3000 kg/mm^2 for all the carbides. A widening of the X-ray diffraction lines accompanied the increase in microhardness.

A review of available data on the thermal expansion of WC was published in India.[121] Also, experiments were performed taking X-ray powder pictures of WC at different temperatures with a high-temperature symmetrical focusing camera. Lattice parameters were

evaluated and compared with previous results. A list of 20 references is included.

Zirconium Carbide

Soviet investigators[122] have reported the results of hot-hardness measurements of sintered ZrC. Two test methods were employed: the static method and the dynamic method (according to the extent of the rebound of the spherical indentor), at 900 to 1650 and 2500°C, respectively. The dynamic tests apparently showed that the hardness of specimens of ZrC decreased markedly with increasing temperature. At room temperature, ZrC is a brittle relatively nonplastic material; but, beginning at 1500 to 1600°C, it undergoes considerable softening (plasticizing). The static tests, on the other hand, indicate that loss of hardness commences at lower temperatures (1000 to 1200°C). The proposed reason for this discrepancy is that the specimens in the static tests contained less carbon, i.e., the content of this component in the alloy did not correspond to its stoichiometric composition. Thus, for example, as the carbon content decreases (compared with its stoichiometric content), hot hardness sharply decreases (roughly in half when the temperature rises from 930 to 1270°C). There was no mention of creep and strain-rate effects on plastic deformation.

Brown et al.[123] have determined the wave velocities that are used for elastic-property calculations at 23°C for monocarbides of Ti, Zr, Hf, Nb, Ta, and W. The data show the expected anisotropy to be found in die-pressed materials. Elastic moduli for ZrC, calculated from the data for isostatically pressed material, show good agreement with previously published data.

Silicon Carbide

Gulden[124] has studied the mechanical properties of chemically vapor-deposited beta SiC between room temperature and 1400°C. Material with grain diameters in the range from less than 1 μ up to 15 μ exhibited bend strengths between 106 and 140 ksi at room temperature. No grain-size dependence of the bend strength of dense (>99% of theoretical) SiC was observed at any test temperature. The fracture strength of dense SiC remained approximately constant between room temperature and about 900°C and then increased sharply up to the maximum test temperature of 1215 or 1400°C. This increase in fracture stress coincided with the onset of detectable plastic yielding in the stress-strain curves. The fracture mode of this material at all test temperatures was transgranular cleavage. The fracture stress of SiC of lower density, which was characterized by the presence of grain-boundary flaws, decreased slightly at high temperature. The fracture mode of this material appeared to be intergranular at high testing temperatures.

Price has reported[125] the effects of fast-neutron radiation on pyrolytic silicon carbide. Samples of pyrolytic polycrystalline beta silicon carbide were irradiated to 2.0 to 4.2×10^{21} neutrons/cm^2 ($E > 0.18$ Mev) at temperatures between 460 and 1040°C. The samples showed an isotropic linear expansion that decreased with increasing irradiation temperature from 0.35% at 460°C to 0.05% at 1040°C. The lattice-parameter changes were equal to the macroscopic dimensional changes, within experimental accuracy. Irradiation caused a slight increase in X-ray line broadening that was attributable to the generation of internal strains. There was no significant change in Young's modulus or the modulus of rupture.

(W. C. Chard)

Concrete

The first prestressed-concrete pressure-vessel reactor (PCPVR) in the United States, a high-temperature gas-cooled reactor, is being built by Gulf General Atomic for the Fort St. Vrain Station, Public Service Company of Colorado.[126] The internal dimensions of the vessel are 31 ft in diameter and 75 ft high. Wall thickness is 9 ft. The vessel is designed to be operated at 700 psig.

Confidence in the expected performance of the PCPVR stems from both model tests and performance data available on operating PCPVR's in France and England. Detailed results of model tests on the Fort St. Vrain reactor have been published.[127] Data were obtained on the creep of concrete in a one-quarter-scale vessel exposed to sustained temperatures up to 140°F (60°C). Both mechanical and thermal loading conditions were investigated.

The measured creep rate of concrete in the model was less than that observed in similar concrete tested as sealed 6-in.-diameter by 12-in.-high cylinders in uniaxial compression. This effect was most pronounced at the elevated temperatures employed in the study. A reasonably good prediction of the creep of the model concrete was achieved through a viscoelastic-finite-element analysis that used creep data obtained on the English Wylfa PCPVR. (D. R. Lankard)

References

1. B. Cox, Effects of Irradiation on the Oxidation of Zirconium Alloys in High-Temperature Aqueous Environments, *J. Nucl. Mater.*, **28**(1): 1-47 (October 1968).
2. A. B. Johnson, Jr., Effects of Nuclear Radiation on the Corrosion, Hydriding, and Oxide Properties of Six Irradiated Zirconium Alloys, USAEC Report BNWL-SA-1719(Rev.), Battelle–Northwest, September 1968.
3. M. S. Hunter and W. G. Fricke, Jr., Study of Crack-Initiation Phenomena Associated with Stress Corrosion of Aluminum Alloys, Report NASA-CR-98161 (N69-13202), Aluminum Company of America Research Laboratory, July 15, 1968.
4. S. B. Brummer, R. O. Bell, F. H. Cocks, A. Cordellos, M. Krebs, and J. Russo, Study of the General Mechanism of Stress Corrosion of Aluminum Alloys and Development of Techniques for Its Detection, Report NASA-CR-98098 (N69-10637), TYCO Laboratories, Inc., 1968.
5. N. Balai, C. R. Sutton, and M. R. Sims, Final Surveillance of EBWR Pressure Vessel Following the Plutonium Recycle Program, USAEC Report ANL-7117(Suppl.), Argonne National Laboratory, September 1968.
6. Atomic Energy of Canada Limited, unpublished data.
7. M. Kowaka and S. Nagata, Transgranular Stress-Corrosion Cracking of Mild Steels and Low Alloy Steels in the H_2O–CO–CO_2 System, *Corrosion*, **24**(12): 427-428 (December 1968).
8. R. B. Benson, Jr., R. K. Dann, and L. W. Roberts, Jr., Hydrogen Embrittlement of Stainless Steel, *Trans. Met. Soc. AIME*, **242**: 2199-2205 (October 1968).
9. L. F. Trueb, Corrosion and Stress-Corrosion Cracking of Explosively Shocked Austenitic Stainless Steels and Explosion-Bonded Stainless Steel-to-Steel Clads, *Corrosion*, **24**(11): 355-358 (November 1968).
10. V. L. Hill, Development of Oxidation-Resistant Hafnium Alloys, April 1, 1967–March 31, 1968, Report IITRI-B6079-4, Illinois Institute of Technology Research Institute.
11. F. Bollenrath and P. Poddey, Oxidation Behavior of Nb Up to 1000°C, *Metall.*, **22**: 702-706 (July 1968).
12. M. Yamawaki and T. Mukaibo, Effect of Zirconium Alloying on High-Temperature Oxidation of Niobium, *Denki Kagaku*, **36**: 671-675 (September 1968).
13. M. S. Tsirlin and L. M. Kovba, X-Ray Investigation of the Scale Formed upon Oxidation of Alloys in the Nb–Zr System, *Vestn. Mosk. Univ., Ser. II Khim.*, No. 5: 4-7 (September–October 1968).
14. I. A. Tregubov and A. T. Grigorev, Investigation of the Oxidizability of the Alloys Nb–V, Nb–Zr, and Nb–Zr–V at the Temperatures 500 and 900°C, *Izv. Akad. Nauk SSSR, Metal.*, No. 4: 209-211 (July–August 1968).
15. C. A. Barrett, Absorption Rate Sticking Probabilities for Oxygen on Columbium and Dilute Columbium–Zirconium Alloys, Report NASA-TN-D-4885, National Aeronautics and Space Administration, Lewis Research Center, November 1968.
16. M. D. Scheer and J. Fine, Reactions of Carbon Monoxide with Tantalum Surface Heated Above 2000°K, *Surface Sci.*, **12**: 102-107 (September 1968).
17. S. S. Brenner and W. J. McVeagh, Field Ion Microscopy Study of the Formation of Oxide Particles on Tungsten, *J. Electrochem. Soc.*, **115**: 1247-1252 (December 1968).
18. S. Hoover, D. Rausch, and P. Gordon, The Role of Contamination in the Kinetics of Oxide Nucleation of Tungsten and Molybdenum, Technical Report No. 2, IIT Project No. 55214, Illinois Institute of Technology, January 1969.
19. H. K. A. Kan and S. Feuerstein, Low-Energy Electron Diffraction Studies of the Interaction of Oxygen with a Molybdenum (1 0 0) Surface, Report SAMSO-TR-68-429, Aerospace Corp., September 1968.
20. N. N. Gratsianskii, N. A. Bogacheva, and S. A. Zhabitskaya, Corrosion Resistance of Pure Niobium in Aggressive Media, *Ukr. Khim. Zh.*, **34**: 1073-1075 (1968).
21. R. Kieffer, H. Bach, and J. Stempkowski, Corrosion Research on Niobium–Tantalum Alloys, *Werkst. Korros.*, **18**: 782-784 (1967).
22. F. F. Faizullin and V. K. Levina, Anodic Passivation and Polishing of Tungsten in Alkali Solutions, *Elektrokhimiya*, **3**: 1225-1228 (October 1967).
23. S. R. Maloof, Dislocation Etch Pitting Studies on Tungsten Single Crystals Under Potentiostatic Conditions, *Corrosion*, **24**: 283-290 (September 1968).
24. J. F. Nejedlik and J. D. Gadd, Coatings for Long Term Intermediate Temperature Protection of Columbium Alloys, Report AFML-TR-68-170, TRW, Inc., October 1968.
25. J. E. Restall, The Development and Testing of Protective Coatings on F48 and SU-16 Niobium Alloys, *J. Less-Common Metals*, **16**(1): 11-36 (September 1968).
26. High Strength Columbium Alloy Coats Itself to Resist Oxidation, *Mater. Eng.*, p. 27 (December 1968).
27. I. M. Miller, An Evaluation of Coated Molybdenum and Columbium Alloys in High-Temperature Supersonic Airstreams, Report NASA-TN-D-4877, National Aeronautics and Space Administration, Langley Research Center, November 1968.
28. J. B. Berkowitz, Mechanism of Oxidation of Ta–10 W Alloy Coated with WSi_2, Report AMMRC-CR-68-08(F), A. D. Little, Inc., April 1968.
29. J. R. Weeks (Comp.), Annual Report of the Nuclear Engineering Department, December 31, 1968, USAEC Report BNL-50149 (S-71), Brookhaven National Laboratory.
30. Atomics International, AEC Unclassified Programs, Quarterly Technical Progress Report, July–September 1968, to be published.
31. General Electric Breeder Reactor Development Operation, Sodium Components Development Program, Mass Transfer Investigations in Liquid Metal Systems, Quarterly Progress Report No. 7, September–November 1968, USAEC Report GEAP-5719, General Electric Company, January 1969.
32. Atomic Power Development Associates, Inc., Quarterly Technical Progress Report on AEC-Sponsored Activities, July–September 1968, USAEC Report APDA-232.
33. M. J. Todd and S. Turner, The Surface Tension of Liquid Sodium and Its Wetting Behaviour on Nickel and Stainless Steels, British TRG-Report-1459, July 19, 1968.
34. D. L. Keller (Comp.), Progress on Development of Materials and Technology for Advanced Reactors During October–December 1968, USAEC Report BMI-1857, Battelle Memorial Institute, January 1969.
35. P. A. Nelson and M. G. Chasanov, Uranium Nitride–

Sodium Paste Fuel for Fast-Reactor Blankets, USAEC Report ANL-7475, Argonne National Laboratory, August 1968.

36. P. Patriarca and W. O. Harms (Comps.), Fuels and Materials Development Program, Quarterly Progress Report for Period Ending September 30, 1968, USAEC Report ORNL-4350, Oak Ridge National Laboratory, February 1969.
37. E. C. Bishop, R. A. Nadler, and G. A. Whitlow, Vanadium Alloy Cladding Development. Quarterly Progress Report for the Period Ending December 31, 1968, USAEC Report WARD-3791-30, Westinghouse Electric Corp., Advanced Reactors Division, February 1969.
38. R. W. Harrison, SNAP-8 Refractory Boiler Development, Corrosion of Oxygen–Contaminated Tantalum in NaK, Topical Report 1, Report GESP-138, General Electric Nuclear Systems Programs, Space Systems, Jan. 14, 1969.
39. A. L. Bement, G. J. Dau, E. A. Evans, and R. E. Nightingale, Reactor Fuels and Materials Development Programs for Fuels and Materials Branch of USAEC Division of Reactor Development and Technology, Quarterly Progress Report, July–September 1968, USAEC Report BNWL-919, Battelle–Northwest, November 1968.
40. J. E. Brocklehurst, Dilation of Neutron Irradiated Graphite Exposed to Liquid Sodium, *Carbon*, 6: 545-554 (August 1968).
41. E. R. Astley, Fast Flux Test Facility Quarterly Technical Report, July–September 1968, USAEC Report BNWL-917, Battelle–Northwest, December 1968.
42. S. J. Rodgers, J. W. Mausteller, and E. F. Batutis, Nickel and Iron Concentration in Sodium, Technical Report No. 27, Mine Safety Appliances Research, June 30, 1954.
43. R. A. Baus, A. D. Bogard, J. A. Grand, L. B. Lockhart, R. R. Miller, and D. D. Williams, The Solubility of Structural Materials in Sodium, in *Proceedings of the International Conference on the Peaceful Uses of Atomic Energy, Geneva, 1955*, Vol. 9, pp. 356-363, United Nations, New York, 1956.
44. Papers presented at the AEC Corrosion Symposium, Battelle Memorial Institute, Columbus, Ohio, May 6, 1968.
    a. R. L. Eichelberger, and R. L. McKisson, Solubility Studies of Metals in Sodium.
    b. R. A. Walker, J. N. Pratt, and B. W. Mott, The Solubility of Metallic Elements in Liquid Sodium.
45. A. W. Thorley and C. Tyzack, Corrosion Behaviour of Steels and Nickel Alloys in High-Temperature Sodium, in *Alkali Metal Coolants*, Symposium Proceedings, Vienna, 1966, pp. 97-117, International Atomic Energy Agency, Vienna, 1967 (STI/PUB/143).
46. R. L. Eichelberger, R. L. McKisson, and B. G. Johnson, Solubility Studies of Refractory Metals and Alloys in Potassium and in Lithium, Report AI-68-110, Atomics International, Feb. 21, 1969.
47. Oak Ridge National Laboratory, Molten-Salt Reactor Program Semiannual Progress Report for Period Ending August 31, 1968, USAEC Report ORNL-4344, February 1969.
48. V. F. Funke, V. K. Dvoryak, and A. V. Kharitonov, Interaction Between Uranium Dicarbide and Molten Readily Fusible Metals (in Russian), *Izv. Akad. Nauk SSSR, Metal.*, 4: 233-237 (July–August 1968).
49. S. Stecura, Solubilities of Vanadium, Titanium, and Zirconium in Liquid Potassium, Report NASA-TN-D-5093, National Aeronautics and Space Administration, Lewis Research Center, March 1969.
50. K. Goldmann and J. M. McKee, Oxygen Effects in a Type 316 Stainless-Steel, Nb–1% Zr, Liquid Potassium System, *Nucl. Appl.*, 6(4): 321-331 (April 1969).
51. J. R. DiStefano, Refluxing Capsule Experiments with Refractory Metals in Boiling Alkali Metals, USAEC Report ORNL-4323, Oak Ridge National Laboratory, January 1969.
52. B. E. Farwell, D. Yee, and S. Nakazato, 9 Cr–1 Mo Steel as a Mercury Containment Material for the SNAP-8 Boiler, Report NASA-CR-72503 (Aerojet 3661), Aerojet-General Corp., January 1968.
53. Argonne National Laboratory, Reactor Development Program Progress Report, November 1968, USAEC Report ANL-7518, Dec. 27, 1968.
54. S. H. Miller, G. J. Moyar, and C. E. Troller, Literature Survey on In-Pile Mechanical Properties; Testing and Theory, USAEC Report KAPL-3453, Knolls Atomic Power Laboratory, Aug. 15, 1968.
55. A. Cowan and W. J. Langford, Effect of Hydrogen and Neutron Irradiation on the Failure of Flawed Zircaloy-2 Pressure Tubes, British TRG-Report-1749, Sept. 4, 1968.
56. R. L. Knecht and P. J. Pankaskie, Zircaloy-2 Pressure Tubing, USAEC Report BNWL-746, Battelle–Northwest, December 1968.
57. C. D. Williams and C. E. Ells, The Influence of Niobium in Irradiation Strengthening of Dilute Zr–Nb Alloy, *Phil. Mag.*, 18(154): 763-772 (October 1968).
58. W. E. Niemuth and J. F. Weissenberg (Eds.), Proceedings of the National Topical Meeting on Fast Reactor Systems, Materials, and Components, Cincinnati, Ohio, April 2–4, 1968, USAEC Report CONF-680419, American Nuclear Society.
59. A. L. Bement, G. J. Dau, E. A. Evans, and R. E. Nightingale, Battelle–Northwest, unpublished, February 1969.
60. E. R. Astley, Battelle–Northwest, unpublished, Mar. 7, 1969.
61. R. E. Skavdahl and E. L. Zebroski, Sodium-Cooled Reactors, Fast Ceramic Reactor Development Program, USAEC Report GEAP-5700, General Electric Company, Advanced Products Operation, November 1968.
62. D. G. Harman, Postirradiation Tensile and Creep-Rupture Properties of Several Experimental Heats of Incoloy 800 at 700 and 760°C, USAEC Report ORNL-TM-2305, Oak Ridge National Laboratory, December 1968.
63. D. A. Woodford, J. P. Smith, and J. Moteff, Effect of Helium Gas Bubbles on the Creep Ductility of an Austenitic Alloy, *J. Nucl. Mater.*, 29(1): 103-110 (January 1969).
64. J. R. Weeks (Comp.), Brookhaven National Laboratory, unpublished, 1968.
65. J. R. Hawthorne and U. Potapoves, Initial Assessments of Notch Ductility Behavior of A533 Pressure Vessel Steel with Neutron Irradiation, USAEC Report NRL-6772, Naval Research Laboratory, July 12, 1968.
66. J. R. Hawthorne and F. J. Loss, Effects of Coupling Nuclear Radiation with Static Service Stresses on Pressure Vessel Material Behavior, *Nucl. Eng. Design*, 8: 108-116 (1968).

67. I. A. El-Shanshowry, I. M. Voronin, and M. S. Abdel-Azirm, Effect of Neutron Irradiation on the Behavior of Copper, Copper + 2 at.% Aluminum and Copper + 2 at.% Magnesium at Elevated Temperatures, *J. Nucl. Mater.*, **29**(2): 161-168 (February 1969).
68. C. E. Ells, Hydride Precipitates in Zirconium Alloys, *J. Nucl. Mater.*, **28**(3): 129-151 (December 1968).
69. D. Lee, Ductility of Textured Zircaloy-2, *Trans. Amer. Soc. Metals*, **61**: 742-749 (December 1968).
70. J. F. R. Ambler, Grain Boundary Hydride Habit in Zircaloy-2, *J. Nucl. Mater.*, **28**(3): 237-245 (December 1968).
71. General Electric Company, Missile and Space Division, AEC Fuels and Materials Development Program, Progress Report No. 76, USAEC Report GEMP-1008, Sept. 30, 1968.
72. W. M. Rumball, the Hardenability of Zr–1.2 Wt.% Cr–0.1 Wt.% Fe, Canadian Report AECL-3050, November 1968.
73. *Selection of Stainless Steels*, American Society for Metals, Metals Park, Ohio, 1968.
74. *Forming of Stainless Steels*, American Society for Metals, Metals Park, Ohio, 1968.
75. *Joining of Stainless Steels*, American Society for Metals, Metals Park, Ohio, 1968.
76. *Machining Stainless Steels*, American Society for Metals, Metals Park, Ohio, 1968.
77. O. Ogunlade and R. D. Watson, Surface Treatments To Improve the Wear Resistance of Type 304 Stainless Steel in Water, Canadian Report AECL-2732, August 1968.
78. E. J. McGowan and J. W. Faber, Effects of Electrical Discharge and Electrochemical Machining on the Fatigue Strength of Selected Structural Materials, USAEC Report WAPD-TM-787, Westinghouse Electric Corp., Bettis Atomic Power Laboratory, January 1969.
79. S. Ray, Effect of Niobium on the Mechanical Properties of an Austenitic Stainless Steel, *Trans. Indian Inst. Metals*, **21**(1): 13-17 (March 1968).
80. Better Nuclear Tube Alloys, *Nucl. Eng. Int.*, **13**(151): 78-79 (December 1968).
81. R. A. Moen, K. R. Wheeler, and J. E. Irvin, Battelle–Northwest, unpublished, December 1968.
82. L. E. Steele, Interim Report of USA Studies on Irradiation Effects to Advanced Pressure Vessel Materials (1967–1968), USAEC Report NRL-Memo-1947, Naval Research Laboratory, Dec. 1, 1968.
83. T. Nishimura, Effect of Chromium Contents on the Isothermal Tempering Characteristics of 3 Mo–Cr Type Steels, *Nippon Kinzoku Gakkaishi*, **32**: 708-713 (1968).
84. G. P. Ray, The Effect of Thermal Cycles on Creep Properties of Alloy Steels for Tubes, *Metallurgia*, **78**: 187-191 (November 1968).
85. T. M. Nilsson, Effect of Working Direction on the Microstructure and Mechanical Properties of an Extruded SAP Alloy, USAEC Report ORNL-TM-2355, Oak Ridge National Laboratory, December 1968.
86. A. L. Dragoo, Diffusion, *Int. At. Energy Agency, Special Issue*, No. 2: 187-202 (July 1968).
87. H. R. Munkelwitz, An Apparatus for Measuring the Diffusion of Impurities in Solids, USAEC Report BNL-13092, Brookhaven National Laboratory, November 1968.
88. M. Rosen and M. Daniel, Zener Diffusion Parameter in the Rare Earth Metals, *J. Less-Common Metals*, **17**: 119-120 (1969).
89. T. C. Wallace, Diffusion and Chemical Kinetics Related to Problems in High Temperature Chemistry of the Refractory Carbides, pp. 133-154, in *Fundamentals of Refractory Compounds*, H. H. Hausner and M. G. Bowman (Eds.), Plenum Press, New York, 1968.
90. H. M. Lee and L. R. Barrett, Diffusion of Carbon and Uranium in Uranium Carbide, *J. Nucl. Mater.*, **27**(3): 275-284 (September 1968).
91. G. Kimmel, A. Bar-Or, and A. Rosen, Interdiffusion Between Nickel and Uranium, *Trans. Amer. Soc. Metals*, **61**(4): 703-710 (December 1968).
92. J. J. Blechet, A. Van Craeynest, and D. Calais, Diffusion and Solubility of Plutonium in Nickel (in French), *J. Nucl. Mater.*, **28**(2): 177-184 (November 1968).
93. S. Peterson (Comp. and Ed.), Metals and Ceramics Division Annual Progress Report Ending June 30, 1968, USAEC Report ORNL-4370, Oak Ridge National Laboratory, October 1968.
94. R. Ducros and P. LeGroff, Measurement of the Coefficient of Diffusion of Carbon in Rhenium (in French), *Compt. Rend., Ser. C.*, **267**: 704-706 (Sept. 16, 1968).
95. G. P. Tiwari and B. D. Sharma, Diffusion of Niobium in Aluminum, *Trans. Indian Inst. Metals*, **20**: 83-86 (June 1967).
96. B. M. Pande, M. C. Naik, and R. P. Agarwala, Diffusion of Chromium and Iron in Zircaloy-2, *J. Nucl. Mater.*, **28**(3): 324-332 (December 1968).
97. R. P. Agarwala and R. A. Paul, Diffusion of Molybdenum in Zirconium, in *Nuclear and Radiation Chemistry*, Symposium Proceedings, Poona, March 6–9, 1967, pp. 542-548, Bhabha Atomic Research Center, Trombay, India, 1967.
98. I. A. Tregubov, L. N. Kuzina, and O. S. Ivanov, Mutual Diffusion of Tantalum and Tungsten (in Russian), *Dokl. Akad. Nauk SSSR*, **180**(2): 423-424 (May 11, 1968).
99. P. L. Gruzin, S. V. Zemskiy, and A. D. Tzutzunnik, Diffusion in Titanium and Titanium-Base Alloys, Report FTD-MT-24-32-68 [translated from *Fiz. Metal. Metalloved.*, No. 5: 366-382 (1958)].
100. D. K. Reimann and T. S. Lundy, Cation Self-Diffusion in UO_2, *J. Nucl. Mater.*, **28**(2): 218-219 (November 1968).
101. F. S. Feates, The Diffusion of Carbon in Single Crystal Graphite, *J. Nucl. Mater.*, **27**(3): 325-330 (September 1968).
102. A. H. Dexter, Measurement of the Permeability of Metals to Hydrogen at Room Temperatures, USAEC Report DP-1108, E. I. du Pont de Nemours & Company, Savannah River Laboratory, April 1968.
103. V. A. Goltsov, P. V. Geld, and V. B. Vykbodets, Activation Energy for the Diffusion of Hydrogen in Metals with F.C.C. Lattices (in Russian), *Fiz. Metal. Metalloved.*, **26**(3): 522-526 (September 1968).
104. D. T. Peterson and C. C. Hammerberg, Diffusion of Hydrogen in Barium Metal, *J. Less-Common Metals*, **16**: 457-460 (December 1968).
105. L. Verdini, Diffusion of Interstitial Helium in Tantalum, *Ric. Sci.*, **38**: 411-417 (May 1968).
106. T. S. Elleman, The Effect of Radiation and Gas Concentrations on Rare Gas Diffusion in Solids: Annual Progress

Report, 1968, USAEC Report ORO-3508-4, North Carolina State of the University of North Carolina, Nov. 1, 1968.

107. H. M. Laska, R. H. Doremus, and P. J. Jorgensen, Permeation, Diffusion, and Solubility of Deuterium in Pyrex Glass, *J. Chem. Phys.*, **50**(1): 135-137 (January 1969).
108. P. L. Raffo, Exploratory Study of Mechanical Properties and Heat Treatment of Molybdenum–Hafnium–Carbon Alloys, Report NASA-TN-D-5025, National Aeronautics and Space Administration, Lewis Research Center, February 1969.
109. H. R. Babitzke, L. L. Oden, and H. J. Kelly, Columbium and Tantalum Alloy Development, USAEC Report BM-RI-7211, Bureau of Mines, Albany Metallurgy Research Center, December 1968.
110. A. D. Feith, Thermal Conductivity and Electrical Resistivity of Tungsten–26 Weight Percent Rhenium, in *Thermal Conductivity*, D. R. Flynn and B. A. Peary, Jr. (Eds.), pp. 371-380, National Bureau of Standards, Washington, D. C., 1968.
111. D. T. Novick and E. S. Machlin, Effect of Rhenium on the Lattice Solid Solubility of Oxygen in Tungsten, *Amer. Soc. Metals, Trans. Quart.*, **61**(4): 777-783 (December 1968).
112. W. L. Barmore, Elevated Temperature Deformation and Electron Microscope Studies of Polycrystalline Tungsten and Tungsten–Rhenium Alloys, USAEC Report UCRL-70524, University of California, Lawrence Radiation Laboratory, October 1968.
113. R. C. Rau and F. T. Williams, Jr., Creep Failure Modes in Arc-Cast and Powder-Metallurgy Tungsten, USAEC Report GEMP-640, General Electric Company, Missile and Space Division, 1967.
114. R. C. Rau, S. F. Bartram, and P. N. Flagella, Microstructure of Arc-Cast Tungsten After High-Temperature Creep Deformation, USAEC Report GEMP-639, General Electric Company, Missile and Space Division, 1967.
115. G. W. King, An Investigation of the Yield Strength of a Dispersion-Hardened W–3.8 Volume Percent ThO_2 Alloy, *Trans. Met. Soc. AIME*, **245**(1): 83-89 (January 1969).
116. R. E. Riley, N. K. Richerson, and D. H. Schell, Extruded Carbide–Graphite Composites, USAEC Report LA-4077, Los Alamos Scientific Laboratory, Oct. 15, 1968.
117. R. P. Adams, M. I. Copeland, D. K. Deardorff, and R. L. Lincoln, Cast Hafnium Carbide–Carbon Alloys, USAEC Report BM-RI-7137, Bureau of Mines, Albany Metallurgy Research Center, June 1968.
118. Bureau of Mines, Albany Metallurgy Research Center, Quarterly Metallurgical Progress Report No. 39, April 1–June 30, 1968, USAEC Report USBM-RC-1347.
119. R. C. Rossi and R. D. Carnahan, Structure-Sensitive Properties of Arc-Melted Carbides, in *Ceramic Microstructures. Their Analysis, Significance, and Production*, R. M. Fulrath (Ed.), pp. 620-635, John Wiley & Sons, Inc., New York, 1968.
120. A. E. Kovalskii, A. I. Prikhna, E. A. Rybakova, I. I. Timofeeva, and A. A. Shul'zhenko, Effect of High Pressure on the Structure and Hardness of Some Refractory Carbides, *Izv. Akad. Nauk SSSR, Metal.*, No. 4: 231-232 (July–August 1968).
121. V. T. Deshpande, R. R. Pawar, and S. V. Suryanarayana, Thermal Expansion of Tungsten Monocarbide, *Curr. Sci. (India)*, **37**: 543-545 (Oct. 5, 1968).
122. N. A. Evstyukhin and V. M. Shchavelin, Investigation of the Hot Hardness of Zirconium Carbide, *Met. Metalloved. Chist. Metal., Sb. Nauch. Rabot*, No. 6: 101-107 (1967).
123. H. L. Brown, P. E. Armstrong, C. P. Kenpter, and J. A. O'Rourke, Directional Variations of Elastic Properties of Some Transition Metal Monocarbide Cubes, *Planseeber. Pulvermet.*, **16**: 114-118 (July 1968).
124. T. D. Gulden, Mechanical Properties of Polycrystalline Beta-SiC, USAEC Report GA-9075, Gulf General Atomic Incorporated, Dec. 31, 1968.
125. R. J. Price, Effects of Fast-Neutron Irradiation on Pyrolytic Silicon Carbide, USAEC Report GA-9042, Gulf General Atomic Incorporated, Nov. 12, 1968.
126. T. E. Northup, Concrete Reactor Vessels Are Coming to U. S., *Power*, pp. 76-78 (February 1969).
127. T. E. Northup and F. S. Ople, Jr., Effects of Temperature on a Prestressed Concrete Reactor Vessel Model, paper presented at the 1968 Fall Convention, American Concrete Institute, Memphis, November 3–8, 1968.

Section
IV
Reactor Materials

Special Fabrication Techniques

Melting, Casting, and Fabrication of Cast Materials

Atomics International[1] conducted an exploratory casting program to determine whether hyperstoichiometric uranium carbide could be cast into rings for fuel for advanced Heavy Water Organic Cooled Reactor (HWOCR) annular element designs. Unique mold-gating systems were developed for both single- and multiple-cavity molds. This resulted in the successful arc casting of uranium carbide fuel rings and hollow cylinders of various outside diameters ranging from 0.75 to 3.5 in., all having a 0.25-in. wall thickness, and lengths up to 6 in. However, additional work is required to resolve existing problem areas and to develop advanced technology for a large-scale, economical, multiple-concentric-ring casting process for the advanced HWOCR fuel concepts.

A review of methods of obtaining high-purity metals has been compiled by Bunshah.[2] Processing and operational steps employed in the preparation of purified compounds for producing high-purity metals are discussed. Chemical reactions that are used to obtain metals from their compounds are also discussed. Vacuum induction melting, vacuum arc melting, electroflux remelting, electron-beam melting, annealing, distillation, casting, and zone refining are discussed as techniques to consolidate and refine primary purified metals. Casting techniques are described, and the capabilities of each process are evaluated. Principles of solidification important to single-crystal growth are given. Techniques used to grow metal single crystals from the melt are described, and a table is included designating the techniques applicable to specific metals. Cutting, handling, and the perfection of melt-grown crystals are discussed. An extensive bibliography is included for each chapter.

Researchers at Oak Ridge[3] are working to improve the strength of zirconium tubing by control of the grain size and texture. They found that the amount of cold work required to obtain fine-grained tubing is more than 20% but less than 54%. Neither reversing the lead ends of tubing in successive passes nor varying the ratio of wall reduction to diameter reduction affected the grain size.

Harvey Aluminum[4] performed a series of upset-forging tests to demonstrate the improvement possible through the use of high-temperature dies. Three materials were used: 7075 aluminum alloy, 811 titanium alloy, and 250 maraging steel.

For 7075 aluminum the material was heated to 800°F, and the dies were heated to 400 to 800°F (205 to 425°C). Increasing die temperatures produced thinner disks with greatly reduced unit forging force. The 811 titanium and 250 maraging steel materials were heated to 1950°F (1065°C), and the dies were heated to 400 to 1400°F (205 to 760°C) in 200°F increments. The 811 titanium data show significant and consistent lowering of the unit forging force and production of thinner disks up through 1200°F (650°C) die temperature. Oxidation and lubrication problems occurred at 1400°F (760°C). The data for maraging steel are incomplete but show a consistent trend of lower unit forging force and thinner disks possible with increasing die temperatures.

Hot-work die steel used for aluminum forging performed very satisfactorily. Inconel 713C used for titanium and maraging steel also performed quite well but showed some shallow thermal cracking attributed to the rapid open-flame heating methods used. The work is not extensive enough to estimate die life. Lubrication problems became serious at temperatures above 800°F (425°C) and particularly so at 1200 and 1400°F (650 and 760°C).

Westinghouse[5,6] is preparing 35- to 40-lb ingots of the following vanadium alloys for evaluation by a number of laboratories as LMFBR (liquid-metal-cooled fast breeder reactor) cladding materials:

V–20 Ti
V–15 Cr–5 Ti
V–9 Cr–3 Fe–1.3 Zr–0.05 C (Vanstar-7)
V–6 Fe–5 Nb–1.3 Zr–0.05 C (Vanstar-9)
V–8 Cr–10 Ta–1.3 Zr–0.05 C (Vanstar-8)

Table IV-1 Extrusion Constants for Vanadium-Alloy Billets[6]

Product	Extrusion ratio, R	Extrusion constant = $P/\ln R$, ksi*				
		V–20 Ti	V–15 Cr–5 Ti	Vanstar-7	Vanstar-8	Vanstar-9
Billets processed at Argonne National Laboratory†						
1.75-in.-diameter bar	3.9 : 1		81.6	77.9	82.3	85.2
0.59-in.-diameter reextruded rod	8.6 : 1	54.3‡	58.4–62.2	46.7–51.9	54.4–59.5	53.6–54.0
0.865-in.-OD by 0.117-in.-wall reextruded tube blank	7.5 : 1		64.8–66.6	51.7–54.7	50.7–57.7	52.2–59.7
0.23- by 0.94-in. reextruded sheet bar		46.0–54.6			50.7–53.4	
Billets processed at Oak Ridge National Laboratory§						
1.81-in.-diameter bar	4.9 : 1		70.0			
0.69- by 3-in. sheet bar	5.7 : 1		71.0	68.0	57.0	74.6
2.12-in.-OD by 0.31-in.-wall tube shell	5.8 : 1		63.0	49.0	55.0	63.0

*For ANL material, P is the average running pressure on stem of extrusion press; for ORNL material, P is the breakthrough pressure on stem of extrusion press; R is the extrusion ratio.

†Billets heated to 1100°C for extrusion.
‡10.5 : 1 extrusion ratio.
§Billets heated to 1200°C for extrusion.

The ingots, prepared by consumable-electrode melting of electrolytically reduced vanadium granules, are being fabricated to rod, sheet, and tubing. High oxygen content of the granules resulted in relatively high oxygen content (800 ppm) in the ingots. Chemical analyses indicated that compositional control of the alloying elements was very good. These ingots were machined to extrusion billets and canned in 304 stainless steel for extrusion at Argonne and at Oak Ridge. The extrusion constants are given in Table IV-1. Both laboratories found that there is little difference in ease of extrusion of the different vanadium alloys. The extrusion constants obtained at Oak Ridge are lower than the primary extrusion constants obtained at Argonne because the extrusion temperature was higher at Oak Ridge. The extruded alloys from both laboratories were to be rolled to rod or sheet or tube, reduced, and drawn. The Vanstar alloys can be rolled at 250°C to sheet, but the V–15 Cr–5 Ti alloy tends to split transversely at mid-thickness. Increasing the rolling temperature is expected to solve this problem.

(D. E. Stellrecht)

Powder-Metallurgy Materials

Consolidation Techniques

The densification of single-phase systems under pressure by hot pressing or pressure sintering was reviewed in a paper[7] presented at the Third International Materials Symposium on Ceramic Microstructure. The number of applications of this technique, where controlled microstructures and improved properties are objectives, is large. A brief evaluation is presented on the state of the art of pressure-sintering-process mechanisms such as phenomenological plastic flow, particle rearrangement by fragmentation and grain-boundary sliding, and enhanced diffusion under stress. Several thermochemical and thermomechanical adaptations of uniaxial pressure sintering are described.

Fabrication of All-Metal Products

Powder-metallurgy wear-resistant alloys have been investigated by Union Carbide.[8] The properties of five wear-resistant alloys made by powder-metallurgy techniques are compared with those made by conventional melting and casting. The alloys concerned were three cobalt-base compositions and one nickel-base and one iron-base alloy. The microstructures of the powder-metallurgy products were much more uniform but had up to 3% porosity. The hardness values were comparable, whereas the tensile properties of the powder-metallurgy products were generally better.

Fabrication of Dispersion-Strengthened Products

The fabrication of a Be–Al composite is the subject of a British patent.[9] Composites of aluminum and beryllium, containing 50 to 90 wt.% beryllium and

having high strength, good ductility, and low specific gravity, are prepared by mixing the beryllium and aluminum powders with an alkaline or alkaline-earth halogen, such as LiF–LiCl, and sintering at 800 to 1100°C for 1 hr. The action of the alkaline-earth halide confines the aluminum within the beryllium, prevents expulsion of the aluminum from the sintered compact, and forms a composite of beryllium particles surrounded by an Al–Be matrix alloy. Density of the compacts can be increased by a double re-press and an intermediate liquid-phase sinter. (C. A. MacMillan)

Plating

Nonelectrolytic Chemical Plating

Preparation of W–5 Re-alloy sheet stock by chemical-vapor deposition was attempted at Oak Ridge.[3] Rhenium and tungsten were codeposited on resistance-heated sheet substrates of Mo–0.5 Ti. The initially observed temperature gradient along the length of the substrate was minimized by reducing the width of the substrate at the ends, where electrical connections to the water-cooled electrodes were made. The alloy was successfully deposited at 750°C, 10 torrs, and using a $H_2/(WF_6 + ReF_6)$ ratio of 12. The direction of gas flow was reversed every 30 min during the 16-hr deposition experiment in an effort to improve thickness uniformity. The average thickness on both sides of the substrate and the rhenium content along the length of the deposit were measured.

A study was initiated at Oak Ridge[3] to determine the metallurgical properties of chloride tungsten, i.e., tungsten deposited from WCl_6, and to elucidate the cause and mechanism for the observed differences in behavior and properties between the chloride and fluoride tungsten. This is discussed in Sec. III under "Metallurgy of Refractory Metals." The possibility of depositing vanadium metal from VF_5, VCl_4, and VCl_3 was also evaluated. Temperatures above 950°C appeared to be required, even for the hydrogen reduction of VCl_3. A considerable amount of that chloride was transferred by argon into the reaction zone along with the hydrogen; however, a somewhat thicker deposit found on the stainless-steel mandrel was identified as principally VCl_2. Construction of a high-temperature induction-heated rig has been in progress for future research on depositing vanadium at higher temperatures.

The vacuum-pack and vacuum-slip-pack processes for forming protective coatings on refractory metals were described by Gadd and coworkers.[10] Apparatus, techniques, and problems associated with laboratory- and production-scale operations were given. The vapor transport and diffusion mechanisms acting during the deposition of the Cr–Ti–Si coating system on niobium, and the process variables, metal-pack or slip composition and particle size, activator type and concentration, system pressure, temperature, diffusion time, and substrate surface preparation, were discussed. Advantages and disadvantages of the vacuum-pack and vacuum-slip-pack processes were considered, and process parameters were listed for depositing various elements on Nb, Ta, Mo, and W.

The behavior of titanium-modified $NbSi_2$ coatings, prepared by siliciding niobium, and Nb–5 Ti, Nb–10 Ti, and Nb–15 Ti alloys, was evaluated by Felten[11] in oxidizing and inert-gas atmospheres between 800 and 1200°C. The oxidation resistance of the coatings was related to the composition of the oxide formed and to thermal-crack formation. It increased with increasing titanium content in the coatings, but the titanium-modified disilicides exhibited a diffusional stability lower than that of $NbSi_2$. Observed at 1000°C and higher was considerable formation of a new titanium-rich ternary phase, "MSi," as a dispersion within the MSi_2 phase and as a discrete layer between the MSi_2 and M_5Si_3 layers in the coating. This ternary phase showed inferior oxidation resistance. Its preferential oxidation was indicated as the potential failure mechanism for titanium-modified silicide coatings of 1200°C and above.

Structure and phase composition of the two- and three-component diffusion coatings of the Cr–Ti–Si system on niobium metal were studied by Zemskov et al.[12] by X-ray and metallographic analyses and microhardness measurements. The chromium diffusion coating consisted of an outer chromium-base solid solution with a precipitated $NbCr_2$ phase at the interface. The titanium coating had a titanium-base solid solution adjacent to a niobium-rich solid-solution layer, and siliciding of the niobium resulted in the formation of $NbSi_2$. X-ray analysis of the Cr–Ti codeposited coating indicated a chromium-rich solid-solution zone at the surface and a layer containing $NbCr_2$ or $(Nb,Ti)Cr_2$ adjacent to it. The Cr–Si coating system had two zones: a mixture or solid solution of $CrSi_2$ and $NbSi_2$ at the surface, followed by a $NbSi_2$ layer. The Ti–Si coating consisted of $TiSi_2$ in the first (surface) zone and of Nb_5Si_3 of various modifications in the second zone. The three-component Cr–Ti–Si coating system was most complex. From the three zones observed, the exterior one had a columnar grain

structure. The composition of this zone, believed to be a complex silicide or a solid solution of silicides, could not be related to any simple silicide of niobium, chromium, and titanium. The third zone was an alloyed $NbSi_2$, and the composition of the middle zone was not resolved. Oxidation of the Cr–Ti–Si coating at 1250°C proceeded 40 to 50 times slower than that of the two-component Ti–Si and Cr–Si coatings.

A generalized description of the ion-plating process along with its various modifications was given by Mattox.[13] The uses and limitations of the process were outlined, and a bibliography of pertinent publications was presented. The ion-plating process has proved to be a useful tool to the laboratory and production technologist. The technique utilizes equipment that is normally associated with vacuum and sputtering technologies and is therefore an easy tool to acquire.

Simultaneous deposition of uranium and carbon from gas mixtures of UF_6 and CH_4 at temperatures ranging from 1400 to 1600°C at pressures of 50 to 150 mm Hg was reported by Marinkovic, Suznjevic, and Dezarov.[14] Highest concentrations of uranium were found in samples deposited at about 1500°C. No definite relation between the amount of incorporated uranium and total gas pressure was observed. Oxidation-kinetics measurements on deposits were made.

The fluidized-bed, entrained-bed, and rotary-drum coating systems have been investigated and considered for remotely coating fuel particles at Oak Ridge.[15] The fluidized-bed coating system appeared to be most suitable, and the design of a remote prototype fluidized-bed coater was completed. The capability of the entrained-bed system to coat, satisfactorily, slightly larger sizes than the fluidized bed was strongly offset by the frequent maintenance requirement of the entrained bed. The 5-in.-diameter fluidized-bed coating unit will permit development of operational and maintenance techniques directly applicable to the fueled graphite line of the Thorium–Uranium Recycle Facility.

Investigation of fluidized-bed coating processes included multiorifice and single-inlet nozzle systems. Coatings were deposited from methane, propane, and acetylene with the multiorifice system showing no significant advantages over the single-inlet nozzle system. The effects of process-controlling parameters (bed temperature, gas flux, inert-gas dilution, charge size, and kernel density and size) on coating density, coating thickness, anisotropy factor of the coating, coating rate, and deposition efficiency using acetylene and a single-inlet system were identified. This evaluation, with the study extended to coatings produced from propane and propylene, was reported by Pratt et al.[16]

Additional studies have been made at Gulf General Atomic[17] on coating conditions and coating properties for coatings produced from methane and propane. The temperature range for the propane-coatings deposition was 1125 to 1700°C and that for methane coatings was 1690 to 1960°C. Coating density was essentially uninfluenced by the propane feed concentration of 20 to 40 vol.%. Coatings deposited from 40 vol.% propane showed a maximum in the deposition rate at a temperature of about 1600°C, where coating density was the lowest. The deposition rate varied with the propane feed concentration. The difference in the deposition rate was greatest at higher temperatures.

Gulf General Atomic[18] also has continued with the evaluation of properties of and irradiation effects in vapor-deposited SiC. Bend strengths of fine-grained (1 μ) and coarse-grained (15 μ) SiC were determined at 25, 1000, 1300, and 1500°C. Preferred orientation in samples of SiC deposited under different conditions was measured. From the X-ray broadening, internal strain measurements were made on a series of deposits prepared between 1300 and 1800°C. Silicon carbide deposited at 1750°C was reported to contain smaller amounts of chlorine than that deposited at 1400°C.

(J. Zupan)

Electroplating

Aluminum electrodeposited in aluminum chloride–lithium aluminum halide–ethyl ether solutions was increased[19] in tensile strength from about 16,000 to 32,300 psi and in yield strength from about 13,000 to 28,700 psi with the addition of pyridine (0.124*M*). Elongation ranged from 8 to 10%. These deposits contained a total of 0.1 wt.% silicon and other metallic impurities, in comparison with 0.04 wt.% metallic impurities for nonstrengthened aluminum electrodeposits. Other organic strengthening agents were identified, but pyridine produced the best results. Among several metallic hardeners, titanium was the most effective. Electrodeposited aluminum containing 0.07 wt.% titanium showed an ultimate tensile strength of 17,400 psi and a yield strength of 14,400 psi when 0.03*M* to 0.04*M* titanyl acetylacetonate had been added to the plating solution.

Nonporous 5-mil-thick zirconium electroplates were deposited at Battelle–Northwest[20] on uranium by using a KF–LiF eutectic containing 2 to 10 mole % ZrF_4. The solution was maintained at 625 to 675°C. The cathodes—uranium fuel elements—were plated at 20 to 40 ma/cm^2. A good bond was obtained. Bath deterioration with use was attributed to chemical decomposition of the electrolyte. Sparging with HF

improved the deposits from an aged, deteriorated solution.

In a Soviet study of the application of ultrasonic energy during the electrodeposition of alloys,[21] it was noted that the molybdenum content of Fe–Ni–Mo alloys was increased with the ultrasonic agitation. This and similar results obtained by others suggest that the concentration of the most active metal (electrochemically) in any alloy system can be increased by ultrasonic agitation of the plating solution. Several metallic electrodeposits have been increased in hardness, according to some reports in the literature on ultrasonics, and some were embrittled. Porosity was reduced, according to some reports. Such generalities may be misleading, however, because there has been no systematic study of the effects of ultrasonics.

An anodic dissolution method was reported by the British[22] for removing thin layers from irradiated silicon wafers. Anodizing at 41 ma/cm^2 in a 0.1*M* aqueous solution of boric acid and sodium tetraborate produced oxide films that were subsequently dissolved in potassium hydroxide solution. The current efficiency for anodic oxidation ranged from 2 to 2.5%, which was higher than the efficiency for any process investigated previously. The rate of oxidation also was higher than the rate for other processes.

(W. H. Safranek)

Explosive Metalworking

A method has been developed by researchers in Italy[23] for explosively welding end plugs onto finned sheaths of tubular fuel elements. It was necessary to modify the conventional explosive-bonding assembly to prevent deformation of the fins. A thick buffer, contoured to fit the outside of the finned tube, was placed between the tube and the explosive; this permitted acceleration of the finned tube to the required collision velocity without any deformation of the fins. Materials bonded (in diameters ranging from 0.7 to 1.4 in.) include SAP and Zircaloy-2. The bonds were helium leak tested and were consistently found to be completely leakfree at temperatures up to 360°C. Work is progressing on the development of a machine capable of producing 100 welded pieces per hour.

A U.S. patent[24] describes the application of explosive-bonding technology to the fabrication of lined bimetallic tubes. In the process the explosive is placed around the outer tube, and a tubular liner is slipped inside, leaving a uniform annular clearance. The liner is filled with water to serve as an internal support mandrel. The water, which behaves as a solid under the high pressure generated during the bonding operation, not only prevents deformation of the tubes but also allows production of lined tubes that have surprisingly close dimensional uniformity. Bimetallic tubes have been produced in the following materials combinations: Admiralty brass–mild steel, stainless steel–mild steel, titanium–mild steel, and aluminum–mild steel. The tubes so made were strong, sound, and metallurgically bonded over their entire interfaces.

Other patents[25,26] describe two specialized applications of the explosive-bonding process. They both employ specially shaped and sized explosive charges to produce controlled-area bonds. One of the patents describes the means by which metal sheets can be explosively spot welded. The explosive charge consists of a small cartridge placed in contact with one of the metal plates and detonated at its top surface. In the other patent a process for producing seam (or line) welds between two or more plates is outlined. This process employs a flexible linear-shaped charge that is placed on the plates to be bonded. Examples of the process are given in which seam welding was used to join up to four plates. It was also shown that two concentric tubes could be bonded together at selected points using this method. (D. Laber)

Welding and Brazing

Welding

Studies related to the molten-salt-reactor program at Oak Ridge[27] indicate that titanium-modified Hastelloy N is a weldable base metal with no problems in the heat-affected zone. Small additions of titanium to Hastelloy N significantly improve its mechanical behavior under irradiation. The titanium-modified material can be welded with filler metals of similar composition. However, cracking problems have been encountered when filler metal from the same heat as the base metal has been used. This is apparently caused by segregation of unidentified elements.

Researchers have also shown that residual welding stresses in Hastelloy N can be reduced by decreasing heat input and by postweld heat-treating. Heat-treatment at temperatures as low as 650°C for 100 hr offers some reduction in stresses. Stresses are almost completely eliminated by treatment at 870°C for 6 hr or 1180°C for 1 hr. Another accomplishment in this program is the satisfactory welding of Hastelloy N that has been irradiated and exposed to fluoride salts. Welds

with properties equal to or better than those of irradiated base metal have been obtained.

During another Oak Ridge program,[3] hot cracking in Inconel 600 weldments is being investigated. Various minor alloying elements have been evaluated for their effects on crack length. Sulfur and phosphorus are both highly detrimental; both manganese and silicon reduce the extent of weld cracking and work better alone than in combination. Titanium and aluminum also reduce the hot-cracking propensity of Inconel 600. It was also shown during this study that silicon, titanium, and phosphorus cause an increase in weld cross-sectional area and depth of penetration, whereas aluminum has the opposite effect.

When circumferential welds are made in tube-to-end-cap joints where high integrity is required, the possibility of cracking should be recognized, according to a recent report by Slaughter et al.[28] Apparently an unusual set of conditions can produce unexpected concentrations of minor elements which cause cracking. This problem was encountered in gas tungsten-arc welding of Inconel fuel elements. Of about 70 welds, 3 were found to be defective. The cracks could not be detected visually or radiographically but were pinpointed by helium sniffing and penetrant methods. They appeared in the tube-and-cap material, and not in the weld metal. A similar problem was encountered in Incoloy 800 welds of the same configuration. The source of contamination could not be determined in either case.

Studies at Rocketdyne[29] with commercial heats of Alloy 718 indicated that manganese in excess of 0.20 wt.%, combined with silicon in excess of 0.25 wt.%, drastically reduces the tendency for microfissuring in welds. This may be attributable to the manganese combining with "free" sulfur to prevent the sulfur from reacting with other elements and causing hot shortness. The high silicon content, on the other hand, may be only coincidental with melting practice. Since all heats in the study had either high or low concentrations of both manganese and silicon, their individual influences could not be assessed.

The presence of magnesium in experimental heats of Alloy 718 in amounts greater than 20 ppm also appeared to inhibit microfissuring and at the same time to improve the tensile properties of the welds. Finally, this research indicated that material with a grain size coarser than ASTM No. 2 has a slightly greater tendency to microfissure than does finer-grained material, even when the Mn–Si content is relatively high.

A state-of-the-art survey[30] on joining ceramics and graphite to other materials, which reviews significant research in this area, has been issued by NASA. An Italian patent[31] has been issued to cover a diffusion welding process for joining dissimilar metals, such as zirconium and steel. The workpieces are first heated to diffusion temperature and then brought sharply into contact, causing plastic deformation. The operation is conducted either in an inert atmosphere or in vacuum.

Brazing

Brazing procedures for metal-to-ceramic seals for thermionic converters are discussed in a Euratom report.[32] Fine-grained, high-density, pure alumina is brazed to Nb–1 Zr using either a palladium alloy or a V–30 Nb–5 Ti alloy. Respective tensile strengths of 10 kg/mm^2 (14.2 ksi) and 8 kg/mm^2 (11.4 ksi) have been obtained with the two alloys. Brazed joints have resisted 100 thermal cycles between 500 and 1200°C. They have also withstood corrosion at 1000°C in cesium vapor under a pressure of 20 torrs for 1000 hr with practically no attack, no loss of vacuum tightness, and no change in tensile strength.

A Ni–19 Cr–10 Si alloy (GE J8100) is being used to braze 347 stainless-steel spacer wires to fuel plates.[33] Optimum brazing conditions are about 2 hr at 2090 to 2120°F (1140 to 1160°C), with the higher temperature apparently producing higher shear strengths. Minor gaps in the brazed joints are successfully rebrazed using Nicrobraz 50 (Ni–13 Cr–10 P). Wires are tacked before brazing by spot welding, using a capacitor-discharge welder with tweezer electrodes. The major problem in brazing these joints is control of the braze-alloy flow. Excessive braze material on the fuel-plate surface interferes with heat transfer and coolant flow. Several control techniques were found to be feasible, although each presents either technical or economic problems.

Brazed joints in Ta–10 W and TZM (Mo–0.5 Ti–0.1 Zr) alloys were tested in shear, with the results shown in Table IV-2. On the whole, the strength was good, even to within a few hundred degrees of the melting point of the brazing alloys. Braze alloys from the Ti–Zr system did not weaken noticeably with aging and were in fact strengthened in most cases. In contrast, the Ti–V brazes all lost strength upon aging, although their actual strengths after aging were still appreciable.

Fluxless brazing of aluminum, once considered impossible, is being utilized to fabricate coldplate for the Apollo Command Module.[34] Coldplate cores, with hundreds of electrical-discharge machined "pins" on one surface, are made of 6061–T651 aluminum alloy.

Table IV-2 Shear Strength of Brazed Joints in Refractory Alloys[33]

Braze alloy composition (balance titanium), wt.%	Melting point, °C	Test temp., °C	Aging temp., °C	Shear strength, ksi: TZM base metal	Ta–10 W base metal (as brazed)	Ta–10 W base metal (aged 50 hr)
45 Zr–10 Ta	1550	RT*	1250	20†	38	30
		1250	1250	6.5	2.5	5.2
42.5 Zr–15 Ta	1525	RT	1250	17‡	37	29
		1250	1250	5.3		5.6
49 Zr–2 Si	1250	RT	1000	25	33	40
		1000	1000	26	5	10
40 Zr–20 Nb	1550	RT	1250	16	48	43
		1250	1250	10	4.7	6.3
46 Zr–8 Ge	1250	RT	1000	36	55	53
		1000	1000	11	27	14
35 Zr–30 Cr	1050	RT	1000	28	49	34
		1000	1000		13	6.7
49 Zr–2 B	1250	RT		40	59	
		1000		36	42	
26 V–10 Nb	1575	RT	1000	19	60	49
		1250	1000	19	51	15
26 V–9 Mo	1550	RT	1250	20	46	37
		1250	1250	8	20.684	12
27 V–5 Mo	1525	RT	1250	12		50
		1250	1250	24	26	14
25 Cr–21 V	1350	RT	1000	25	51	32
		1000	1000	19	33	13

*RT, room temperature.
†TZM aged 50 hr at 1250°C, 19 ksi.
‡Specimen broke in base metal.

Table IV-3 Recommended Alloys for Brazing Beryllium[35]

Designation*	Capillary flow: T-joints, in.	Capillary flow: Residue	Butt-joint tensile stress, ksi: RT	300°F	600°F	1000°F	Double-lap-joint shear stress, ksi: RT	300°F	600°F	1000°F	Metallography, mils: Interaction	Beryllide	Tolerance: Capillary flow, in.†	Honeycomb
A	0.95	None	36.4	42.0	34.0	28.8	10.5	11.0	9.9	8.6	0.1	0.1	0.35	Good–fair
D	1.0	Slight	30.0	44.3	36.0	28.0	11.2	13.4	9.8	6.7	0.2	0.2	0.65	Excellent
E	1.0	None	18.4	26.3	23.2	22.6	11.0	12.0	8.8	7.9	0.1	0.1	0.75	Very good
L	1.0	Slight	24.0	35.0	41.0	29.0	10.5	11.0	9.6	7.7	0.2	0.2	0.55	Excellent
M	1.0	None	24.0	36.0	39.4	24.6	11.5	8.2	10.0	8.4	0.2	0.1	0.60	Excellent
O	1.0	None	24.7	27.0	27.4	27.8	11.1	10.0	6.4	7.3	0.1	0.1	0.60	Good

*All data are based on 1400°F/10-min braze except tolerance at 1400°F/20 min and honeycomb at 1420°F/15 min.
†Compositions: A = Ag–59.4 Cu–9.5 Ge–1.9 Ti–5 Mn; D = Ag–25.2 Cu–9.5 In–5 Mn; E = Ag–23.6 Cu–8.9 In–8.8 Pd–2 Ti; L = Ag–24.6 Cu–9.5 Sn–5 Mn; M = Ag–33 Cu–7 Sn–3 Mn; O = Ag–53 Cu–5 Zn–0.2 P
‡Mean flow for two braze conditions at 1400°F.

The facing skins are made of No. 23 aluminum brazing sheet, which consists of an aluminum 6951 core material clad on one side with 4045 braze alloy. Brazed joints are made between the core "pins" and the facing sheet. The fabrication procedure involves a very rigidly controlled 14-step cleaning process. Brazing is performed in a vacuum using a retort and heated platen presses in order to meet stringent flatness requirements. The brazing-temperature range is 1055 to 1095°F (570 to 590°C), held for 10 to 11 min. The brazed joints, which must be capable of withstanding internal pressures of 1000 psig, have in fact withstood pressures exceeding 2200 psig without failure.

Solar has reported results on a program to develop alloys for brazing beryllium below the recrystallization temperature.[35] Silver-, titanium-, and aluminum-base alloys were evaluated for melt properties, capillary flow, joint strength, and tolerance for changes in brazing conditions. T-specimens, butt and lap-shear coupons, and simulated honeycomb panels were used. As a result of this research, six silver-base alloys have been recommended for brazing at 1400°F (760°C) and above, as shown in Table IV-3. In addition, one titanium-base alloy (Ti–46.6 Zr–5.3 Ni–3.2 Ag–4.5 Be) was recommended, although its joint strength is slightly lower than those of the silver-base alloys. Acceptable wetting and flow could not be obtained with aluminum-base alloys.

(J. E. Mortland and R. M. Evans)

Nondestructive Testing

Ultrasonic Techniques

Engineers at Battelle–Northwest have developed a system for remote inspection of fueled isotope capsules.[36,37] An ultrasonic testing tank is located in the reactor. The test tank has means for rotating the capsule, translating the transducer axially, positioning the transducer both linearly and angularly, monitoring the location of the incident ultrasonic beam on the capsule, and circulating water for cooling. The capsules are inspected with the major axis in the vertical position. The capsule is rotated at 3 rpm, and the transducers traverse the specimen at 0.003 in./revolution.

The grain size relative to the wavelength is a major factor in determining the attenuation of ultrasonic energy through a metal. Detecting large grain size in materials is often done on the basis of ultrasonic attenuation. A frequency is chosen which is especially sensitive to grains at or above the reject size, i.e., with a wavelength approximately equal to the rejectable average grain diameter. Deleuze[38] has devised a method of measuring grain size in hemispherical parts in which he compares the transmission of ultrasonic energy through the test specimen with that through a series of standards of different but known average grain size. He assumes that the grain size in the specimen is equal to that of the one standard which causes the same amount of signal loss as does the specimen.

An electromagnetic transducer developed at Argonne[39] may become competitive with piezoelectric transducers. The transducer produces either shear or longitudinal waves at 5 Mc. Whether shear waves or longitudinal waves are generated is controlled by the relative orientations of the field of a permanent magnet and that of an a-c coil.

The fact that the frequency spectrum of an ultrasonic pulse is initially controlled by the transducer and the electronic system is well known to those using ultrasonics for nondestructive testing. It is also true that factors along the path of propagation also affect the frequency content of the pulse. Measurements of the effects of orientation of the transducer axis with the reflecting surface and of the length of the water path on the spectrum of a pulse reflected from the surface of a large, flat plate have been reported[3] by Oak Ridge. Researchers at Battelle–Northwest[40] have also shown effects on the spectral content of ultrasonic pulses reflected from defects of various geometrical shapes (spheres, disks, and ribbons). Extension of studies of these phenomena could contribute much to the value of ultrasonic energy for analytical purposes.

(D. Ensminger)

NDT Methods Other Than Ultrasonics

A new type of acoustic-emission transducer utilizing a split piezoelectric disk element to achieve a differential response has been successfully fabricated by investigators at Livermore.[41] It is reported that this transducer is much better suited than single-ended types for recording acoustic emissions in the presence of high-electrical-noise backgrounds. The investigators state that this transducer should be of considerable importance to many nondestructive acoustic-emission testing programs that involve working around electric motors, furnaces, and other r-f generating devices.

The phase-sensitive eddy-current meter developed at Oak Ridge has been used with considerable success for nondestructive measurement of the oxide content in aluminum wafers and billets.[42] The apparent accu-

racy is about ¼% of oxide difference. Information for construction of the instrument is available.

A literature survey on uses of neutron radiography has been prepared by Oak Ridge.[43] Approximately 65 references are noted, with special emphasis on uses and radioisotope sources.

Libby of Battelle–Northwest has prepared a report[44] covering several new eddy-current developments now under study there which will be of interest to others working with eddy-current systems. The subjects covered are control of the curvature of test-coil-impedance loci, temperature stabilization of eddy-current test coils, eddy-current ultrasonic transducers, impedance of a solenoid encircling a bar (covering a comparison of units and dimensions used by Foerster, Hochschild, and Libby), flow of eddy currents, and an operational test for phase detectors. Ten important references are listed.

Libby has also prepared a report on investigation of a broad-band, pulsed, eddy-current system with multiple-parameter extraction capabilities.[45] Preliminary results show the separation of signals from irregularities in a short section of ½-in.-diameter 304L stainless-steel tubing with a 0.050-in. wall. An inside circular test coil about 7/16 in. in diameter was used. Signals from probe wobble and a small piece of ferrous material outside the tubing were discriminated against, and signals caused by a notch on the inside wall and a notch on the outside wall were separated from one another and read out on separate channels. It is concluded that, although work remains to be done, the method has been developed sufficiently to proceed with the development of either a plating-thickness test or a tubing test using the principles described.

Further studies of acoustic emission by Battelle–Northwest have recently been reported in useful detail.[46] It is concluded from the work in progress that (1) detection of acoustic emission above about 1.5 Mc appears to be unaffected by hydraulic noise (even cavitation), and all emissions at least from steel are sharp-rise transients that will produce response in transducers in excess of 30 Mc; (2) the edge-mounted shear-wave sensor produces a much sharper and shorter response to acoustic emission than does the surface-mounted longitudinal sensor, which is of significance to detection resolution and to accuracy in source location; (3) the surface-mounted longitudinal sensor is not suitable for use if cavitation is occurring; and (4) edge-mounted shear sensors on a block attached to the specimen surface do not give optimum response, and thus better techniques for using the transducers in the field are being sought. (A. F. Leatherman)

References

1. N. H. Katz, Heavy Water Organic Cooled Reactor. Preliminary Annular UC Fuel Casting Development, USAEC Report AI-CE-45, Atomics International and Combustion Engineering, Inc., Mar. 15, 1969.
2. R. F. Bunshah, Techniques of Materials Preparation and Handling, in *Techniques of Metals Research*, Vol. I, Part 2, John Wiley & Sons, Inc., New York, 1968.
3. P. Patriarca and W. O. Harms (Comps.) and D. J. Rucker (Ed.), Metals and Ceramics Division, Fuels and Materials Development Program Quarterly Progress Report for Period Ending September 30, 1968, USAEC Report ORNL-4350, Oak Ridge National Laboratory, February 1969.
4. J. R. Long, Research Program To Develop a Technology Improvement Program for Closed Die Forging, Report NASA-CR-96323 (N68-32735), Harvey Aluminum, Inc., November 1966.
5. E. C. Bishop, R. A. Nadler, and G. A. Whitlow, Vanadium Alloy Cladding Development, Quarterly Progress Report for the Period Ending September 30, 1968, USAEC Report WARD-3791-25, Westinghouse Electric Corp., Advanced Reactors Division, October 1968.
6. E. C. Bishop, R. A. Nadler, and G. A. Whitlow, Vanadium Alloy Cladding Development, Quarterly Progress Report for the Period Ending December 31, 1968, USAEC Report WARD-3791-30, Westinghouse Electric Corp., Advanced Reactors Division, February 1968.
7. R. M. Spriggs and L. Atteraas, Densification of Single-Phase Systems Under Pressure, in *Ceramic Microstructures. Their Analysis, Significance, and Production*, pp. 701-727, John Wiley & Sons, Inc., New York, 1968.
8. F. L. Carlsen, Jr., and D. G. Dreyer, Properties of Powder Metallurgy Wear Resistant Alloys, *J. Inst. Powder Met.*, 4(4): 31-37 (October 1968).
9. Beryllium–Aluminum Composite, British Patent 1,128,188, Sept. 25, 1968.
10. J. D. Gadd, H. A. Fish, H. A. Kmieciak, and E. E. Jones, Vacuum Pack and Vacuum Slip-Pack Processes for Coating Refractory Metals, *Electrochem. Technol.*, 6(11-12): 379-388 (November–December 1968).
11. E. J. Felten, Oxidation Behavior of Silicided Columbium–Titanium Binary Alloys, *Electrochem. Technol.*, 6(11-12): 438-447 (November–December 1968).
12. G. V. Zemskov, R. L. Kogan, V. M. Luk'yanov, and V. S. Viderman, Structure and Phase Composition of Silicide Coatings on Niobium, *Fiz. Metal. Metalloved.*, 25(4): 762-764 (April 1968).
13. D. M. Mattox, Ion Plating, Report SC-R-68-1865, Sandia Corp., November 1968.
14. S. Marinkovic, C. Suznjevic, and I. Dezarov, Simultaneous Vapor Deposition of Uranium and Carbon, *Bull. Boris Kidric Inst. Nucl. Sci., Chem.*, 19(1): 1-3 (January 1968).
15. R. G. Wymer and A. L. Lotts (Comps.), Status and Progress Report for Thorium Fuel Cycle Development for Period Ending December 31, 1966, USAEC Report ORNL-4275, Oak Ridge National Laboratory, January 1969.
16. R. B. Pratt, J. D. Sease, W. H. Pechin, and A. L. Lotts, Pyrolytic Carbon Coating in an Engineering-Scale System, *Nucl. Appl.*, 6(3): 241-255 (March 1969).

17. Gulf General Atomic Incorporated, Public Service Company of Colorado 330-MW(E) HTGR Research and Development Program, Quarterly Progress Report for the Period Ending December 31, 1968, USAEC Report GA-9130, Jan. 29, 1969.
18. Gulf General Atomic Incorporated, HTGR Base Program, Quarterly Progress Report for the Period Ending November 30, 1968, USAEC Report GA-9090, Dec. 30, 1968.
19. R. Guidotti and K. Lui, The Development of Technology Required for the Successful Deposition of Aluminum Alloys and Beryllium, Report NASA-CR-66344, Electro-Optical Systems.
20. D. A. Nissen and R. W. Stromatt, Zirconium Electroplating on Uranium from Molten Alkali Fluoride Salts, USAEC Report BNWL-825, Battelle–Northwest, June 1, 1968.
21. N. Y. Fedotova, T. A. Ginberg, and A. T. Vagramyan, Activation Mechanism of the Electrode-Position of an Iron–Nickel–Molybdenum Alloy in an Ultrasonic Field (in Russian), *Electrokhimiya*, 3: 1111-1114 (September 1967).
22. M. A. Wilkins, Anodic Oxidation of Silicon, British Report AERE-R-5875, August 1968.
23. J. Amesz, H. Holtbecker, M. Montagnani, and G. Verzeletti, Explosive Welding of a Fuel Element, *Nucl. Eng. Design*, 8: 337-344 (1968).
24. J. Barrington, Explosive Tube Bonding, U. S. Patent 3,364,561, to E. I. du Pont de Nemours & Company, Inc., Feb. 10, 1966.
25. M. Kameishi, Line Welding Method for Metals by Explosives, U. S. Patent 3,344,510, Feb. 19, 1964.
26. T. Suzuki, Spot Welding Method for Metals by Explosives, U. S. Patent 3,316,627, Nov. 5, 1963.
27. Oak Ridge National Laboratory, Molten Salt Reactor Program Semiannual Progress Report for Period Ending August 31, 1968, USAEC Report ORNL-4344, February 1969.
28. G. M. Slaughter, E. A. Franco-Ferreira, E. L. Long, and G. Hallerman, Unusual Weld Cracking Problem in Inconel, *Welding J. (N. Y.)*, 47(10): 479s-480s, (October 1968).
29. T. J. Morrison, C. S. Shira, and L. A. Wersenburg, The Influence of Minor Elements on Alloy 718 Weld Microfissures, paper presented at the Welding Research Council Symposium, Houston, Tex., (October 2–5, 1967).
30. H. E. Pattee, Joining Ceramics and Graphite to Other Materials, Report NASA-SP-5052, Battelle–Columbus, 1968.
31. G. Perona and G. Volta, Diffusion Welding Process, Italian Patent 821,522, 1968.
32. C. M. Cappelletti, C. A. Busse, and E. A. Dorre, Metal-to-Ceramic Seals for Thermionic Converters, Report EUR-4210 (CONF-680508), paper presented at Second International Conference on Thermionic Electrical Power Generation, Stresa, Italy, May 27–31, 1968.
33. V. M. Kolba, C. V. Pearson, and W. C. Kramer, Development of Brazing Techniques and Procedures for Fabricating Fuel Subassemblies for the Argonne Advanced Research Reactor (AARR), USAEC Report ANL-7458, Argonne National Laboratory, August 1968.
34. C. S. Beuyokian, Fluxless Brazing of Apollo—Coldplate—Development and Production, *Welding J. (N. Y.)*, 47(9): 710-719 (September 1968).
35. R. G. Bogowitz and A. G. Metcalfe, Brazing Beryllium by Capillary Flow, Report AFML-TR-67-14, Part II, International Harvester Co., Solar Division, July 1958.
36. R. W. Steffens and F. M. Coffman, Nondestructive Testing of Isotope Containment Capsules: Remote Ultrasonic Test Station UT-40, USAEC Report BNWL-918, Battelle–Northwest, November 1968.
37. R. W. Steffens, Ultrasonic Test Support for Container Integrity Assurance, USAEC Report BNWL-SA-2111, Battelle–Northwest, Sept. 23, 1968.
38. M. P. Deleuze, Ultrasonic Measurement of the Grain Size of Hemispherical Parts Made of Uranium Alloy Containing 0.2% Vanadium by Weight, French Report CEA-CONF-1081.
39. Argonne National Laboratory, Reactor Development Program Progress Report, November 1968, USAEC Report ANL-7518, Dec. 27, 1968.
40. A. L. Bement, G. J. Dau, E. A. Evans, and R. E. Nightingale, Battelle–Northwest, unpublished, February 1969.
41. H. L. Dunegan, A. E. Brown, and P. L. Knauss, Piezoelectric Transducers for Acoustic Emission Measurements, USAEC Report UCRL-50553, University of California, Lawrence Radiation Laboratory, Dec. 13, 1968.
42. H. L. Whaley, Development of Nondestructive Tests for Intermediate Fabrication of Sintered Aluminum Products, USAEC Report ORNL-4352, Oak Ridge National Laboratory, February 1969.
43. M. Gerrard, Uses of Neutron Radiography, USAEC Report ORNL-IIC-16, Oak Ridge National Laboratory, October 1968.
44. H. L. Libby, Miscellaneous Eddy Current Techniques, USAEC Report BNWL-996, Battelle–Northwest, January 1969.
45. H. L. Libby, Broadband Electromagnetic Testing Methods. Part V, Pulsed Eddy Current Method, USAEC Report BNWL-976, Battelle–Northwest, January 1969.
46. Battelle–Northwest, Nuclear Safety Quarterly Report, August–October 1968, for Nuclear Safety Branch of AEC Division of Reactor Development and Technology, USAEC Report BNWL-926, December 1968.

AEC Critical Review Series

REACTOR-NOISE ANALYSIS IN THE TIME DOMAIN

Nicola Pacilio
Argonne National Laboratory
Comitato Nazionale per l'Energia Nucleare

Recent research and new instrumentation emphasize once again the importance of time-analysis methods in the study of neutron noise. The second book in the AEC Critical Review Series is therefore a timely summary and evaluation of past and present research in this field and an indication of future developments in noise analysis.

The author organizes the state of the art of time analysis into four main categories under which he describes 15 different methods. For each method he gives the mathematical formulation, the means of data collection, and the experimental procedure. More important, however, he interprets the results and looks ahead to the uses, limitations, and potentialities of each method. With this added dimension the book becomes a valuable guide for reactor personnel. (102 pp., 18 figs., paperbound, chronological list of references.)

FOUR MAIN CATEGORIES

I: Time-correlation analysis among the neutron-detection pulses

II: Analysis of the moments of neutron distribution

III: Analysis of the probability of neutron detection

IV: Correlation analysis among the signs of the fluctuations

The contents also include:
General considerations on reactor-noise analysis
Synopsis of neutron statistics methods
Conclusions
Index

Available for $3.00 as TID-24512 from

Clearinghouse for Federal Scientific and Technical Information
Springfield, Virginia 22151

LEGAL NOTICE

This journal was prepared under the sponsorship of the U. S. Atomic Energy Commission. Neither the United States, nor the Commission, nor any person acting on behalf of the Commission:

A. Makes any warranty or representation, expressed or implied, with respect to the accuracy, completeness, or usefulness of the information contained in this journal, or that the use of any information, apparatus, method, or process disclosed in this journal may not infringe privately owned rights; or

B. Assumes any liabilities with respect to the use of, or for damages resulting from the use of any information, apparatus, method, or process disclosed in this journal.

As used in the above, "person acting on behalf of the Commission" includes any employee or contractor of the Commission, or employee of such contractor, to the extent that such employee or contractor of the Commission, or employee of such contractor prepares, disseminates, or provides access to, any information pursuant to his employment or contract with the Commission, or his employment with such contractor.

Nuclear Science Abstracts

The U. S. Atomic Energy Commission, Division of Technical Information, publishes *Nuclear Science Abstracts (NSA)*, a semimonthly journal containing abstracts of the literature of nuclear science and engineering.

NSA covers (1) research reports of the U. S. Atomic Energy Commission and its contractors; (2) research reports of government agencies, universities, and industrial research organizations on a worldwide basis; and (3) translations, patents, books, and articles appearing in technical and scientific journals.

Complete indexes covering subject, author, source, and report number are included in each issue. These indexes are cumulated and sold separately.

Availability of NSA

SALE *NSA* is available on subscription from the Superintendent of Documents, U. S. Government Printing Office, Washington, D. C. 20402, at $42.00 per year for the semimonthly abstract issues and $38.00 per year for the cumulated-index issues. Subscriptions are postpaid within the United States, Canada, Mexico, and all Central and South American countries, except Argentina, Brazil, Guyana, French Guiana, Surinam, and British Honduras. Subscribers in these Central and South American countries, and in all other countries throughout the world, should remit $52.50 per year for subscriptions to semimonthly abstract issues and $47.50 per year for the cumulated-index issues. The single-copy price for the abstract issues is $1.75 postpaid, with this exception: Add one-fourth of $1.75 for mailing to the countries to which the $52.50 subscription rate applies.

EXCHANGE *NSA* is also available on an exchange basis to universities, research institutions, industrial firms, and publishers of scientific information. Inquiries should be directed to the Division of Technical Information Extension, U. S. Atomic Energy Commission, P. O. Box 62, Oak Ridge, Tennessee 37830.

DOCUMENTS
OCT 14 1969
MICHIGAN STATE UNIVERSITY
LIBRARIES

TECHNICAL PROGRESS REVIEWS may be purchased from Superintendent of Documents, U. S. Government Printing Office, Washington, D. C. 20402. *Nuclear Safety* at $3.50 per year (six issues) for each subscription or $0.60 per issue; each of the other journals at $2.50 per year (four issues) or $0.70 per issue. The use of the order form below will facilitate the handling of your order.

POSTAGE AND REMITTANCE: Postpaid within the United States, Canada, Mexico, and all Central and South American countries except Argentina, Brazil, Guyana, French Guiana, Surinam, and British Honduras. For these Central and South American countries and all other countries: add, for each annual subscription, $1.00 for *Nuclear Safety* and $0.75 for each of the other journals; for single issues, add one-fourth of the single-issue price. Payment should be by check, money order, or document coupons, and MUST accompany order. Remittances from foreign countries should be made by international money order or draft on an American bank payable to the Superintendent of Documents or by UNESCO book coupons.

order form

SUPERINTENDENT OF DOCUMENTS
U. S. GOVERNMENT PRINTING OFFICE
WASHINGTON, D. C. 20402

Please send — 1, 2, or 3 years

- ☐ Isotopes and Radiation Technology ____
- ☐ Nuclear Safety ____
- ☐ Reactor and Fuel-Processing Technology ____
- ☐ Reactor Materials ____

Enclosed: document coupons ☐ check ☐ money order ☐

Charge: Superintendent of Documents No._____

SUPERINTENDENT OF DOCUMENTS
U. S. GOVERNMENT PRINTING OFFICE
WASHINGTON, D. C. 20402

(Print clearly)

_____
Name

_____
Street

_____
City, State, ZIP Code